Protein-protected metal nanoclusters as diagnostic and therapeutic platforms for biomedical applications

Iman Zare, Daniel M. Chevrier, Anna Cifuentes-Rius, Nasrin Moradi, Yunlei Xianyu, Subhadip Ghosh, Laura Trapiella-Alfonso, Ye Tian, Alireza Shourangiz-Haghighi, Saptarshi Mukherjee, et al.

▶ **To cite this version:**

Iman Zare, Daniel M. Chevrier, Anna Cifuentes-Rius, Nasrin Moradi, Yunlei Xianyu, et al.. Protein-protected metal nanoclusters as diagnostic and therapeutic platforms for biomedical applications. Materials Today, 2023, 66, pp.159-193. 10.1016/j.mattod.2020.10.027 . hal-04454481

HAL Id: hal-04454481
https://hal.science/hal-04454481

Submitted on 16 Feb 2024

HAL is a multi-disciplinary open access archive for the deposit and dissemination of scientific research documents, whether they are published or not. The documents may come from teaching and research institutions in France or abroad, or from public or private research centers.

L'archive ouverte pluridisciplinaire **HAL**, est destinée au dépôt et à la diffusion de documents scientifiques de niveau recherche, publiés ou non, émanant des établissements d'enseignement et de recherche français ou étrangers, des laboratoires publics ou privés.

Distributed under a Creative Commons Attribution 4.0 International License

Graphical abstract

Protein-protected metal nanoclusters as diagnostic and therapeutic platforms for biomedical applications

pp xxx–xxx

Iman Zare, Daniel M. Chevrier, Anna Cifuentes-Rius, Nasrin Moradi, Yunlei Xianyu, Subhadip Ghosh, Laura Trapiella-Alfonso, Ye Tian, Alireza Shourangiz-Haghighi, Saptarshi Mukherjee, Kelong Fan *, Michael R. Hamblin *

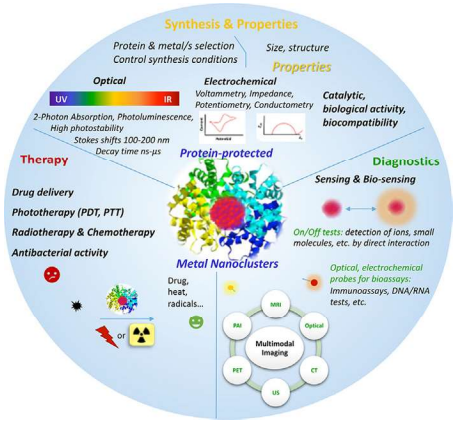

Uncorrected Proof

Materials Today • Volume xxx, Number xx • xxxx 2020 RESEARCH

ELSEVIER

RESEARCH: Review

Protein-protected metal nanoclusters as diagnostic and therapeutic platforms for biomedical applications

Iman Zare [1], Daniel M. Chevrier [2,†], Anna Cifuentes-Rius [3], Nasrin Moradi [4], Yunlei Xianyu [5], Subhadip Ghosh [6,7], Laura Trapiella-Alfonso [8], Ye Tian [9], Alireza Shourangiz-Haghighi [10], Saptarshi Mukherjee [11], Kelong Fan [12,13,*], Michael R. Hamblin [14,*]

[1] Department of Biology, Faculty of Basic Sciences, Semnan University, Semnan 35131-19111, Iran
[2] Aix-Marseille Université, CEA, CNRS, BIAM, 13108 Saint Paul lez Durance, France
[3] Monash Institute of Pharmaceutical Sciences, Monash University, Parkville Campus, 381 Royal Parade, Parkville, Victoria 3052, Australia
[4] Department of Chemistry, Tarbiat Modares University, Tehran 14115 175, Iran
[5] College of Biosystems Engineering and Food Science, Zhejiang University, Hangzhou 310058, Zhejiang, China
[6] Program in Biophysics, University of Michigan, Ann Arbor, Michigan 48109 USA
[7] Department of Chemistry, The Pennsylvania State University, University Park, PA 16802, United States
[8] Chimie ParisTech, PSL University, CNRS 2027, Institute of Chemistry for Life and Health Sciences, SEISAD, 11 rue Pierre et Marie Curie, 75005 Paris, France
[9] Department of Chemistry, Stanford University, Stanford, USA
[10] Department of Mechanical and Aerospace Engineering, Shiraz University of Technology, Shiraz, Iran
[11] Department of Chemistry, Indian Institute of Science Education and Research Bhopal, Bhopal Bypass Road, Bhauri, Bhopal 462066, Madhya Pradesh, India
[12] CAS Engineering Laboratory for Nanozyme, Key Laboratory of Protein and Peptide Pharmaceutical, Institute of Biophysics, Chinese Academy of Sciences, 15 Datun Road, Beijing 100101, China
[13] Academy of Medical Sciences, Zhengzhou University, 40 N Daxue Road, Zhengzhou 450052, China
[14] Laser Research Centre, Faculty of Health Science, University of Johannesburg, Doornfontein 2028, South Africa

The use of protein templates for the controlled synthesis of inorganic nanostructures has gained considerable attention in multidisciplinary fields, including electronics, optics, energy, sensing, and biomedicine, owing to their biocompatibility and structural programmability. The possible synergistic combination of protein scaffolds (and other biomolecules/biopolymers) with metal nanoclusters (MNCs) has created a new class of highly photoluminescent nanoprobes and nanodevices. For the first time, we discuss the different types of protein templates used for MNC preparation with an emphasis on their optoelectronic properties for application. In particular, applications of protein-coated MNCs for chemosensing or biosensing of cancer biomarkers, neurotransmitters, pathogenic microorganisms, biomolecules, pharmaceutical compounds, and immunoassays are discussed in detail herein. Fluorescence-based and multimodal molecular imaging, both *in vitro* and *in vivo* based on functional proteins are also covered. Furthermore, we discuss the burgeoning growth of protein-coated MNCs (*e.g.*, gold (Au) and silver (Ag) NCs) to develop synergistic nanotherapeutics with potential biomedical applications in chemotherapy, radiotherapy, photodynamic therapy (PDT), photothermal therapy (PTT), and antibacterial activity, as well as MNC-containing nanocomposites for enhanced bioimaging and controlled drug release. Overall, this review highlights the recent progress, technical challenges

* Corresponding authors.
E-mail addresses: Fan, K. (fankelong@ibp.ac.cn), Hamblin, M.R. (hamblin.lab@gmail.com).
† These authors made equal contribution.

1369-7021/© 2020 Elsevier Ltd. All rights reserved. https://doi.org/10.1016/j.mattod.2020.10.027

Please cite this article in press as: I. Zare et al., Materials Today, (2020), https://doi.org/10.1016/j.mattod.2020.10.027

Uncorrected Proof

Nomenclature

AChE	Acetylcholinesterase
AIE	Aggregation-induced emission
ALP	Alkaline phosphatase
AD	Alzheimer's disease
Ab	Antibody
antiSA–IgG	Anti-staphylococcal immunoglobulin
Asc	Ascorbyl
Asp	Aspartic acid
ATT	6-aza-2-thiothymine
BSA	Bovine serum albumin
BTB	Bromothymol blue
CFFs	Carbon fiber fabrics
CAT	Catalase
cfu	Colony-forming unit
CT	Computed tomography
Ce6	Chlorin e6
CSH	Cysteamine
Cyt c	Cytochrome c
dBSA	Denatured bovine serum albumin
DAPI	4′,6-diamidino-2-phenylindole
DTPA	Diethylene triamine pentaacetic acid
DOX	Doxorubicin
ESM	Eggshell membrane
EWA	Egg white albumin
EWP	Egg white protein
ECL	Electrochemiluminescence
EPR	Enhanced permeability and retention
EGFR	Epidermal growth factor receptor
EGCG	Epigallocatechin gallate
EDTA	Ethylenediaminetetraacetic acid
FITC	Fluorescein-5-isothiocyanate
FRET	Fluorescence resonance energy transfer
FLFIA	Fluorescent lateral flow immunoassay
FSs	FluoSpheres
FR	Folate receptor
FA	Folic acid
GEM	Gemcitabine
GOD	Glucose oxidase
GSH	Glutathione
AuNRs	Gold nanorods
GO	Graphene oxide
GFP	Green fluorescent protein
Hb	Hemoglobin
HRP	Horseradish peroxidase
HSA	Human serum albumin
HER2	Human epidermal growth factor receptor 2
HA	Hyaluronic acid
5-HT	5-hydroxytryptamine
ICG	Indocyanine green
INS	Insulin
Ils	Ionic liquids
IONPs	Iron oxide nanoparticles
pI	Isoelectric point
a-LA	a-lactalbumin
Lf	Lactoferrin
Arg	L-arginine
LFIA	Lateral flow immunoassay
LOD	Limit of detection
LHRH	Luteinizing hormone-releasing hormone
LYZ	Lysozyme
MRI	Magnetic resonance imaging
MG	Malachite green
MSN	Mesoporous silica nanoparticle
Met	Methionine
MNCs	Metal nanoclusters
MNPs	Metal nanoparticles
MOFs	Metal organic frameworks
MRSA	Methicillin-resistant Staphylococcus aureus
MSSA	Methicillin-sensitive Staphylococcus aureus
MCF-7	Michigan Cancer Foundation-7
MES	2-(N-morpholino) ethanesulfonic acid
MFNC	Multifunctional nanocarrier
NIRF	Near infrared fluorescent
NGF	Nerve growth factor
NSE	Neuron-specific enolase
OVA	Ovalbumin
PPI	Pea protein isolate
PEP	Pepsin
PA	Picric acid
PEG	Polyethylene glycol
PEI	Polyethylenimine
PET	Positron emission tomography
PBS	Phosphate buffered saline
PAI	Photoacoustic imaging
PDT	Photodynamic therapy
PEC	Photoelectrochemical
PL	Photoluminescence
PS	Photosensitizer
PTT	Photothermal therapy
PPi	Pyrophosphate ion
QC	Quantum cluster
QD	Quantum dot
QY	Quantum yield
RF	Radiofrequency
ROS	Reactive oxygen species
RBC	Red blood cell
RuS	Ruthenium sulfide
SF	Silk fibroin
sgRNA	Single guide RNA
SPECT	Single photon emission computed tomography
siRNA	Small interference RNA
SEB	Staphylococcal enterotoxins B
TMB	Tetramethylbenzidine
TAT	Transactivor of transcription
Trf	Transferrin
TRY	Trypsin
US	Ultrasound imaging
UV	Ultraviolet
Van	Vancomycin
ZIF	Zeolite imidazole framework

Uncorrected Proof

and new horizons in this field, and summarizes our understanding of how MNC properties interact with the biological function of protein scaffolds to develop synergistic nanotherapeutics towards clinical translation.

Please cite this article in press as: I. Zare et al., Materials Today, (2020), https://doi.org/10.1016/j.mattod.2020.10.027

Introduction

Proteins are complex biomolecules made up of amino acids, which provide structural integrity and take part in most chemical reactions in all living organisms. The use of protein templates for the synthesis of uniform inorganic nanostructures has gained considerable attention in multidisciplinary fields, including electronics, optics, energy, sensing, and biomedicine. The distinctive features of these nanostructures, particularly metal nanoclusters (MNCs), are their optical, electronic, magnetic, and chemical properties, which have been ascribed to the extremely small dimensions and special nature of the surface [1–8]. Quantum confinement of the electrons in MNCs (*e.g.*, AuNCs and AgNCs) occurs due to the ultrasmall particle sizes of these nanoparticles (with diameters ≤ 2 nm), creating more discrete energy levels of the metal particle with distinct molecule-like electronic transitions in the valence states (*i.e.*, HOMO–LUMO transitions) [9]. This endows MNCs with properties such as photoluminescence (PL) at wavelengths ranging from the ultraviolet (UV) to near-infrared (NIR), wavelength-tunable emission, quantized charges, magnetism, and optical chirality [1,2,6,10,11]. The tremendous progress in research on MNCs suggests they could be employed in many biomedical applications due to such intrinsic properties [2,12–14].

Despite the myriad advantages of MNCs in several fields, synthesis procedures often require long reaction times and harsh conditions, such as organic solvents and hazardous reducing agents, as well as high reaction temperatures. To address the synthetic preparation issues of MNC, researchers have turned to biological systems to direct the synthesis of inorganic nanostructures [15–21]. The use of biological systems that can simultaneously act as reducing and protecting agents is a stepping stone towards developing clean or green procedures for the synthesis of MNCs using milder reaction conditions [22–24]. Protein-directed synthesis of MNCs using bovine serum albumin (BSA) as a bio-scaffold was reported by Xie et al. for the first time [25]. It was reported that aromatic amino acid groups reduced metal ions through donating electrons to gold ions, whereby AuNCs were formed.

Since the discovery of this clean synthesis procedure for BSA-AuNCs, there has been a growing number of studies using biomolecules, proteins, and biomaterials to produce templated metal and alloy NCs [26,27]. These proteins have included ovalbumin (OVA), glucose oxidase (GOD), lysozyme (LYZ), trypsin (TRY), transferrin (Trf), pepsin (PEP), egg white albumin (EWA), insulin (INS) and hemoglobin (Hb) [26,28–34]. In addition to proteins, recently it has been reported that cancerous cells and normal mammalian cells are able to direct the synthesis of MNCs, such as Au, Ag, zinc (Zn), and platinum (Pt) [35–38]. Because the protein coating on the MNCs acts as an interface between the NCs and the biological environment, the proteins surrounding the MNCs can determine the key parameters, which are of great significance in biological settings, including water solubility, excellent stability, low toxicity, and abundance of functional groups. The intrinsic fluorescence of protein-templated MNCs arising from their metallic core makes them promising fluorescent probes in both pre-clinical and clinical applications [39–43]. These properties have emerged as a whole new direction in biomedical research. However, although the synthesis, properties and biomedical applications of some biomolecule-protected NCs have been published in recent years, there are few comprehensive reviews covering the biomedical applications of protein-encapsulated MNCs [17,22,44–55].

The integration of many advantageous features including optical, electronic, and catalytic properties of MNCs [56] with the abundant active functional groups of proteins within a single structure make protein-protected MNCs outstanding among other nanostructures. Protein-MNCs can be used as tracking and carrier agents in biolabeling, biosensing, bioimaging, targeted cancer therapy and drug delivery applications. In some respects, protein-protected MNCs are preferable to conventional fluorescence probes or stains (*e.g.*, 4′,6-diamidino-2-phenylindole (DAPI) and green fluorescent protein (GFP)) and quantum dots (QDs) (*e.g.*, cadmium selenide (CdSe) and gallium arsenide (GaAs)) due to their prolonged fluorescence lifetime, biocompatibility and good stability [57,58] This is due to the surrounding protective protein layer, since the fluorescence of the metal core is shielded from nonspecific bio-macromolecular interactions or unwanted cellular sequestration that could lead to photobleaching and quenching in biological environments [59,60]. Moreover, unlike QDs where the core stability is prominent and the functional coating determines the QDs toxicity leading to restrictions in their bio-application, the multifunctionality of the protein coating on MNCs is useful for post-synthesis modification for a variety of biomedical applications, particularly biomarker sensing, drug loading, imaging-guided drug delivery as well as cancer therapy (Fig. 1). Nevertheless, there are still concerns about the practical application of MNCs for biomedical purposes. One concern for using protein-MNCs as staining probes in bioimaging applications is the weaker luminescence of protein-MNCs. In terms of quantum yield (QY), protein-MNCs are slightly inferior compared to conventional fluorescence probes and semiconductor QDs, thus different approaches for enhancing the fluorescence intensity of MNCs are of importance. Another growing concern about the practical *in vivo* applications of MNCs is the possible toxicity issue, which will be further discussed in Section 2. According to a few studies that assessed the toxicity of protein-protected MNCs, the toxicity of BSA-protected MNCs towards some cell lines has been reported [61,62]. Considering the progress and the current limitations, we suggest that prospects for employing MNCs in biology and medicine are encouraging, but will require judicious consideration for their future clinical translation.

In this comprehensive overview, we will focus on the advantages and limitations of a broad range of protein-protected MNCs in biomedical research (Fig. 1). First, we will introduce the emergent properties of protein-protected MNCs in terms of structure, electronic, and optical properties (Section 2). Next, in Section 3, we will focus on chemical and biological sensing applications as fluorescent labels in assays. These include sensing and detection of cancer biomarkers, biomolecules, pharmaceutical compounds, neurotransmitters, pathogenic microorganisms, and pH and temperature monitoring. Fluorescence-based imaging and multimodal imaging strategies for biological systems, both *in vitro* and *in vivo* are presented in Section 4. In Section 5, we highlight the

Uncorrected Proof

Please cite this article in press as: I. Zare et al., Materials Today, (2020), https://doi.org/10.1016/j.mattod.2020.10.027

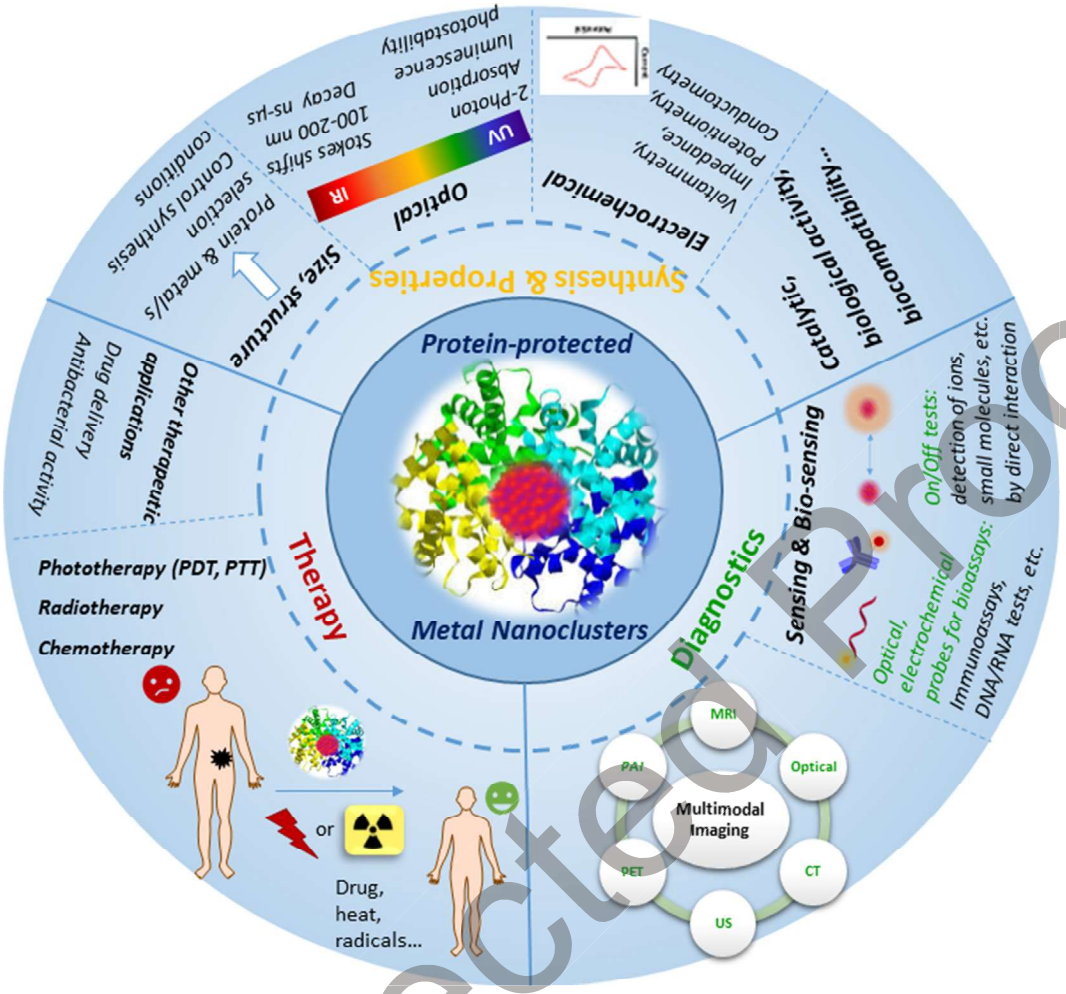

FIGURE 1

Protein-protected MNCs have been widely used in many fields, and their synthesis and properties, and use in diagnostics, and therapy is shown.

progress in emerging therapeutic applications of protein-protected MNCs such as chemotherapy, radiotherapy, PDT, PTT, antibacterial activity and drug/gene delivery. Lastly, the outlook and future perspectives for protein-protected MNCs are discussed with consideration of recent progress, key opportunities and remaining challenges. This is towards the goal of creating next-generation diagnostic and therapeutic agents in translational medicine.

Emergent properties of protein-protected MNCs

Only recently has the marriage between MNCs and proteins (and other biomolecules/biopolymers) created a new class of highly photoluminescent nanoprobes and nanodevices. In particular, the protecting protein plays an important role in directing the formation and stabilization of MNC structures. When combined together, the stabilizing protein molecule and the MNC component give rise to robust emergent properties, such as PL and the ability for sensitive analyte detection. Before a complete understanding of these properties can be ascertained, protein-protected MNCs require more in-depth structural characterization, especially concerning the MNC component. It should be mentioned that several other biomolecular scaffolds can be utilized to stabilize an even broader range of MNCs, which include single amino acids, peptides, DNA and other biopolymers [11]. Similar emergent properties can also be found with these systems which arise from synergetic interaction between the MNC and the stabilizing biomolecule [63]. Nevertheless, these systems may not be directly applicable to understanding protein-protected MNCs. Unlike smaller biomolecules, a variety of proteins, with the combination of proximal amino acid residues, enable the binding and accumulation of metal ions [64]. The spatially confined nature and specific concentration of these accumulation sites could also give rise to unique MNC structures and properties. Protein-MNCs, furthermore, possess additional advantages over other biomolecule-protected systems, including:

(i) protein molecules have an intrinsic capability for highly specific molecule-/analyte–protein interaction that leads to a recognition/sensing property;
(ii) with further improvements to the synthetic protocol, it may be possible to preserve the protein conformation during the MNC formation, thereby retaining some of the protein's biological activity;

Uncorrected Proof

Please cite this article in press as: I. Zare et al., Materials Today, (2020), https://doi.org/10.1016/j.mattod.2020.10.027

(iii) the protein scaffold has a wide range of chemical functionalization possibilities for drug delivery and other biomedical applications.

The one-pot synthesis protocol

It has been demonstrated that several combinations of protein molecule and metal ion precursors can lead to MNC formation under the direction of the protein molecule in a facile, aqueous, one-pot synthesis procedure, while the same approach cannot as easily be applied to smaller ligand molecules (*e.g.*, organothiolates, amines, carboxylates, single amino acids, *etc.*). This was demonstrated in a seminal report on the preparation of red luminescent BSA-protected AuNCs by Xie et al. [25]. Under ambient reaction conditions (water-based, incubation and mixing at 37 °C) metal ions interact with protein residues, leading to reduction of the metal ions and protein–metal bond formation. With a balanced number of metal ions to protein molecules, emergent MNC properties were created including (most notably) intense luminescence, selective analyte interaction (*e.g.*, mercury ions (Hg^{2+}) sensing) and good photostability (*i.e.*, limited photobleaching and photoblinking), which taken together are beneficial for a range of imaging, sensing and detection applications. Following on from this report, similar one-pot mixing and incubation synthesis approaches have yielded several other protein-MNCs with luminescence properties (Fig. 2). It is thus understandable how such a breakthrough in luminescent MNC synthesis has created a burgeoning area of research for these nanomaterials. Of course, the protocol has adapted over the last decade, for example, to reduce synthesis time with higher reaction temperatures, and the addition of microwave-induced reduction have been reported [65]. Regarding point ii) made above, the ability to improve the preservation of protein conformation will impact future applications of protein-MNCs. High alkalinity and chemical reactions with reactive metal precursors (*e.g.*, $HAuCl_4$) are still needed in most one-pot approaches to create the luminescent MNC component, which will change the native state of the protecting protein [66,67]. Nevertheless, alternative synthetic strategies that allow the conjugation of a preformed MNC with protein molecules could provide an alternative approach to protein-MNCs materials [68].

Optoelectronic properties

The intriguing optoelectronic properties of protein-MNCs can be attributed to a combination of a highly confined ultra-small MNC component (tens of metal atoms per protein molecule) with discrete molecule-like electronic transitions, protein residues capable of stabilizing single metal atom coordination sites, and MNC species with significant charge transfer interactions, governed by the conformation of the protein host. The most notable property of protein-MNCs is the luminescence, which spans the visible to near-infrared wavelengths, determined by the particle size regime and the electronic structure of the metal atom type itself. The brightest luminescence can occur in small clusters of late transition metals [69]. In addition to clusters of metal atoms, strong luminescence can be observed in a variety d^8 to d^{10} metal–ligand complexes [70]. Research efforts thus far suggest that the combination of the protein molecule, metal precursor, and suitable reaction conditions can produce a vast range of different MNC sizes (measured as number of metal atoms per protein determined by mass spectrometry) and emission properties. Fig. 2a provides a representative overview of some protein–metal combinations and the resultant optimized emission wavelengths. The emission energy of protein-MNCs is not fully tunable across the whole of the visible range. Maximal optimized emission peaks are often reported around 400–500 nm and 600–700 nm. Interestingly, green emission (500–550 nm) is less common, having only been observed for BSA-PtNCs and lysed PEP-AuNCs [71,72]. However, higher energy emission (~400–450 nm) may originate from the protein itself and not from the MNC component; for example, it may arise from dityrosine residues [6]. According to some studies, the maximal emission peak can shift during optimization of the QY by varying the metal ion to protein concentration, or by adjusting pH conditions, for example [73,74]. Significant tuning of the emission energy through modification of the synthetic procedure will likely lead to lower emission efficiency, indicating that the optimal emission wavelength may inherently depend on the precise combination of metal atom and protein. One potential method for tuning the optical properties of protein-MNCs is to introduce a combination of different metals. This has been demonstrated in a few studies using a mixture of Au and Ag precursors with BSA in a protein-directed synthesis, or by adding ions such as Ag(I), Cd (II) or Pb(II) to AuNCs post-synthesis [25,65,75,76]. This approach could enhance the QY, as has been shown for other Au/AgNC systems [77], providing more tunable control over the emission energy. QY values are reported for most combinations plotted (Fig. 2a). Lower QY of ~0.01 is typically reported when a strong reducing agent is required to induce MNC formation with the protein (*e.g.*, BSA-AgNCs) [78], though this is not the case for some CuNCs and PtNCs, where hydrazine and ultrasonication (combined with ascorbic acid reduction) were used, respectively, to produce MNCs with QY > 0.15 [71,79]. It will be interesting to see the progress made with other noble metals such as Cu and Pt and to understand the nature of the MNC protected by the protein molecule.

Structure-optoelectronic relationship of protein-MNCs

It is well known that a variety of different MNC compositions (metal types and cluster sizes) can yield strong luminescence, and that larger metal cluster sizes (above ~3 nm in NP diameter) will not yield strong luminescence emissions. Thus, the discrete HOMO–LUMO electronic transitions between metal-centered states and significant ligand–metal charge transfer of protein-MNCs provide a suitable platform for molecule-like optoelectronic properties [9]. Regarding the origin of the strikingly intense luminescence property in certain MNCs, recent studies have suggested that the significant enhancement can be explained by increased rigidity of the ligand shell surrounding the MNC, or an aggregation-induced-emission (AIE) occurring between clusters [80]. It is possible that this emission mechanism could apply to protein-protected MNCs as well. For example, the intense luminescence would not be achieved for MNCs without protein molecules to confine the MNC into a rigidified state, and to isolate them from solvent interactions. The concept of a rigidified MNC within a protein molecule was suggested in a recent

Uncorrected Proof

Please cite this article in press as: I. Zare et al., Materials Today, (2020), https://doi.org/10.1016/j.mattod.2020.10.027

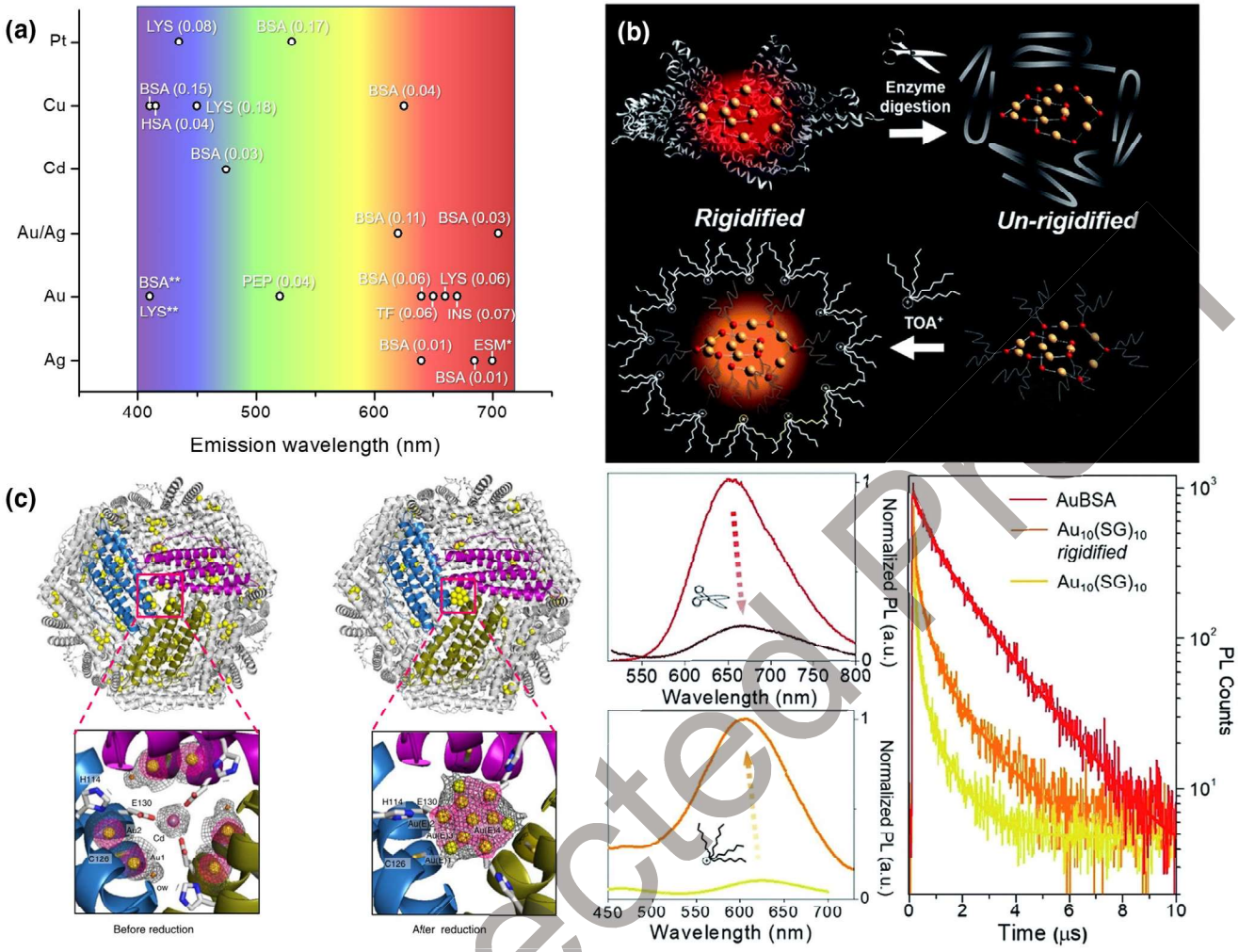

FIGURE 2

On the relationship between luminescence-composition and -structure of protein-MNCs. (a) Representative overview of protein-type and metal-type with wavelength of optimized emission maxima (LYZ [79,107,111], BSA [25,29,30,71,75,78,106,110], HAS [105], PEP [72], Trf [34], INS [109], ESM (LYZ) [32]) and QY reported in parentheses rounded to nearest 0.01. *no QY reported, **emission potentially originates from protein (b) Rigidified and non-rigidified conditions of $Au_{10}(SG)_{10}$ [72] and BSA-AuNCs, bottom plots show emission spectra and PL lifetime decay [81]. Reproduced with permission from Ref. [81]. Copyright 2018 Royal Society of Chemistry. (C) Crystal structures of mutant-apo-ferritin protein with accumulated Au atoms before and after reduction [84]. Reproduced with permission from Ref. [84]. Copyright 2017 Nature Publishing Group.

report on BSA-AuNCs [81]. This was demonstrated (depicted in Fig. 2b) by the enhanced luminescence of SG-AuNCs (SG = GSH) via a phase-transfer process, where SG-AuNCs were encapsulated with bulky counterions, while on the converse, BSA protein was digested for BSA-AuNCs using the TRY enzyme to significantly decrease the MNC luminescence, thereby removing the conditions enforcing rigidity.

Depending on the metal atom type, certain amino acid residues can form covalent interactions with metal species or provide stabilization through weaker interactions with a zero-valent metal core [64,82]. The specific inter-metal interactions involved, and the structural architecture of the MNC itself, are still uncertain and could vary markedly across different combinations of protein molecules and metal species. Albeit, the composition of MNCs coated with protein molecules could very well be polydisperse, although many reports have aimed at preparing a single MNC protein composition. If protein-MNCs were truly monodisperse clusters, a well-resolved absorbance spectrum might be expected, showing distinct optical transitions. Instead, a broader and weaker absorption spectrum is typically found in the visible region, with a strong onset of absorption in the visible blue and UV regions arising from the aromatic protein residues. Moreover, a recent report even suggested that the luminescence of BSA-AuNCs may originate from Au(III)–BSA complexes without any reduction of the Au(III) precursors [83]. A step in the right direction for understanding the interactions between the MNC and the protein molecule was reported by Maity et al. [84], where they were able to crystallize an AuNC within a mutant apo-ferritin protein cage (Fig. 2c). Although the report of this system did not describe any application-based properties such as luminescence or sensing, it did provide direct structural evidence for the assembled AuNC structure and identified metal ion accumulation sites.

Uncorrected Proof

Please cite this article in press as: I. Zare et al., Materials Today, (2020), https://doi.org/10.1016/j.mattod.2020.10.027

Toxicity of protein-MNCs

Despite these advantages, a growing concern associated with the practical *in vivo* application of protein-protected MNCs is their possible associated toxicity. Therefore, recent scientific efforts have been devoted to evaluate the intrinsic toxicity of protein-stabilized MNCs.

Studies assessing the toxicity of protein-protected MNCs have shown the non-toxicity of BSA-protected MNCs towards some model cell lines [61,62]. For instance, Rotomskis et al. investigated the toxicity of BSA-encapsulated and 2-(N-morpholino) ethanesulfonic acid (MES)-capped AuNCs. The BSA-AuNCs exhibited insignificant cytotoxicity compared to MES-AuNCs, suggesting the important contribution of the protein coating to the biocompatibility. The main reason for this is that the BSA template prevents exposure of the Au core to biological components, significantly reducing any negative effects on cell viability. On the contrary, cell viability decreased after incubation of cells with non-coated MES-AuNCs, due to reactive oxygen species (ROS) generation, which is a common observation for MNCs [61]. Similarity, Sarkar et al. showed that protein-protected AgNCs impregnated onto graphene oxide (GO) sheets had no significant effects on cell viability, confirming that protein coating could modulate the toxicity of AgNCs [85]. Conversely, some papers studying the toxicity of BSA-MNCs showed there was an adverse effect on cell viability, depending on the incubation time and dose [86,87]. According to their results, the BSA-AuNCs exhibited cytotoxicity against both cancer and normal cell lines over a certain range of concentration and time via intracellular generation of ROS. Interestingly, this toxicity could be alleviated by addition of additional free BSA molecules. The ultra-small size enabled GSH-protected MNCs to be metabolized, consequently decreasing their toxicity. These GSH-MNCs showed higher renal clearance and lower toxicity after 24 h compared to AuNCs stabilized in BSA [86]. Hence, these studies suggest that the eventual use of protein-MNCs in clinical applications requires judicious consideration.

Fluorescence enhancement strategies

There are numerous examples showing that the size, shape and surface chemistry of protein-protected MNCs can be readily tuned by adjusting the environmental conditions, including the structure of the protein, synthesis method used, temperature, and pH, which will determine their resulting PL properties [88]. Despite the many advantages of using proteins to template MNCs, their use is limited given their weak luminescence compared to conventional fluorescent dyes or QDs.

There are certain strategies known to increase the luminescence of MNCs including: 1) increasing the electron donation density of the ligands; 2) increasing the electro-positivity of the metal core; 3) AIE; and 4) using ligands containing electron-rich elements [80,89]. In general, for protein-protected MNCs, it has been shown that biomolecules with a large number of electron-rich atoms (*e.g.* N and O) or groups (*e.g.* –COOH and –NH_2) can increase the number of reduced metal ions in the MNC leading to luminescence enhancement. For instance, Shamsipour and coworkers investigated the reason underlying the QY enhancement of Hb-AgNCs [90]. They found that the mechanism involved in the MNC redox reactions mediated by Hb led to AIE, resulting in a significant increase in fluorescence. The Ag(I) precursor was first converted into oligomeric Ag(I)-X complexes (X: thiol, carboxyl and amine groups) in alkaline media, and was then reduced to Ag(0) metal by ligands with electron-rich atoms, (*e.g.* tryptophan, tyrosine and phenylalanine) which are abundant in human Hb (Fig. 3). Subsequently, the Ag(0)NCs–Ag(I)Hb complex core–shell nanostructure led to a dual emission/single excitation nanoprobe with a high QY.

Other strategies have focused on reducing the size of the MNCs in order to maximize their photoluminescent properties. For example, the presence of metal ion binding sites within the protein template is an effective mechanism to enhance the QY of protein-protected MNCs [91]. Rao et al. used metallation of the protein template using external ions as a strategy for improving the fluorescence intensity of AuNCs formed by α-lactalbumin (α-LA). In this study, the addition of lanthanum ions (La^{3+}) occupied the metal ion binding sites within the protein and restricted AuNC growth, so that smaller AuNCs with higher emission intensity were formed. Another approach to increase the QY of MNCs has been the use of ionic liquids (ILs) as the reaction medium. Studies from Wang et al. showed that the use of imidazolium ILs in the synthesis process of BSA-AuNCs resulted in an enhancement in fluorescence intensity and improved stability. Direct donation of delocalized electrons from the imidazolium ring structure contributed to restricting the size of the MNCs formed and thus, to the luminescence enhancement [92]. Metal-enhanced luminescence is another effective technique to maximize the QY. Muhammed et al. showed improved quantum efficiency of luminescent mercaptosuccinic acid-protected AuNPs by employing BSA as an etching agent [93]. It is likely that BSA could etch the surface atoms of the NPs, leading to a reduction in the Au core size resulting in highly luminescent AuNCs. Also, the metal-ion-induced luminescence enhancement can be used to synthesize cluster systems with enhanced optical properties and different ion-cluster interactions can be used to develop metal ion sensors as illustrated recently by Pradeep et al. with Au_{38}-BSA [76]. Other approaches that have been successfully applied to enhance the QY of MNCs include i) using sonochemical and microwave synthetic pathways, ii) forming "protein-corona"-like assemblies on the surface of NCs, iii) encapsulating NCs into metal–organic frameworks (MOFs), and iv) using mixed proteins for coating [71,94–97].

Considering that protein-MNCs are situated between the realms of metallic semiconductors and molecular systems, or are hybrids of such systems, it is of interest to understand how the MNC component contributes to the observed optical properties. The photoexcitation and emission mechanism of protein-MNCs is coming into focus from recent studies on atomically-precise MNCs. For example, correlating precise structure, HOMO–LUMO electronic energy levels, and optical properties of $Au_{25}(SR)_{18}$ NCs has enabled a detailed understanding on the origin of the optical properties [98,99]. This information can somewhat be translated to protein-MNCs to help understand their PL mechanism since similar structures as S–Au(I)–S oligomers are likely to exist [81]. If the MNC structure takes the form of $Au_{25}(SR)_{18}$, it has been suggested for BSA-AuNCs that an efficient intersystem crossover event occurs during the photo-

Uncorrected Proof

Please cite this article in press as: I. Zare et al., Materials Today, (2020), https://doi.org/10.1016/j.mattod.2020.10.027

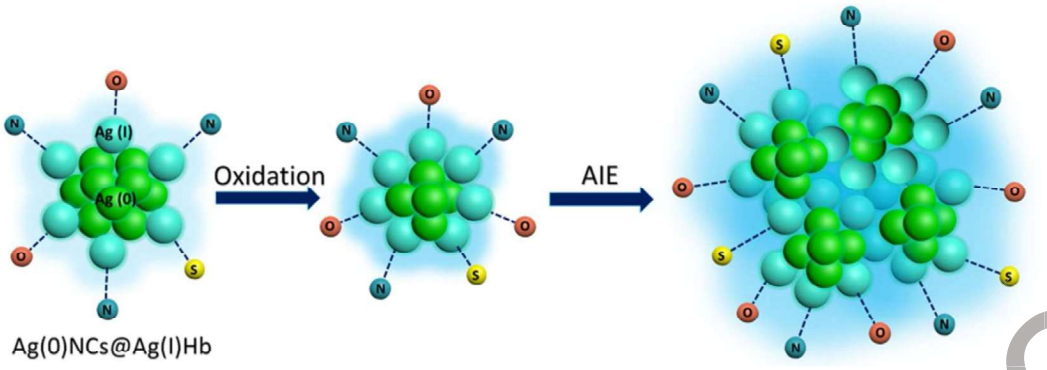

FIGURE 3

Synthesis mechanism identification of Hb protected AgNCs [90]. Reproduced with permission from Ref. [90]. Copyright 2018 American Chemical Society.

relaxation process due a small energy gap between singlet state and S–Au(I)–S triplet states leading to the observed decay times from ns to μs [100,101].

Parameters such as Stokes shift and PL decay time can provide some information regarding the nature of the MNC and the interaction between the MNC and the protein molecule. Large Stokes shifts more than 150 nm have often been reported for protein-MNCs, which indicate significant metal–ligand charge transfer as a result of which, photoexcitation can cause a large degree of relaxation to the ground state. Moreover, reorientation of dipoles can occur via vibrational energy dissipation from the MNC, leading to the stabilization of the protein residues with respect to the surrounding solvent molecules. If the MNC component is only weakly bound to the protein molecule, a smaller Stokes shift might be expected due to lower protection from solvent interactions. For instance, dendrimer-stabilized AuNCs of various sizes (but similar in size to AuNCs protected by proteins) are only weakly-protected metal clusters and show emission across the visible range with Stokes shifts <100 nm [102]. Considering the PL decay time, metallic clusters with fewer metal–ligand interactions (having a zero valence state) should exhibit a fast decay on the order of ps to ns due to the increased rate of excitation/relaxation electronic transitions [103]. If the MNC can be regarded as molecular in structure, having more interactions with the protein on average per metal atom (and likely in an oxidized valence state), or having inter-metal d^{10}–d^{10} interactions, the PL decay time may be two to three magnitudes longer than that of a metallic particle [104]. Taking into account these two photophysical properties, a significant difference in the structural environments of protein-MNCs and thus, molecular orbital levels, may cause the difference in PL decay time. For example, protein-MNCs formed from CuNCs (HSA, BSA, LYZ) [79,105,106], PtNCs (BSA, LYZ) [71,107] and AgNCs (BSA) [108] have Stokes shifts of <150 nm and average luminescence decay times of ~1 ns, whereas protein-MNCs formed from AuNCs (INS, Trf, BSA, LYZ) [109–111] have Stokes shifts >150 nm and average PL decay times of ~100–1000 ns.

The second interesting property of protein-MNCs is the possibility of selective and sensitive physicochemical interactions with analytes ranging from metal ions to enzymes (as will be discussed in detail in the following sections). These specific protein-MNC–analyte interactions have often been explored as potential platforms for sensing/diagnostic applications, which can achieve detection limits of nM or even pM [112]. The method of analyte detection is typically based on an increase or decrease in luminescence intensity, which can either occur due to protein-analyte or metal–analyte binding or recognition, and is sometimes reversible, rendering the protein-MNC sensor reusable [113]. The decrease in protein-AuNC luminescence when interacting with heavy metal ions such as Hg^{2+} has been attributed to closed-shell, metallophilic interactions (d^{10}–d^{10}). Through this interaction, Hg^{2+} ions interrupt charge carriers after photoexcitation of protein-AuNCs [114,115]. On the other hand, other heavy metals such as Pb^{2+} can cause aggregation of the protein-MNCs, as was shown for BSA-CuNCs [106]. In this case, a conformational change to the protein molecule around the MNC will also cause a change in the luminescence intensity [116,117]. For detection of molecular analytes, quenching of the luminescence can occur through oxidation of protein amino acid residues that bind to the MNC, for example, the oxidation of thiols in horseradish-AuNCs can be caused by hydrogen peroxide (H_2O_2) [118]. There is also the possibility of an etching process of the MNC itself, as shown by the interaction between BSA-AuNCs and cyanide ions [119]. For detection of biomolecules and larger molecules, strong binding affinities between certain metal ions and these biomolecules can be exploited to develop a sensing mechanism using protein-MNCs as the platform. This was demonstrated using EWP-AuNCs in which Cu^{2+} ions had been employed to quench the luminescence. In the presence of ATP, Cu^{2+} ions would dissociate from the protein-AuNC conjugates by an interaction with the ATP, thereby restoring the luminescence of the protein-AuNCs as an ATP biosensor [120].

Diagnostic applications in biomedicine

Chemical and biological sensing applications

The sensing of important chemical and biological analytes has great significance in biomedical, forensic and environmental sciences [121,122]. The design of highly sensitive, cost-effective, biocompatible sensors requires advanced technology which involves fundamental knowledge of chemistry, biology and material science [123,124]. In general, the functional operation of sensors requires two stages: (i) a recognition element to provide selective/specific binding to the target species; (ii) a

Uncorrected Proof

Please cite this article in press as: I. Zare et al., Materials Today, (2020), https://doi.org/10.1016/j.mattod.2020.10.027

transducer component to provide a measurable signal of the binding event. The efficiency of these two stages governs the overall efficiency of the sensor in terms of response time, selectivity, and limit of detection (LOD) [125]. The ideal sensor should be facile to produce, robust, yet delicate enough for optimum performance. The detection of toxic chemicals containing Hg, lead (Pb), Cd, chromium (Cr) and arsenic (As) ions is of utmost importance due to their long-term bioaccumulation in vital organs and tissues, resulting in alteration of physiological functions causing serious health hazards [126,127]. Recently, protein-protected MNCs have shown great potential as chemical sensors and biosensors with very low LODs [128]. Besides being non-toxic as compared to many organic molecules/dyes and QDs, these MNCs are intrinsically luminescent which makes their detection process label free and highly sensitive [129].

Cancer biomarker detection

Cancer continues to be a major cause of death across the world as evident from the latest GLOBCAN 2018 report, which estimates 18.1 million new cases of cancer and 9.6 million deaths due to 36 different types of cancer [130] This number seems to escalate every year, and hence detection at early stages and precise diagnosis of cancer is highly desirable for the successful treatment of the disease. In this context, a cancer biomarker is a molecular indicator of the presence of cancer in the body or changes in cancerous cells in response to different kinds of therapy [131] Cancer biomarkers are typically concerned with DNA, RNA, cell metabolites, or membrane receptors specific to tumor cells, and these play a crucial role in cancer diagnosis and treatment [132]. The use of protein-MNCs simplifies the post modification process with various available functional groups, allowing specific identification, interaction, differentiation and imaging of tumor-specific moieties. Out of all the reporter methods employed for cancer detection by MNCs, electrochemistry, colorimetry, and fluorimetry techniques have been mostly used.

Zhou et al. designed a ternary nanostructure based on an electrochemiluminescence (ECL) technique comprising BSA-AuNCs as the luminophore, tris(3-aminoethyl)amine as a co-reactant, and Pd–CuO as an accelerator [133]. This ECL assay could efficiently measure carcinoembryonic antigen (a protein derived from colon cancer and embryonic tissue). The ECL signal of the luminophore (which was normally weak) was greatly amplified due to the combination of the luminophore, co-reactant, and the accelerator resulting in ultrasensitive detection [133]. In another study, BSA-AuNCs were incorporated inside porous $CaCO_3$ nanospheres, and subsequently, these hybrids were further surface decorated with an antibody (Ab) against neuron-specific enolase (NSE), conjugated to horseradish peroxidase (HRP) to form the sensor ($CaCO_3$-BSA-AuNCs-HRP-Ab_2) [134]. This hybrid biosensor served as a versatile fluorescence as well as electrochemical probe for the detection of the NSE cancer biomarker. The sensor specifically bound to NSE attached to modified carbon nanotubes. After that, NSE was detected by fluorescence upon the release of AuNCs from the substrate in the presence of ethylenediaminetetraacetic acid (EDTA), whereas, for electrochemical detection a H_2O_2-mediated HRP catalyzed reaction was employed [134].

AuNCs have been reported to display intrinsic peroxidase-like activity which could be useful for designing bioassays [135,136]. Using this strategy, Tao et al. synthesized LYZ-AuNCs and attached them to GO via electrostatic interactions. The peroxidase activity of the GO-LYZ-AuNCs was tested in the presence of 3,3′,5,5′-tetramethylbenzidine (TMB) and H_2O_2, whereby a strong blue color could be detected by the naked eye. GO-LYZ-AuNCs were then covalently modified with folic acid (FA) to form an ultrasensitive colorimetric cancer detection assay by selectively binding to the folate receptors (FRs) expressed on cancer cells [137]. In another continuation of this work, Tao et al. exploited the same peroxidase activity of AuNCs (stabilized with BSA instead of LYZ) to develop a robust assay for colorimetric sensing of human epidermal growth factor receptor 2 (HER2)-positive breast cancer cells. Based on the change in the absorbance produced by the catalytic reaction in the presence of TMB and H_2O_2, the HER2 Abs (Ab-HER2) anchored to the surface of AuNCs-loaded liposomes (AuNCs-LPs) (BSA-AuNCs-LPs-Ab-HER2) that were adsorbed to SKBR3 (HER2 high) and Michigan Cancer Foundation-7 (MCF-7) (HER2 low) breast cancer cells could be detected by UV–Vis spectrometry [138].

Liu et al. took advantage of NIR fluorescence of TRY-AuNCs to target HeLa cells. TRY-AuNCs were surface-modified with FA, which enabled them to selectively detect FR positive HeLa tumor cells with high affinity [31]. Pradeep and co-workers prepared BSA-AuNCs with a similar FA surface conjugation. This fluorescent probe specifically detected FR positive oral cancer KB and breast cancer MCF-7 cells, whereas FR negative lung cancer A549 cells remained unstained by the probe [139]. Some enzymes like telomerase can act as a useful cancer biomarker because telomerase is activated in almost 85% of cancer cell types. When telomerase is activated and the telomeres become elongated in the cancer cells, the deoxy-ribonucleoside triphosphates are converted into nucleic acids along with the formation of pyrophosphate ions (PPi) molecules as byproducts [140]. Addition of telomerase to the medium containing BSA-AuNCs-Cu^{2+} provided a simple and sensitive real time analysis of telomerase activity as a cancer biomarker by measuring changes in the fluorescence intensity of the probe [140]. Thus, protein-MNCs, because of their emissive properties, could provide sensitive detection of extracellular cancer biomarkers based on changes in fluorescence intensity [141] (Fig. 4). Besides the fluorescence properties of protein-MNCs, their electrochemical effect could also be utilized for biomarker assays. Mousavi and coworkers described BSA-protected PbNCs for an electrochemical immunoassay for epidermal growth factor receptor (EGFR) detection. The signal of the immunosensor was dual-amplified by the electrochemical stripping current of Pb and PbNCs, which enabled detection of very low quantities of EGFR [142].

Biomolecules and pharmaceutical compounds

By exploiting their stable fluorescence properties and biocompatibility, protein-protected MNCs have played a major role in the sensing of biological molecules for more than a decade [128]. Small molecules such as GSH have important biological significance. The detection and quantification of GSH as the most abundant thiol in cells is important because it takes part in several biological reactions such as neutralizing free radicals and per-

Uncorrected Proof

Please cite this article in press as: I. Zare et al., Materials Today, (2020), https://doi.org/10.1016/j.mattod.2020.10.027

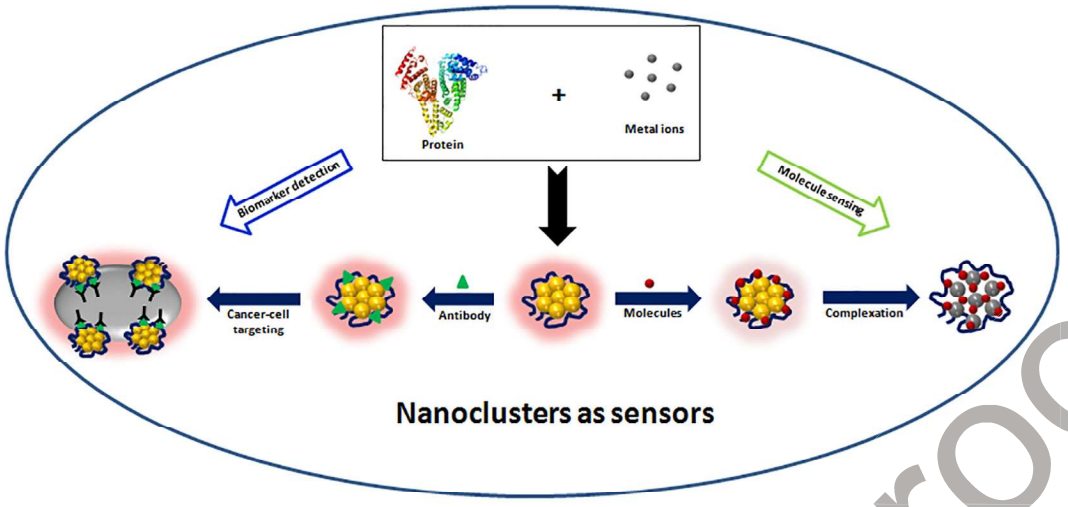

FIGURE 4

Schematic showing the mechanism of cancer biomarker detection and molecular sensing by protein-protected MNCs.

oxides, and is associated with HIV expression and cancer therapy [143]. Kailasa and co-workers synthesized amylase-protected AuNCs as a GSH biosensing assay. The gradual addition of GSH to these AuNCs resulted in quenching of the NCs fluorescence due to the formation of a non-fluorescent complex [144]. Similarly, LYZ type-VI stabilized blue-emitting AuNCs were synthesized for highly sensitive detection of GSH with a LOD as low as 20 nM [145]. Lin et al. synthesized BSA-AuNCs for sub-nanomolar detection of cystatin C, a cysteine protease inhibitor. Their procedure involved quenching of the fluorescence intensity of the AuNCs in the presence of papain (a cysteine protease that destroyed the BSA coating), whereas the absence of papain resulted in the retention of fluorescence [146]. A similar fluorescence recovery procedure was also demonstrated using gluten-protected AuNCs for "turn-on" sensing of creatinine in human blood. The fluorescence of the AuNCs was initially "turned-off" by addition of picric acid (PA), however, on subsequent addition of creatinine to these quenched AuNCs, the fluorescence was recovered due to the formation of a creatinine–PA complex, which had stronger binding affinity than the initial gluten–PA complex [147].

Glucose is the major source of energy in living cells, however, its over-abundance may cause diseases such as diabetes, and hence its quantitative detection is essential [148,149]. The sensing of glucose can be monitored by the formation of H_2O_2 as a reaction by-product during the enzymatic oxidation of glucose [129,150]. The generated H_2O_2 may induce degradation of the MNC core resulting in the quenching of fluorescence, and therefore, the levels of glucose can be determined. This technique was demonstrated by Jin et al., where they synthesized BSA-AuNCs that exhibit emission in the NIR region. These fluorescent BSA-AuNCs showed good performance for the detection of H_2O_2, which significantly quenched the fluorescence intensity of the MNCs. Glucose detection by BSA-AuNCs was enabled by the catalytic oxidation of glucose in the presence of GOD with the generation of H_2O_2 as a by-product. From quenching results, the LOD for glucose was estimated to be 5 μM [151]. Apart from BSA, LYZ-CuNCs have also been used to detect glucose based on fluorescence quenching, however in this work, glucose was simply added to the NCs sample without applying any catalytic procedure [152]. It is worth noting that glycoprotein-functionalized AuNCs could be attractive tools for the analysis and understanding of carbohydrate–protein interactions as recently demonstrated by Reichardt [153]. The biological molecule bilirubin is an important product of the biological breakdown of heme. An excess of bilirubin in the blood (greater than 50 μM) is found in a serious disease called jaundice, which necessitates its detection efficiency [154]. In two different studies, BSA-CuNCs [155] and HSA-AuNCs [156] were successfully employed for highly sensitive detection of bilirubin in blood and serum samples. The mechanism of bilirubin sensing by BSA-CuNCs involved fluorescence recovery of the MNCs, which was initially "turned-off" in the presence of Fe^{3+} but subsequently "turned-on" due to an interaction between Fe^{3+} and bilirubin that removed Fe^{3+} ions from the system. On the other hand, quenching of fluorescence was observed when bilirubin was added to HSA-AuNCs [156].

Other biomolecules like mangiferin have also been detected by BSA-CuNCs with a low LOD value [157]. In addition to serum proteins, the chicken egg protein, OVA, has also been used to synthesize MNCs with good biocompatibility and optical properties, which enabled them to act as efficient sensors for different biomolecules. OVA-CuNCs successfully detected another essential biomolecule, FA (LOD ~ 0.18 μM) [158], and also the toxic compound ricin (LOD ~ 4.6 μM) [159]. Shamsipour and co-workers developed Hb-protected AuNCs for the analysis of cytochrome c (Cyt c), a biomarker for the apoptotic process in cells. The fluorescence of AuNCs had decreased due to the fluorescence resonance energy transfer (FRET) from Hb-AuNCs, as a donor, to the heme group in Cyt c as an acceptor. The decrease in fluorescence intensity of AuNCs enabled this "turn-off" assay to measure Cyt c at nanomolar level [160]. Ghosh et al. used HSA as a template to synthesize blue-emitting HSA-AgNCs. When AgNCs were treated with the serine protease, TRY, the fluorescence was significantly quenched due to the proteolysis of HSA into smaller peptide fragments. The quenching was accompanied by the gen-

Uncorrected Proof

Please cite this article in press as: I. Zare et al., Materials Today, (2020), https://doi.org/10.1016/j.mattod.2020.10.027

eration of an unusual red emission band with an enhanced QY. These AgNCs provided a new approach to sense TRY as well as to study protein metabolism involved in the proteolytic process [161]. In another recent study, a hybrid platform comprising of reduced GO and BSA was created for *in situ* synthesis of AuNCs that could detect TRY with a sensitivity of 100 ng/ml [162].

Protein-protected MNCs have also shown the ability to sense pharmaceutical molecules and drugs. BSA-AuNCs detected the antibacterial drug ciprofloaxin [163], and the neurotransmitter dopamine [164]; whereas papain-AuNCs were able to sense D-penicillamine [165]. The mechanism of drug sensing for both these AuNCs involved Cu^{2+}-mediated fluorescence quenching of the MNCs. With the gradual addition of the drug, a complex was formed between the protein template and the drug dissociating the Cu^{2+} and restoring the fluorescence of AuNCs. BSA-protected MNCs were able to sense rutin [166], clenbuterol [167], metronidazole [168] and nitroimidazole [168]. The sensing mechanism for all of these drugs involved direct quenching of MNC fluorescence, which was either ascribed to electron transfer from the MNC to the drug molecule or to chemical reaction [166–168]. The detection of cysteamine (CSH), involved chemical etching of the MNC core by CSH causing a loss of fluorescence [168]. MNCs have also shown the ability to selectively detect *Escherichia coli* bacteria involving a fluorescence recovery mechanism. The fluorescence of the Cu^{2+}-BSA-AuNC complex was recovered by copper binding involving the redox pathways of *E. coli*. The other three types of bacteria that were used as controls were not able to "turn-on" the fluorescence of the NCs in the same way [169].

Metal ions and small molecules

The unique fluorescence characteristics of protein-protected MNCs have been applied for metal ion sensing and quantification. Some of these metal ions are essential biological components, while others are environmentally toxic causing health hazards; either way, it is important to detect these metallic elements with high precision and sensitivity. Heavy metal ions such as Hg^{2+} and $Pb^{2+}$are highly toxic to human health and the environment [170]. During the past decade, there have been numerous reports describing heavy metal detection exploiting the change in the fluorescence of photostable protein-protected MNCs (Fig. 4) [171,172]. The complex formation between Hg^{2+} and the cysteine residues in BSA through Hg-S bond formation was primarily responsible for the fluorescence quenching of BSA-AuNCs which enabled sensitive and selective detection of Hg^{2+} in different samples [173]. Another plausible mechanism for the fluorescence "turn-off" behavior of MNCs may be the presence of a large number of non-reduced M^+ ions on the surface of the protein-MNCs which direct the high-affinity d^{10} (Hg^{2+})–d^{10} (M^+) metallophilic interaction. This Hg^{2+}–M^+ bond attenuates the fluorescence of MNCs, allowing the detection and quantification of Hg^{2+} ions [115]. Recently a variety of protein-templated MNCs, such as GOD-templated AuNCs [33], TRY-AuNCs [174], β–lactoglobulin-AuNCs [175], casein-AuNCs [176], bimetallic Au-AgNCs protected by keratin [177], bimetallic Pt-AuNCs protected by BSA [178] and mixed proteins (BSA/LYZ) stabilized Au/AgNCs [94] have all been shown to function as efficient Hg^{2+} sensing assays, mostly via "turn-off" fluorescence, with very low LODs and practical applicability in actual sample analysis. Lin et al. reported LYZ type-VI protected AuNCs that could selectively detect Hg^{2+} as well as CH_3Hg^+ ions with LODs of 0.003 nM and 4 nM, respectively [112]. The LODs met the limits set for permitted Hg levels in drinking water by the U.S. Environmental Protection Agency (EPA). In addition, bimetallic Pt-AuNCs protected by BSA showed ratiometric sensing for cysteine in the presence of Hg^{2+} ions involving strong interaction between the thiol group of cysteine and Hg^{2+} ions [178].

The detection of another heavy metal Pb is also important due to its toxic effects on the human nervous system [125,179]. Pal and co-workers developed BSA-protected luminescent CuNCs which acted as highly sensitive and selective "turn-off" fluorescence sensors for Pb^{2+} ions [106]. On the other hand, Kawasaki et al. synthesized PEP-stabilized AuNCs with a dual metal sensing ability, where in the presence of Hg^{2+} ions fluorescence quenching occurred, and with the addition of Pb^{2+} ions enhanced the fluorescence of the MNCs by almost 8-fold [72]. Although the mechanism responsible for this dual sensing was not discussed in detail, a possible explanation may be due to metallophilic interactions as described above.

The detection of other metal ions, namely Cu, Zn and Co is also important because excessive amounts in the human body might have adverse effects such as cellular damage, causing heart, lung, liver, kidney and brain disorders [180–182]. In an interesting work, Yang et al. synthesized lysine-AuNCs, which cooperatively interacted with BSA-AuNCs to show enhanced fluorescence. The nanoconjugate selectively detected Cu^{2+} ions by interactions with surface ligands such as COOH and NH_2 groups of BSA and lysine resulting in fluorescence quenching of AuNCs [183]. Similarly, Hb-AuNCs have been found to be a selective and sensitive fluorescence "turn-off" probe for the quantification of low concentrations of Cu^{2+}. The interaction between the Hb protecting shell and the Cu^{2+} ions induced the aggregation, which led to fluorescence quenching of Hb-AuNCs [28]. Fan et al. showed that BSA-AgNCs combined with a zeolite imidazole framework (ZIF) was capable of ultrasensitive detection of Cu^{2+} in blood [95]. Ghosh and co-workers synthesized two different types of AgNCs utilizing HSA as template with interconvertible fluorescence characteristics. The blue-emitting AgNCs independently detected Co^{2+} (via fluorescence quenching) and Zn^{2+} ions (via fluorescence enhancement). The successive addition of Co^{2+} followed by Zn^{2+} ions to the same sample restored the fluorescence of the AgNCs to its original value. Interestingly, by changing the emission from blue to red, these AgNCs were able to sense Hg^{2+} at the LOD of environmental standards. The sensing mechanism for all three ions (Co^{2+}, Zn^{2+}, Hg^{2+}) was ascribed to an electronic phenomenon involving excited states of MNCs [184]. In another study, BSA-AuNCs has been shown to detect heavy metals Co and Cd via differential interaction which resulted in "turn-off" and "turn-on" luminescent properties, respectively [185].

In addition, several other protein-MNC-based assays have been developed for selective and specific metal ion detection, which include papain-AuNCs for Cu^{2+} detection [73], BSA-AuNCs for Zn^{2+} detection [186] and protamine-AuNCs for Pb^{2+} detection [187]. In addition to metal cations, the detection of anions is equally important. Inorganic ions like CN^-, S^{2-} and

Uncorrected Proof

Please cite this article in press as: I. Zare et al., Materials Today, (2020), https://doi.org/10.1016/j.mattod.2020.10.027

NO_2^- are known to have an adverse impact on cellular respiration, or can act as potential carcinogens [128]. Recently, fluorescent BSA-AuNCs were applied as a chemosensor for CN^- ions. The mode of action of the sensor involved the formation of a very stable $Au(CN)_2^{2-}$ complex accompanied by fluorescence attenuation of the AuNCs. The CN^- mediated etching reaction of the BSA-AuNCs could be detected visually by a color change from deep brown to colorless, thus facilitating highly specific sensing in the simultaneous presence of interfering species [119]. A similar CN^- ion detection method was also demonstrated for LYZ-AuNCs [188]. Zhang et al. showed that addition of S^{2-} ions to silk fibroin (SF)-CuNCs resulted in AIE with an almost 3-fold increase in fluorescence, thus providing a platform for "turn-on" detection of S^{2-} ions [189]. On the other hand, BSA-AuNCs showed fluorescence quenching behavior in the presence of S^{2-} ions due to the formation of insoluble Au_2S precipitates [190]. Yang and coworkers utilized BSA-AuNCs for the fabrication of a Boolean "NAND" logic gate for the detection of NO_2^- ions [191]. It was observed that under strongly acidic conditions that NO_2^- in the presence of H_2O_2 quenched the fluorescence of BSA-AuNCs via oxidation of the BSA scaffold. This finding was used to design a Boolean NAND logic gate using NO_2^- and H_2O_2 as inputs and the fluorescence intensity ratio (F/F_0; where F and F_0 correspond to the fluorescence in the presence and absence of the inputs) as the output [191]. For ion sensors, the most crucial parameter is to evaluate the sensitivity and specificity of the probe. The conventional way to determine the sensing efficiency is by constructing Stern-Volmer intensity plots. In addition, the specificity of a sensing probe can be tested with the addition of similar but different ions, or when other interfering species are added to the analyte in the medium.

Protein-MNCs have also been used for the sensing of small molecules. AgNCs stabilized by denatured LYZ (dLYZ-AgNCs) exhibited a ratiometric fluorescent sensing ability for H_2O_2 and hydroxyl radicals (.OH) by displaying a dual emission. In the presence of Fenton reagent, dLYZ-AgNCs behaved as a "turn-off" fluorescence sensor for H_2O_2 monitored at 640 nm due to .OH-induced quenching. In contrast, it behaved as a "turn-on" fluorescence sensor when monitored at 450 nm due to .OH-induced oxidation of the tyrosine residues in LYZ. The ratio of fluorescence changes of the two emission peaks (F_{450}/F_{640}) was used to quantify H_2O_2 with adequate LOD. As shown by confocal imaging, dLYZ-AgNCs possessed sensitivity towards the fluctuation of .OH levels in living cells, hence it could be used as a promising tracker for ROS-induced oxidative damage to proteins [192]. In another study, polymeric microcapsules were fabricated co-encapsulating BSA-AuNCs and FluoSpheres (FSs). From the dual emission peak of the microcapsule, it was observed that the fluorescence peak due to BSA-AuNCs (red emission) was highly sensitive to the H_2O_2 concentration, showing quenching behavior, whereas, the FSs were found to be insensitive to H_2O_2 and the fluorescence peak (green emission) remained unchanged. Based on this finding, a novel ratiometric fluorescence sensor was designed for ultrasensitive detection of H_2O_2. When internalized within macrophage cells, the microcapsules could detect intracellular H_2O_2 fluctuations occurring in response to external chemical stimuli [193]. HRP-AuNCs were employed for quantitative detection of H_2O_2 by exploiting the catalytic activity of HRP towards H_2O_2. The oxygen radicals that were generated from the reaction between H_2O_2 and HRP oxidized Au-S bonds leading to the formation of S-S bonds and aggregation of AuNCs accompanied by fluorescence quenching [118]. HRP-AuNCs were also used in a microfluidic droplet configuration for the detection of 200–400 attomoles of H_2O_2. With this microfluidic technique, which contained an ultrasmall volume (4.2 nL) of a microdroplet of HRP-AuNCs, H_2O_2 secreted from a single cell, which was introduced in the setup, was sufficient to induce pronounced fluorescence quenching of HRP-AuNCs. The study also provided a method to distinguish between cancerous and normal cells since the former has a higher H_2O_2 content leading to greater quenching of HRP-AuNC fluorescence when compared to the signal observed in the presence of normal cells [194]. Apart from H_2O_2, TRY-AgNCs were used for the sensing of NADH and ethanol via an enzyme-catalyzed reaction [195]. BSA-AuNCs were employed for ratiometric detection of malachite green (MG) involving a FRET mechanism. When MG was added gradually to BSA-AuNCs, a significant energy transfer took place from the donor (AuNCs) to the acceptor MG, resulting in fluorescence quenching of AuNCs. Since FRET is primarily a dynamic quenching process, fluorescence lifetime measurements confirmed its validity [196]. BSA-AuNCs were also used as sensors for melamine [197] and salicylaldehyde [186].

Temperature and pH sensing

The effect of temperature is another parameter of interest to monitor in many biological processes since the activity of enzymes and other cellular processes is temperature-dependent. A small change in temperature can lead to major alterations in biological reactions [198–200]. Temperature sensors like thermocouples are not realistic for *in vivo* temperature sensing since their mode of action is in 'contact' with the target location [199,200]. In this context, protein-protected MNCs have shown great potential as *in vivo* thermometers. By exploiting their stable fluorescence properties, water solubility and biocompatibility, the MNCs can operate as 'non-contact' probes for temperature sensing at sub-micron scales [199]. Ghosh et al. synthesized HSA-protected blue-emitting CuNCs which could act as reversible temperature sensor. When the HSA-CuNCs were heated and subsequently cooled within the temperature range of 20–55 °C, a fluorescence "turn-off" with a ~25% drop in fluorescence intensity was observed during heating, which was restored to ~100% during a subsequent cooling process. The sensing procedure was highly versatile as was evident from hysteresis results, which showed almost the same fluorescence properties after 5 cycles of temperature variation. The temperature sensing ability of these photo-stable HSA-CuNCs was further demonstrated via reversible FRET experiments using an external organic dye [105]. In another study, Baker and co-workers synthesized BSA-AuNCs with similar reversible sensing characteristics. The red emission of the AuNCs dropped ~40% upon increasing the temperature from 10 to 45 °C. However, when cooling back to 10 °C, the emission was restored, but with a slightly higher value than the initial fluorescence intensity due to hysteresis. After several synthetic modifications, they were finally successful in demonstrating that these BSA-AuNCs could function as efficient

Uncorrected Proof

Please cite this article in press as: I. Zare et al., Materials Today, (2020), https://doi.org/10.1016/j.mattod.2020.10.027

"nano"thermometers [201]. Gelatin-stabilized AgNCs [202] and EWP-AuAgNCs [203] were also demonstrated to act as reversible temperature sensors in the temperature range 10–60 °C. The mechanism for this reversible temperature sensing was ascribed to the thermal unfolding of the protein scaffolds during the heating process, while subsequent cooling caused refolding. This phenomenon directly affected the optical properties of the MNCs, where the loss/gain in fluorescence was proportional to the rate of non-radiative decay pathway, depending on the protein structure. Importantly, in all of the above studies, the upper temperature limit was set ≤65 °C because refolding of the protein conformation becomes impossible at higher temperature [105,201–203].

Regulation of the intracellular pH also plays an important role in many cellular functions like ion transport, signaling, and membrane dynamics [204]. The physiological pH varies within the range of 7.0–7.4 due to the balance of dissolved ions. In this context, protein-templated MNCs also exhibit pH-dependent optical properties, which have been exploited by several research groups to develop versatile and reversible pH sensors for biological applications. TRY-CuNCs were synthesized and tested for pH sensing over a wide pH range from 2 to 12 using a series of buffer solutions. The fluorescence intensity of the CuNCs exhibited a linear decrease with increasing pH, with the highest emission at acidic pH, but negligible emission under alkaline conditions due to the formation of precipitates at high pH. It was also shown that the changes in fluorescence were reversible because they remained the same after varying the pH over 7 cycles [205]. SF-protected CuNCs were also found to be highly efficient and reversible pH sensors. However, in contrast to TRY-MNCs, the fluorescence intensity of SF-CuNCs exhibited an increased emission with increasing pH which was attributed to the deprotonation of the amide and carboxyl groups in SF at alkaline pH [206]. Similarly, CuNCs stabilized by EWP [207] and BSA [208] also displayed pH sensing properties. The fluorescence response of the CuNCs stabilized by these two proteins showed similar pH dependence to those found with SF. Interestingly, BSA and EWP possess isoelectric points (pI) at acidic pH (~4.5), whereas the pI of TRY is at alkaline pH (~10). When the pH ≈ pI, proteins tend to precipitate out of solution and the MNCs lose their fluorescence. Hence the plot of fluorescence response against pH showed an opposite trend when the CuNCs were stabilized by BSA/EWP in contrast to TRY. Wang et al. synthesized BSA-AuNCs which functioned as an "ON/OFF" pH switch based on the fluorescence signal. The fluorescence of the sensor was highly sensitive to pH value; at pH > 5 fluorescence was "turned-on" and at pH < 5 it was "turned-off". In addition, these BSA-AuNCs could be immobilized on a highly stable and porous agarose hydrogel to construct a pH indicator that allowed visual detection [209]. Aly and co-workers reported that BSA-templated AuNCs could be applied as intracellular pH sensors. BSA-AuNCs were labeled with a pH indicator bromothymol blue (BTB) to modulate the pH sensitivity of the fluorescent MNCs. The emission of the native BSA-AuNCs was found to be pH independent within the range 2–11. On the other hand, BTB-labelled BSA-AuNCs were shown to detect post-mortem changes in blood pH that occur after the death of the red blood cells (RBCs). Hence this nanosensor could be used as a potential forensic tool for estimating the time passed since death [210]. In another study, a dual temperature/pH-responsive fluorescent probe was constructed based on the integration of a pH-sensitive organic dye, fluorescein-5-isothiocyanate (FITC) and BSA-AuNCs. The fluorescence of this hybrid compound was sensitive to both temperature and pH changes. The resultant FITC-labelled BSA-AuNCs were applied as an "AND" logic gate with temperature and pH as inputs and the ratiometric fluorescence signal of FITC-labelled BSA-AuNCs as the output. The fluorescence signal ratio of FITC to BSA-AuNCs was used for intracellular temperature and pH monitoring in HeLa cells [211]. Wei et al. synthesized BSA-protected AuNCs that showed enhancement in QY by varying the pH of the reaction medium and also the temperature. The synergistic effect of these two parameters resulted in core–shell MNCs comprising of Au(0)–Au(I) aurophilic interactions which stabilizes the excited state of the NCs and increases its luminescence [212].

Detection of neurotransmitters

Neurotransmitters are chemicals that function as messengers of neural activity and can be classified into several groups such as biogenic amines, amino acids, peptides, and gaseous neurotransmitters. Common neurotransmitters include dopamine, acetylcholine, epinephrine, 5-hydroxytryptamine (5-HT; serotonin), histidine and hydrogen sulphide (H_2S), which have all been detected by using the protein-MNCs [213–218].

Dopamine is an important neurotransmitter released by neurons that plays a significant role in the central nervous, renal, hormonal, and cardiovascular systems. It is also an important biomarker for diseases such as schizophrenia and Parkinson's. Conventional methods for dopamine detection generally rely on electrochemistry, but this can be interfered with by other reducing agents. The fluorescence properties and the charge transfer property of MNCs offer an excellent platform for developing dopamine sensors.

By using fluorescent TRY-AuNCs as the probe, a "turn-off" sensing platform has been developed for dopamine detection with high sensitivity [219]. The TRY-AuNCs present strong red fluorescence at 665 nm upon excitation at 520 nm. Dopamine can greatly quench the red fluorescence of TRY-AuNCs with good selectivity and sensitivity, showing a detection limit of 0.14 nM. This facile "turn-off" method has been successfully used to detect dopamine in pharmaceutical samples, showing good precision and accuracy. Fluorescent AuNCs can be also used to detect dopamine in cerebrospinal fluid based on an electron transfer mechanism [213]. Dopamine was oxidized to dopamine o-quinone that acted as the electron acceptor while the AuNCs acted as the electron donor, leading to fluorescence quenching depending on the concentration of dopamine. This approach enabled the detection of dopamine spiked into cerebrospinal fluid with a linear range from 0 to 10 nM and a LOD of 0.83 nM.

Apart from their fluorescent properties, MNCs also have catalytic activities that mimic those of natural enzymes. Hb-stabilized AuNCs, for example, were reported to exert a peroxidase-mimicking activity that can catalyze a chemiluminescence reaction between luminol and $NaIO_4$, while dopamine can inhibit this catalytic reaction [220]. Dopamine is a reducing

Uncorrected Proof

Please cite this article in press as: I. Zare et al., Materials Today, (2020), https://doi.org/10.1016/j.mattod.2020.10.027

agent and can act as a scavenging agent of the ROS generated in the chemiluminescence reaction, leading to a decrease in the chemiluminescence signal. With this method, dopamine concentrations ranging between 0.3 and 9.0 nM can be detected with a LOD of 0.1 nM. Besides AuNCs, CuNCs can be also used to develop fluorescent sensors for dopamine detection [221]. BSA-protected CuNCs emit a blue fluorescence and dopamine can interact with BSA-CuNCs that leads to a fluorescence quenching. Another interesting feature of BSA-CuNCs is that they possess an intrinsic peroxidase-like activity that can be employed for colorimetric detection of dopamine. A LOD 0.1637 pM was achieved, and BSA-CuNCs have been successfully applied for dopamine detection in serum samples with recoveries in the range 90–98.33%.

Acetylcholinesterase (AChE) is an enzyme that can catalyze the breakdown of acetylcholine, an important neurotransmitter that functions in both the central and peripheral nervous systems. By using bimetallic BSA-AuAgNCs [222], researchers have developed a simple, cost effective and ultrasensitive method for detecting AChE (Fig. 5a). The assay is based on the "ON/OFF" sensing strategy. Cu^{2+} can quench the fluorescence of bimetallic AuAgNCs. In presence of AChE, it can catalyze the enzymatic reaction to generate thiocholine that can switch on the fluorescence of BSA-AuAgNCs. This method can be used to sensitively detect AChE as well as its inhibitors such as ethyl parathion. Apart from dopamine and AChE, many other biomolecules are associated with neurodegenerative disorders such as epinephrine and 5-HT [223]. For instance, an elevated epinephrine concentration in human body fluids such as blood and urine is highly associated with Parkinson's and Alzheimer's diseases. High QY (12%) BSA-AuNCs were prepared through a reflux hydrothermal method, showing an average diameter of 3.3 ± 1.82 nm [214]. Epinephrine can significantly enhance the fluorescence intensity of BSA-AuNCs that may relate to the electron transfer during the polymerization of epinephrine (Fig. 5b). The fluorescence enhancement is concentration-dependent that can be used to detect epinephrine, and a LOD of 0.91 nM was achieved in samples from Alzheimer's patients. Acting as a monoamine neurotransmitter, 5-HT is widely distributed in the central nervous system and contributes to the feelings of happiness. Highly sensitive and rapid detection of 5-HT is of great importance to help understand its biological function in neurological diseases. Trf-AuNCs have been prepared to detect 5-HT based on a "turn-on" strategy of the fluorescence (Fig. 5c) [216]. The presence of 5-HT can trigger the aggregation of Trf-AuNCs because of the specific interaction between 5-HT and the sialic acid residues of Trf. The aggregation-enhanced emission feature of Trf-AuNCs resulted in a significant enhancement in the fluorescence intensity, thus a "turn-on" fluorescent assay can be developed with high selectivity and sensitivity. The linear detection range for 5-HT detection is 0.2–50 μM ($R^2 = 0.994$), and this approach has a detection limit of 0.049 μM (S/N = 3). 5-HT detection has been challenged in serum samples with recoveries of 96.20–108.6%, suggesting the effectiveness of this "turn-on" biosensor.

Detection of pathogenic microorganisms

Microorganisms can be harmful to human health and cause severe diseases, such as bacterial infections. AuNCs have been used to detect *Staphylococcal* enterotoxins B (SEB) that can cause food contamination and lead to serious diseases (Fig. 6a) [224]. Eggshell membrane (ESM)-templated AuNCs showed intense fluorescence but weak enzymatic activity. In contrast, GSH templating

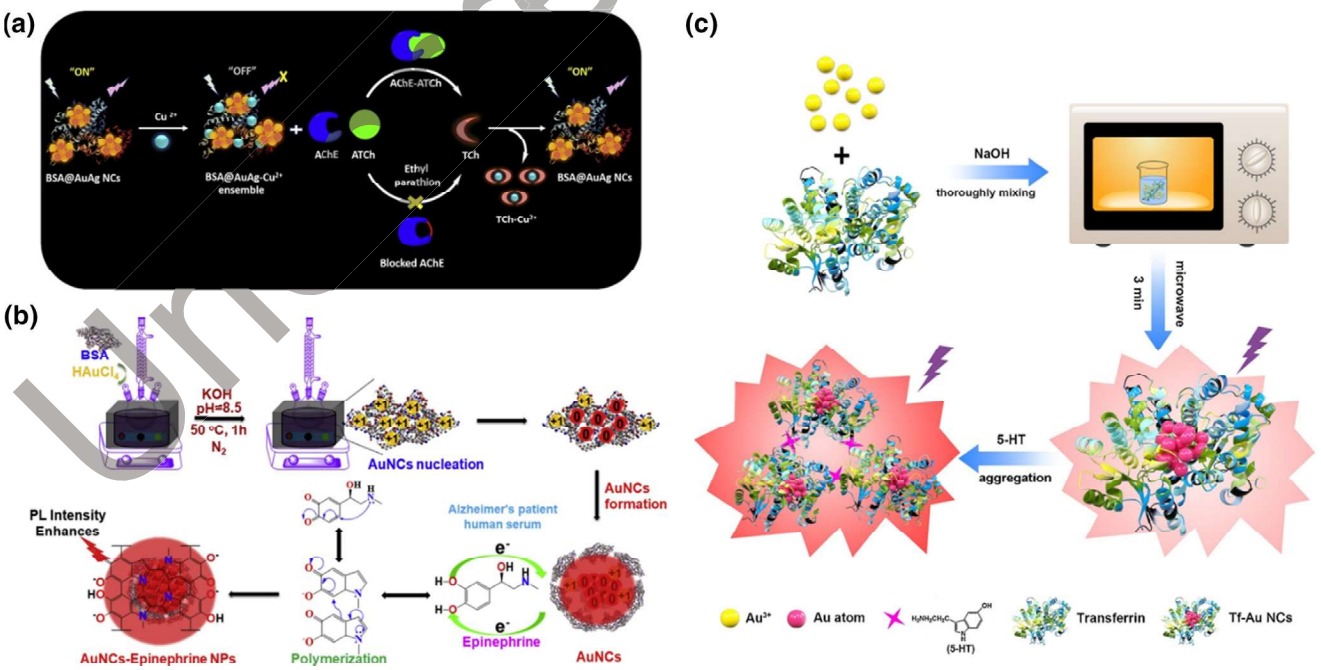

FIGURE 5

Functionalized MNCs for detection of neurotransmitters. (a) BSA-AuAgNCs for AChE detection [222]. Reproduced with permission from Ref. [222]. Copyright 2020 Elsevier. (b) BSA-AuNCs for epinephrine detection [214]. Reproduced with permission from Ref. [214]. Copyright 2019 Elsevier. (c) Trf-AuNCs for 5-HT detection [216]. Reproduced with permission from Ref. [216]. Copyright 2019 Elsevier.

Please cite this article in press as: I. Zare et al., Materials Today, (2020), https://doi.org/10.1016/j.mattod.2020.10.027

Uncorrected Proof

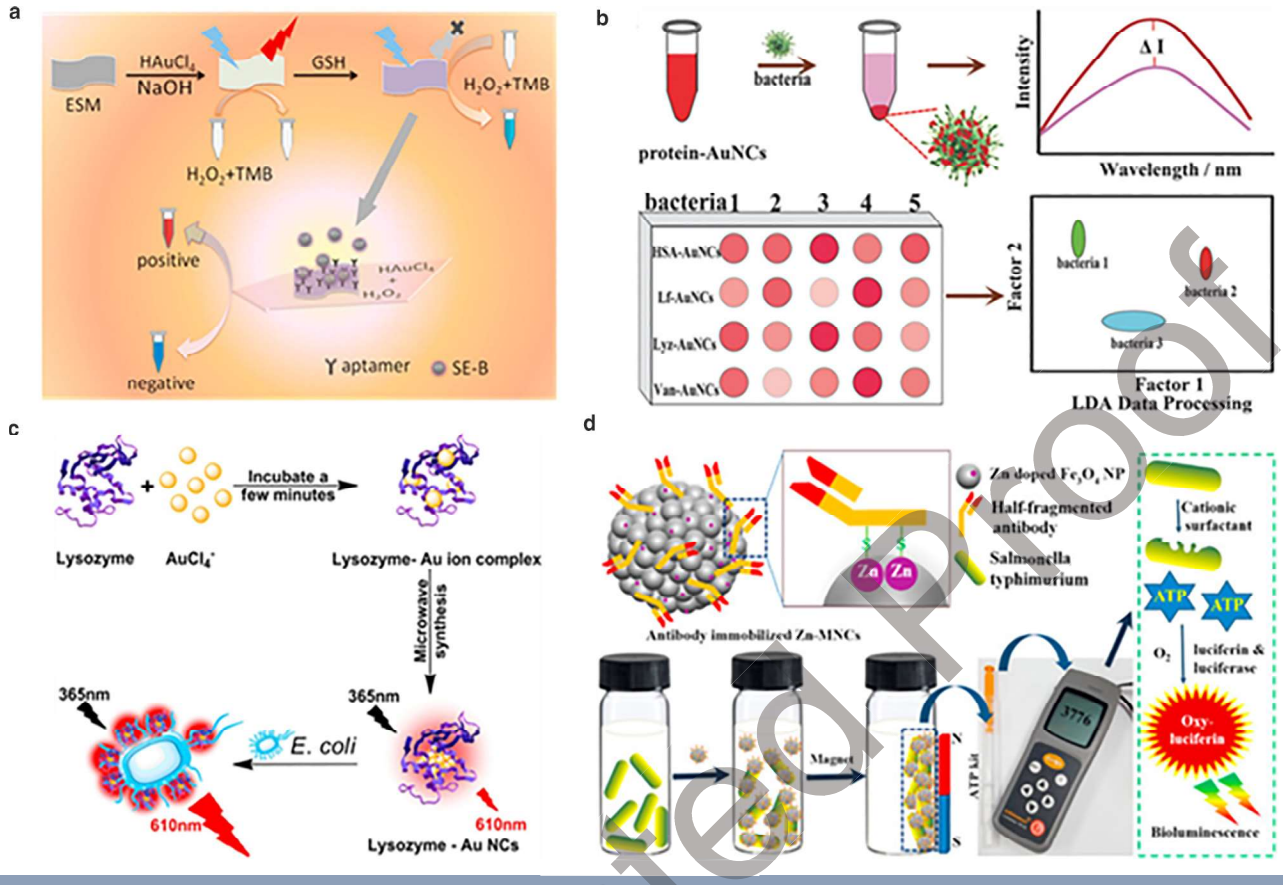

FIGURE 6

MNCs for detection of pathogenic microorganisms. (a) Peroxidase-mimicking AuNCs for detection of SEB [224]. Reproduced with permission from Ref. [224]. Copyright 2019 Elsevier. (b) Functionalized AuNCs used in fluorescent sensor arrays as "chemical tongue" for bacteria identification [227]. Reproduced with permission from Ref. [227]. Copyright 2018 Wiley. (c) LYZ-AuNCs for *E. coli* detection [229]. Reproduced with permission from Ref. [229]. Copyright 2015 Elsevier. (d) Zn-MNCs combined with an ATP luminometer for *Salmonella* detection [230]. Reproduced with permission from Ref. [230]. Copyright 2017 Elsevier.

allowed the NCs to show a higher peroxidase-like activity but weak fluorescence. By modulating the catalytic activity of the MNCs, researchers developed an immunoassay for the rapid and on-site detection of SEB. A concentration range of 0.4–20 ng/mL could be detected with a LOD of 0.12 ng/mL, providing a promising platform for the point-of-care testing of pathogenic microorganisms for food safety applications. Combined with aptamers, BSA-AuNCs can be employed for colorimetric detection of *Salmonella typhimurium* based on the peroxidase-like activity of aptamers-BSA-AuNCs [225]. Bacteria of micron size can bind with aptamers-BSA-AuNCs which further catalyze the reaction to generate a blue color, enabling a colorimetric detection of bacteria. This allowed detection of *S. typhimurium* in the range of 10^1–10^6 colony-forming unit (cfu)/mL with a detection limit of 1 cfu/mL.

As a Gram-positive food-borne bacterial pathogen that can lead to listeriosis and meningitis, the rapid detection of *Listeria monocytogenes* species from contaminated food samples is important to protect human health [226]. Leucocin A, a potent antimicrobial peptide against *Listeria*, was immobilized on a glass slide and could capture *L. monocytogenes* in the samples. Fluorescent AuNCs spontaneously assembled onto the peptide-bound bacteria *in situ* with an emission wavelength at 612 nm after excitation at 304 nm. This approach allowed rapid detection of bacteria with a LOD of 2000 cfu in a 10 μL sample that was promising for bacterial screening in food safety. Apart from *in situ* formation, functionalized MNCs can also be used to develop fluorescent sensor arrays that act as a "chemical tongue" to identify bacteria (Fig. 6b) [227]. Several proteins including HSA, LYZ, and lactoferrin (Lf) were used as templates to prepare the probes, which had different binding affinities to bacteria depending on the protein template. The different physicochemical properties of bacteria resulted in different responses of the sensor array, and the fingerprint-like pattern generated enabled the identification of different bacteria including *Staphylococcus aureus*, *E. coli* and their drug-resistant strains methicillin-resistant *S. aureus* (MRSA) and kanamycin-resistant *E. coli*. Bacterial infection with MRSA can be fatal if improperly treated due to the antibiotic-resistant properties of the bacteria. HSA-AuNCs were found to have a specific affinity toward *S. aureus* and MRSA [228]. The peptide binding motifs identified in HSA were also used to functionalize AuNCs to generate peptide-bound AuNCs that showed high binding affinity with *S. aureus* and MRSA. It provided a straightforward and practical way for the naked-eye identification of bacteria with a sensitivity of ~10^6 cells/mL.

Uncorrected Proof

Please cite this article in press as: I. Zare et al., Materials Today, (2020), https://doi.org/10.1016/j.mattod.2020.10.027

The choice of the template for the synthesis of the MNCs plays an impotent role in developing assays. LYZ-AuNCs have been reported as appropriate sensors for bacterial detection (Fig. 6c) [229]. LYZ has several advantages in this regard including (1) amino acid residues that are beneficial for the nucleation and growth of MNCs (2) good biocompatibility and MNC stability make the assay dependable and (3) it belongs to a family of bacteria-recognizing and bacteria-killing enzymes. Fluorescent LYZ-AuNCs can attach to the surface of *E. coli* with red fluorescence that was linearly responsive over the range of 2.4×10^4 – 6.0×10^6 cfu/mL of *E. coli* with a LOD of 2.0×10^4 cfu/mL. In contrast, BSA-AuNCs could not recognize *E. coli* and no fluorescence enhancement was observed. Magnetic NCs can be also used for bacterial detection. Zn-doped magnetic NCs (Zn-MNCs) were hydrothermally synthesized and employed to detect pathogenic bacteria in milk (Fig. 6d) [230]. The accessible Zn sites on the MNCs enabled bacterial-targeted Ab immobilization by Zn-S bonding, as a facile procedure avoiding the tedious steps for Ab functionalization on other metallic NPs. In addition, the magnetic properties of the Zn-MNCs allowed the capture and magnetic separation of *Salmonella* bacteria in milk. The captured bacteria could be quantified with a commercial ATP luminometer. With the help of the ATP luminometer assay, this method could achieve a detection limit of only 10 cfu/mL in *Salmonella*-spiked milk. Because different Abs can be conjugated onto the Zn-MNCs, this type of assay could be useful for rapid and sensitive detection of various pathogenic bacteria.

Protein-protected MNCs as nanoprobes for immunoassays

Protein-protected MNCs have been exploited in the development of immunoassays thanks to their electrochemical, catalytic, and optical properties. When electrochemical detection is used, MNCs act either as signal probes [142,231–233] or as modifiers of the electrode surface to enhance the transduction of the signal [234] or even as blocking agents of the signal [235,236]; whereas when optical properties are used, MNCs are the signal nanoprobes [237–241]. One of the trends in the field is the use of protein-protected MNCs as a component of a nanocomposite, which acts as the signal nanoprobe for further enhancement of the detection signal, thus rendering the immunosensor more sensitive [242–244]. MNCs can be used as nanocarriers of the detection molecule due to the surface binding capacity to decrease the number of molecules that can be detected and for stabilizing the signal [245]. In the following paragraphs, recent strategies and formats of immunoassays based on protein-protected MNCs will be briefly discussed (a recent review was dedicated to a general overview of MNCs as probes for diagnostic applications [2]).

Gold is the most commonly used metal for the MNC core [2,246], however, other metals have been utilized including Ag, Cu, Cd, and Pb. Another approach is bimetallic MNCs, such as Au/Pt [242], with a positive synergistic effect compared to the properties exhibited by individual MNCs. BSA is the preferred protein template in most studies, but other biomolecules such as hormones (dopamine), amino-acids [239] (cysteine, tyrosine), enzymes [241] (PEP, GSH) and also DNA [240] have been widely used to create robust nanoprobes for the development of immunoassays (see Table 1).

Classical formats of immunoassays (sandwich and competitive) have been performed using different detection strategies thanks to the versatility of the MNCs. A variety of signal generation processes have been investigated (Fig. 7) resulting in ultrasensitive immunoassays with LODs in the range of lower parts per trillion (*i.e.*, pg/L), and reliable assays with a reproducibility ≤ 8%. In addition, these strategies have been applied directly to clinically/environmentally relevant samples including water, urine, serum, or even cancer cells.

Several studies have employed MNCs as electrochemical signal enhancers using the classical method of acidic digestion of MNCs followed by electrochemical detection of the generated free metal ions [142,231,233]. Because each MNC contains only tens to hundreds of metal atoms, the electrochemical signal is enhanced, offering the potential to create sensitive immunoassays. In addition, this strategy allows for the detection of several target molecules at the same time, using a mixture of different metal cores for each target (Fig. 7a). Another interesting detection strategy is the use of MNCs as a catalyst in the detection reaction [242,243]. To increase the catalytic effect, a nanocomposite can be developed based on a NP support (PtNP or C_{60}) allowing the decoration of its surface with the protein-protected MNCs, which will then act as a catalyst for the detection reaction. In a study by Chen et al.[242], bimetallic MNCs were shown to increase the catalytic effect compared to single metal-core MNC, and achieved a LOD two hundred times lower than a conventional ELISA (Fig. 7b). Another approach is a photoelectrochemical (PEC) immunoassay [235,236] where the CuNCs that were attached to the recognition molecule (*e.g.*, Ab or aptamer) were used as blocking agents of an electrochemical signal after digestion and conversion to Cu^{2+} ions that intercalated into the electron-hole pair of the electroactive nanoparticles (at the electrode surface), thus blocking the transmission of the photocurrent (Fig. 7c). MNCs can also be used as modifiers of the electrode surface to improve the electronic conduction of the signal, providing a signal enhancement of 28% compared to an unmodified surface electrode [234].

Fluorescence is the most often used reporter for MNCs in labels in immunoassays and can be tuned either by changing the nature of the metal core, or by varying the biomolecule used as the scaffold for the MNC synthesis. Different immunoassays have been developed using direct measurement of the fluorescence of the MNCs [238,239,244]. Peng et al. reported [239] the simultaneous determination of clenbuterol and ractopamine in swine urine using a lateral flow immunoassay (LFIA) format with green-emitting Arg/ATT/AuNCs as detection probes (Fig. 7d), providing the most sensitive LFIA to date and decreasing the LOD for both targets up to two orders of magnitude compared with previous reports. Several studies have described the production of switchable (ON/OFF) immunoassays using quenching and/or enhancement of the MNC fluorescence (Fig. 7e) [237]. This strategy relies on the generation of structural defects by exposure to oxidants that quench the fluorescence from MNCs, and the regeneration of the fluorescence emission when MNCs were exposed to a reconditioning medium containing reducing agents [237,241]. An innovative strategy for signal generation consisted of the *in situ* formation of fluorescent MNCs as the final product of detection (Fig. 7f). This approach was pro-

Uncorrected Proof

Please cite this article in press as: I. Zare et al., Materials Today, (2020), https://doi.org/10.1016/j.mattod.2020.10.027

TABLE1

Application of functionalized MNCs as fluorescent/catalytic probes in the detection of different analytes.

Metal(s)	Protecting layer	Biomarker(s)	LOD	Sensing strategy	Refs
Au	GOD	Hg^{2+}	7.5 μM	Quenching of the fluorescence intensity	[33]
Au-Ag	BSA, LYZ	Hg^{2+}	0.7 nM.	The fluorescence quenching	[94]
Ag	LYZ	H_2O_2	0.2 μM	Ratiometric fluorescent quenching	[192]
Au	BSA	Dopamine	0.830 nM	Quenching of the fluorescence intensity	[213]
Au	BSA	Epinephrine	0.91 nM	Enhancement in the fluorescence intensity	[214]
Au	dBSA	AChE	0.02 mU mL^{-1}	Quenching of the fluorescence intensity	[215]
Au	Trf	5-HT	0.049 μM	Enhancement in the fluorescence intensity	[216]
Au	TRY	Dopamine	0.14 nM	Quenching of the fluorescence intensity	[219]
Au	Hb	Dopamine	0.1 nM	Peroxidase-mimicking activity	[220]
Cu	BSA	Dopamine	0.1637 pM	Quenching of the fluorescence intensity	[221]
Au	ESM	SEB	0.12 ng/mL	Peroxidase-mimicking activity	[224]
Au	BSA	*S.* Typhimurium	1 cfu/mL	Peroxidase-mimicking activity	[225]
Au	HSA, LYZ, and Lf	*S. aureus*, *E. coli*, and drug-resistant bacteria	1.2×10^7 cells/mL	Fluorescent sensor array	[227]
Au	HSA	*S. aureus*	10^6 cells/mL	Enhancement in the fluorescence intensity	[228]
Au	LYZ	*E. coli*	2.0×10^4 cfu/mL	Enhancement in the fluorescence intensity	[229]
Zn-Fe	Ab	*Salmonella*	10 cfu/mL	Magnetic separation and ATP luminometer	[230]
Au	BSA	ALP	0.002 U L^{-1}	Switch-on fluorescent immunoassay	[237]
		Mouse-IgG	1.5 pg mL^{-1}		
Au	BSA	INS	0.11 ng mL^{-1}	Fluorescent immunoassay	[238]

posed by Li et al.[240] and took advantage of the rapid formation of DNA-templated CuNCs (within 5 min) in the presence of the reducing agent produced by the enzymatic reaction of alkaline phosphatase (one of the enzymes often used in ELISA assays), expanding its use into highly sensitive fluorimetric immunoassays (LOD of human-IgG was 7 pg/mL) (Table 2).

ECL has also been used as signal detection for immunoassays, and in a recent work MNCs have demonstrated advantages in the field by offering the possibility to expand the optical window to the NIR spectrum and increasing the sensitivity of the bioassay [247]. Thus, a new family of ECL tags is possible. Very recently has been probed the use of Abs as scaffolds for the synthesis of MNCs and thus allowing the development of dot-blot immunoassays [248]. The bioactivity of modified IgG has been evaluated by surface plasmon resonance measurement suggesting that the IgG-AuNCs binds to its antigen with an affinity constant of 6.28×10^{-8} M probing that any loss of activity is observed. This work opens the door to a new application of MNCs into the classical biological techniques.

Diagnostic imaging of biological systems *in vitro* and *in vivo*

In vitro imaging

Bioimaging is a common technique used to understand biological processes and for effective medical diagnosis [249]. Bioimaging techniques based on magnetic (*e.g.*, magnetic resonance imaging (MRI)), radiation-based (*e.g.*, computed tomography (CT), positron emission tomography (PET), single photon emission computed tomography (SPECT)) and optical approaches (fluorescence imaging) have different properties in terms of spatial resolution, sensitivity, and depth of tissue penetration. Optical imaging is a non-invasive technique known for providing information at a cellular and/or molecular level with a relatively low cost and high sensitivity even at the single molecule level [250]. Many studies have reported the use of protein-templated NCs as fluorescence probes for cancer cell imaging. Cancer cells often over-express certain cell receptors that can be targeted by MNCs, and thus cancer cells can be imaged and distinguished from normal cells [251,252]. To provide cell receptor-specific targeting properties, MNCs can be functionalized with targeting moieties such as FA, hyaluronic acid (HA), Trf, steroids, aptamers, or Abs (*e.g.* Herceptin) [253–256]. Retnakumari et al. described Au quantum cluster (AuQC)-BSA conjugated with FA as a targeting agent which could recognize KB carcinoma cells that overexpress FR. FA-conjugated BSA-AuNC exhibited bright and stable florescence in the NIR, and showed significant internalization by FR-positive oral carcinoma KB cells through FA-mediated endocytosis [139]. Another study reported functionalization of BSA-protected AuNCs with Herceptin to visualize cancer cells [257]. The bioconjugated AuNCs-Herceptin effectively localized within the nuclei of breast cancer cells that overexpressed the receptor tyrosine-protein kinase Erbb2. Chattopadhyay et al. developed a novel composite based on Zn phosphate-decorated AuNCs protected with BSA fragments and used them as a bioimaging agent to target HeLa cancer cells [62]. Efficient internalization of $AuNCZn_3(PO_4)_2$ by cancer cells was tracked by their bright luminescence (Fig. 8). Additionally, their resistance to proteases could open up their practical application for clinical purposes. In addition to Au clusters, Cu clusters stabilized by proteins could also be utilized as bioprobes for *in vitro* imaging. Trf-directed CuNCs with a high QY were used to stain HeLa cells [258]. In this study, Wen et al. used Trf not only as a synthesis template, but also as a molecular recognition agent for targeting of Trf receptors which are overexpressed on HeLa cells as well as other cancer cells. Strong red fluorescence was emitted from HeLa cells treated with the Trf-CuNCs, indicating the efficient targeting of the Trf-CuNCs. In addition to recognition and imaging of cancer cells, the affinity of protein-protected MNCs towards metal ions can be leveraged to visualize the distribution of ions within cells. For instance, a "turn-on" sensor based on Hb-incorporated iron QCs (Hb-FeQCs) was designed for the detection and cellular imaging of Zn(II) [259]. The enhancement of emission intensity

Uncorrected Proof

Please cite this article in press as: I. Zare et al., Materials Today, (2020), https://doi.org/10.1016/j.mattod.2020.10.027

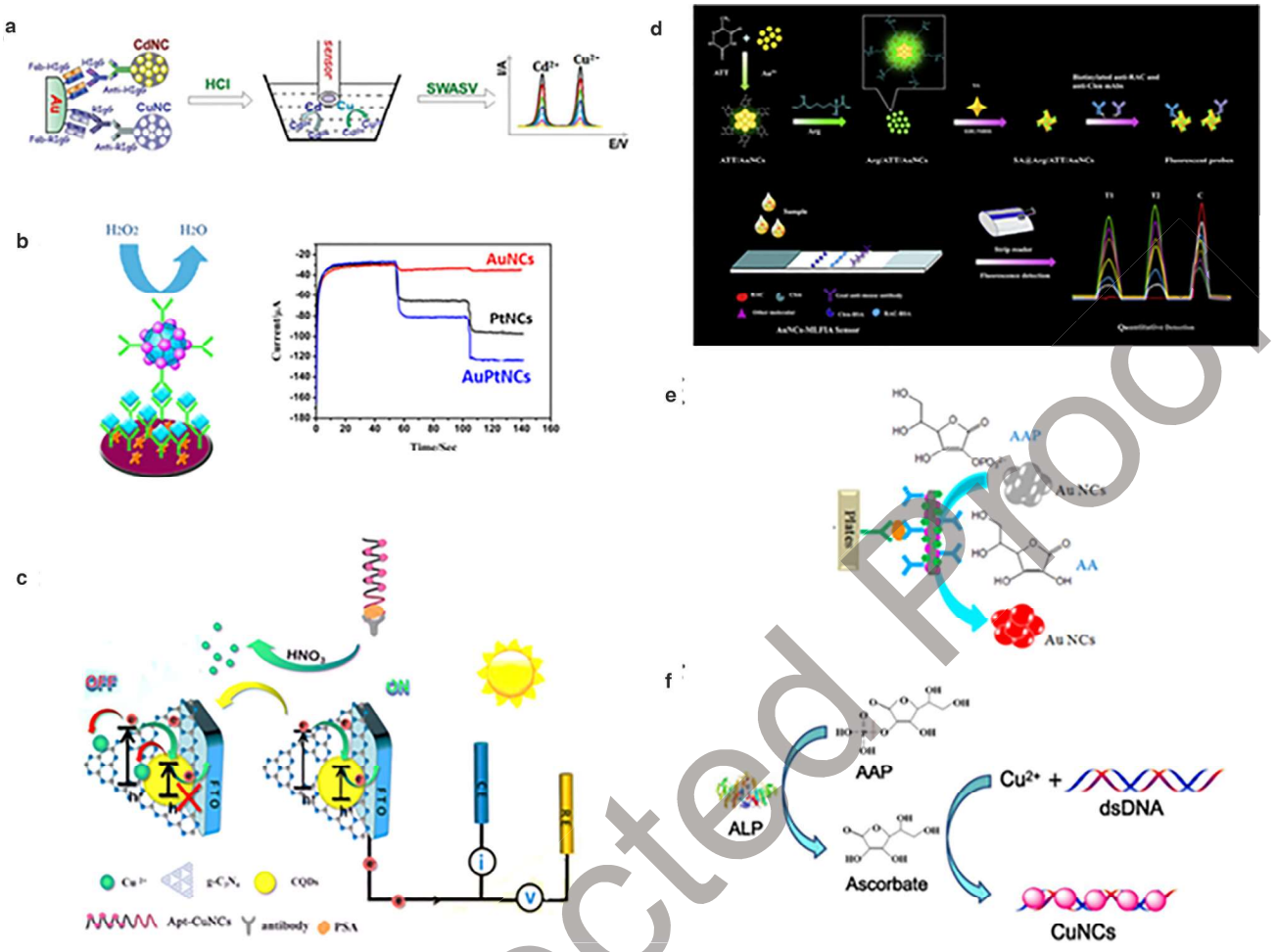

FIGURE 7

Different signal transduction processes in immunoassays based on MNCs. (a) Direct electrochemical detection of the metal ions that compose the MNCs [233]. Reproduced with permission from Ref. [233]. Copyright 2017 Royal Society of Chemistry. (b) MNCs acting as a catalyst of the detection reaction [242]. Reproduced with permission from Ref. [242]. Copyright 2016 Elsevier. (c) PEC immunoassay using CuNCs as blocking agents of the photocurrent [235]. Reproduced with permission from Ref. [235]. Copyright 2017 American Chemical Society. (d) Synthesis of green-emitting Arg/ATT/AuNCs and bioconjugation to streptavidin (top scheme); and schematic representation of the FLFIA process at the bottom [239]. Reproduced with permission from Ref. [239]. Copyright 2018 Elsevier. (e) Switch ON/OFF strategy of the MNCs fluorescent signal [237]. Reproduced with permission from Ref. [237]. Copyright 2016 Elsevier. (f) *In situ* generation of fluorescent MNCs [240]. Reproduced with permission from Ref. [240]. Copyright 2019 Elsevier.

was due to the formation of a complex between Zn ions and Hb-FeQCs, and this nanoplatform displayed good cellular uptake and viability confirming the excellent cellular imaging capability of protein-MNC-based fluorescent probes.

In vivo imaging

The ability of *in vivo* nanoprobes to accumulate within the tumor tissue via the enhanced permeability and retention (EPR) is pivotal. They should possess long circulation times in the blood and have low toxicity. The ultrasmall size and biocompatibility of protein-protected MNCs meet all these desired criteria. In terms of size, NPs with a hydrodynamic diameter >6–8 nm tend to accumulate in the liver, giving rise to concerns associated with possible toxicity. The ultrasmall size of MNCs is lower than the size threshold for renal excretion, which enable them to be rapidly cleared through the kidneys with minimal accumulation in other organs [260,261]. Their ultrasmall size also allows them to accumulate in solid tumors facilitated by the EPR effect due to abnormalities in vascular architecture and poor lymphatic drainage of tumors [262]. It has been proved that their renal clearance does not interfere with their tumor accumulation [253]. Similarly to *in vitro* imaging, the presence of multiple functional groups on the MNCs surface enables their functionalization with targeting moieties, facilitating their accumulation and internalization into tumor cells by receptor-mediated endocytosis [263]. Their tunable emission ranging from UV to NIR solves an important problem for *in vivo* imaging, that is absorption and scattering of short-wavelength light by biological tissues [264]. For instance, there was an interesting report demonstrating for the first time the use of long-lived BSA AuNCs as time-gated intensity imaging probes. Since the fluorescence lifetime of BSA-AuNCs is several hundred fold longer than the tissue autofluorescence, the contribution of background fluorescence and light scattering could be suppressed by collecting the emission of AuNC-BSA 50 ns after the excitation pulse [265]. Protein-MNCs emitting in the biologically transparent NIR window are

Uncorrected Proof

Please cite this article in press as: I. Zare et al., Materials Today, (2020), https://doi.org/10.1016/j.mattod.2020.10.027

TABLE.2

Imaging applications of protein-protected MNCs.

Metal cluster(s)	Protecting ligand(s)	Surface functionalization	Diagnostic modality	Refs
Cu	BSA	N/A	*In vitro* cell imaging	[29]
Au	TRY	FA	*In vivo* HeLa tumor cell imaging	[31]
Au	Human Trf	FA	Cellular imaging	[34]
AuNCs-MSNs	BSA	N/A	*In vivo* tumor imaging	[41]
Au-$Zn_3(PO_4)_2$	BSA	N/A	*In vitro*/*in vivo* imaging	[62]
AgNCs/GO	BSA/HSA	N/A	CT imaging	[85]
Au	BSA	FA	*In vitro* cell imaging	[93]
Au	INS	N/A	The two-photon red fluorescence imaging/X-ray/CT	[109]
Au	BSA	FA	Targeted cancer imaging	[139]
Au/Ag	Egg white	N/A	Cell imaging	[203]
Au	BSA	FA and HA	Tumor-targeted imaging	[251]
Au	BSA	FA	Turn on fluorescence imaging	[256]
Cu	Trf	N/A	Targeted imaging of cancer cells	[258]
Au	BSA	N/A	Time gated intensity imaging	[265]
Au	BSA	N/A	*In vivo* and *ex vivo* fluorescence imaging	[267]
Au	BSA	N/A	Two photon *in vitro* imaging	[269]
Au	Albumin NPs	N/A	Two-photon imaging of cancer cells	[270]
Au	LYZ	FA	NIRF/CT dual-modal bioimaging	[272]
Gd_2O_3/Au	BSA	RGD	NIR/MRI/*in vivo* targeted tumor imaging	[274]
Au	BSA	ICG	*In vivo* NIRF imaging/PAI	[275]
Gd_2O_3-Au	BSA	ICG	X-ray CT/NIRF/MRI	[276]
IONPs/AuNCs	BSA	N/A	MRI/*in vitro*	[277]
Cu	BSA	LHRH	PET imaging	[278]
Au- GO	Trf	N/A	NIR/*in vivo* imaging	[279]
Au	BSA	Met	NIR tumor imaging	[280]
^{64}Cu-AuNCs	HSA	N/A	PET and NIR imaging	[281]
Au	BSA	FA	Targeted imaging in cancer cells	[282]
Au	OVA	FA	*In vitro* Imaging	[283]
Au	BSA	N/A	Cellular and bacterial imaging	[284]
Au	BSA	N/A	NIR FL imaging	[285]
Au	BSA	DTPA, GdIII	NIRF/CT/MRI	[286]
Au	Ribonuclease-A	Vitamin B12	Cancer targeting and imaging	[287]
Au	BSA	FA	Targeted tumor cellular dual-modality imaging	[288]
Au	Egg white	N/A	Cellular imaging	[289]

advantageous for *in vivo* imaging, including deep tissue penetration, reduced light scattering, minimal background interference, minimized autofluorescence, and less photodamage to biological samples [168,266].

Qing et al. were the first group to employ BSA-AuNCs as fluorescent probes for *in vivo* imaging in HeLa tumor-bearing mice. Fluorescence imaging confirmed the accumulation of the NIR-emitting BSA-protected AuNCs in the tumor via the EPR effect. More significantly, their results showed negligible uptake of BSA-AuNCs by the reticuloendothelial system with no potential for toxicity [267]. Following this study, Huang et al. demonstrated the application of HA-functionalized BSA-AuNCs as a tracking agent for tumor-targeted imaging in tumor-bearing nude mice [251]. Since HA can recognize CD44 receptor, which is over-expressed on Hep-2 cells, Hep-2 tumors could be visualized by the bright fluorescence of AuNC taken up by cells through receptor-mediated internalization. Pea protein isolate (PPI)-stabilized AuNCs were employed as an *in vitro* staining probe and for *in vivo* imaging [268]. In order to enhance the blood circulation time, they were further coated with RBC membranes. Significant fluorescence could be detected at the tumor site after the injection of AuNCs/PPI-RBC, confirming their efficiency as an *in vivo* imaging nanoprobe.

Multimodal imaging

Despite many successful applications of fluorescence-based imaging techniques using protein-MNCs, one major limitation concerns the lack of resolution, especially in deep tissue. Given that three-dimensional resolution using tomographic techniques provide much more information than fluorescence imaging alone, protein-MNCs have been utilized in multimodal imaging approaches, including multi-photon imaging, traditional CT, PET, MRI, ultrasound imaging (US), and photoacoustic imaging (PAI).

Two-photon excitation fluorescence microscopy provides deeper imaging inside tissue. The two-photon luminescence behavior of BSA-AuNCs was investigated by Gryczynski et al. [269]. In their study, BSA-AuNCs exhibited two-photon excitation luminescence within the 560–1100 nm optical window which allowed deep tissue imaging. A quadratic relation between excitation power and emission intensity of BSA-AuNCs demonstrated their ability to be used as probes for multiphoton microscopy [269]. Chattopadhyay et al. validated the use of AuNCs embedded in BSA-NPs for two-photon imaging of cancer cells [270]. The internalization of the AuNCs in cancer cells was confirmed by luminescence emission in the biological window after two-photon excitation. Fukumura et al. reported a procedure to con-

Uncorrected Proof

Please cite this article in press as: I. Zare et al., Materials Today, (2020), https://doi.org/10.1016/j.mattod.2020.10.027

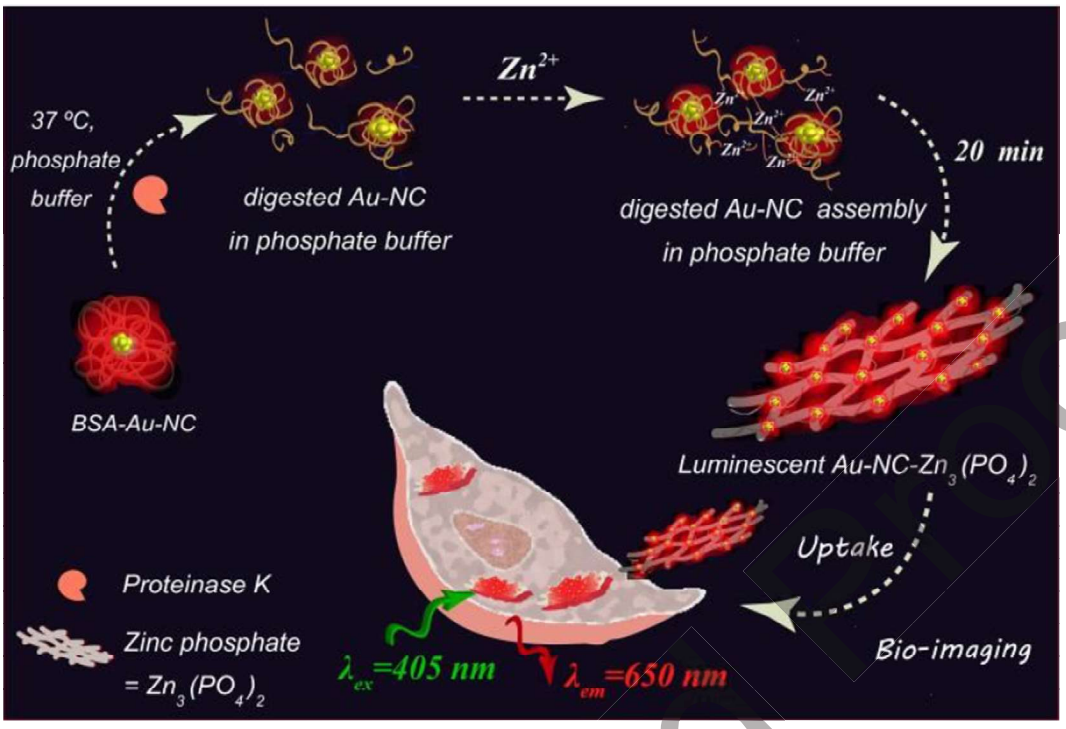

FIGURE 8

Schematic description of the biomimetic pathway towards Zn phosphate crystallization in protein fragment stabilized AuNC assembly and their uptake in cancer (HeLa) cells for bio-imaging [62]. Reproduced with permission from Ref. [62]. Copyright 2017 Royal Society of Chemistry.

trol the number of AuNCs (formed by 8 Au atoms) in one BSA molecule [271]. They showed that BSA units with multiple Au_8-NCs act as an effective and biocompatible luminescence probe for two-photon *in vivo* imaging.

The ability of protein-protected AuNCs to function as a contrast agent in CT has also been investigated. Among the various contrast agents used in CT imaging, AuNPs possess X-ray attenuation properties due to their high atomic number. Motivated by this property of AuNPs, considerable attention has been dedicated to investigate if protein-protected AuNCs could also be used in CT imaging in combination to their intrinsic fluorescence. Li et al. reported a strong dual imaging contrast signal (CT and fluorescence) for LYZ–AuNCs [272]. *In vivo* CT imaging along with fluorescence imaging of HeLa tumor-bearing nude mice indicated that AuNCs not only exhibited NIR fluorescence signal – thus avoiding the autofluorescence of biological tissue, but also displayed promising X-ray attenuation properties. In another study, the use of INS-AuNCs as a multimodal imaging probe was assessed by Chou and coworkers [109]. A two-photon z-stacking study confirmed the internalization of INS-AuNCs by C2C12 cells through endocytosis. Differentiated C2C12 myoblasts showed strong CT signal enhancement by these fluorescent INS-AuNCs (Fig. 9).

In addition to the aforementioned imaging techniques, protein-MNCs as a contrast probe for simultaneous MRI and fluorescence or CT imaging have also been investigated. For example, the efficiency of iodinated BSA-GdNPs (I-BSA-GdNPs) as a dual MRI/CT imaging probe was evaluated both *in vitro* and *in vivo* by Wang et al. [273]. The high relaxivity coefficients of the I-BSA-GdNPs supported their MR imaging ability, resulting in MRI contrast enhancement and enhanced CT signals clearly observable in orthotopic osteosarcoma tumor models (Fig. 10). In another study, *in vivo* multimodal imaging with a BSA-Gd_2O_3/Au nanoprobe in the MR blood pool was explored [274]. Intense NIR fluorescence and MR signals with excellent contrast, as shown in Fig. 11, were demonstrated, illustrating the ability of protein-protected MNCs as MRI agents.

Therapeutic applications in biomedicine

Chemotherapy

The introduction of nanomedicine is expected to revolutionize cancer chemotherapy, with the potential to benefit millions of cancer patients. NPs offer an exciting route to deliver chemotherapeutic drugs more exclusively to the tumor site, using both passive (EPR) and active (through specific over-expressed cell receptors) targeting strategies. Improved targeting can diminish side effects and increase the overall efficacy of the drugs. Researchers in the field have concentrated their efforts in designing a wide range of different protein-MNCs as nanotherapeutics with the capacity to deliver drugs selectively into tumors. For example, the anti-cancer drug cisplatin was conjugated to BSA-AuNCs together with FA – used as active targeting moiety – for 4 T1 breast cancer cells [290]. The nanoformulation induced cellular apoptosis, exhibited high accumulation in orthotopic breast tumors and decreased the metastatic burden in the lungs. Overall, this work confirmed the efficiency of the AuNC-based nanomedicine as a theranostic platform for targeted chemotherapy and bioimaging of breast cancer. Doxorubicin (DOX) has also been conjugated to FA-functionalized BSA-AuNCs to induce cytotoxicity in lung, liver, breast and colon cancer cells [253].

Uncorrected Proof

Please cite this article in press as: I. Zare et al., Materials Today, (2020), https://doi.org/10.1016/j.mattod.2020.10.027

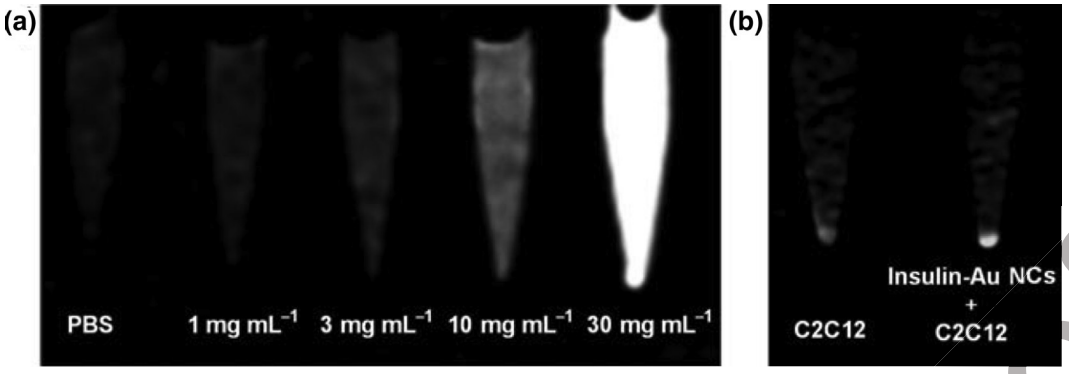

FIGURE 9

Dual-modality CT-fluorescence imaging with INS–AuNCs. (a) CT imaging of INS–AuNCs at sequential concentrations; and (b) differentiated C2C12 myoblasts with (20 mg/mL, right) and without (left) INS–AuNCs [109]. Reproduced with permission from Ref. [109]. Copyright 2011 Wiley.

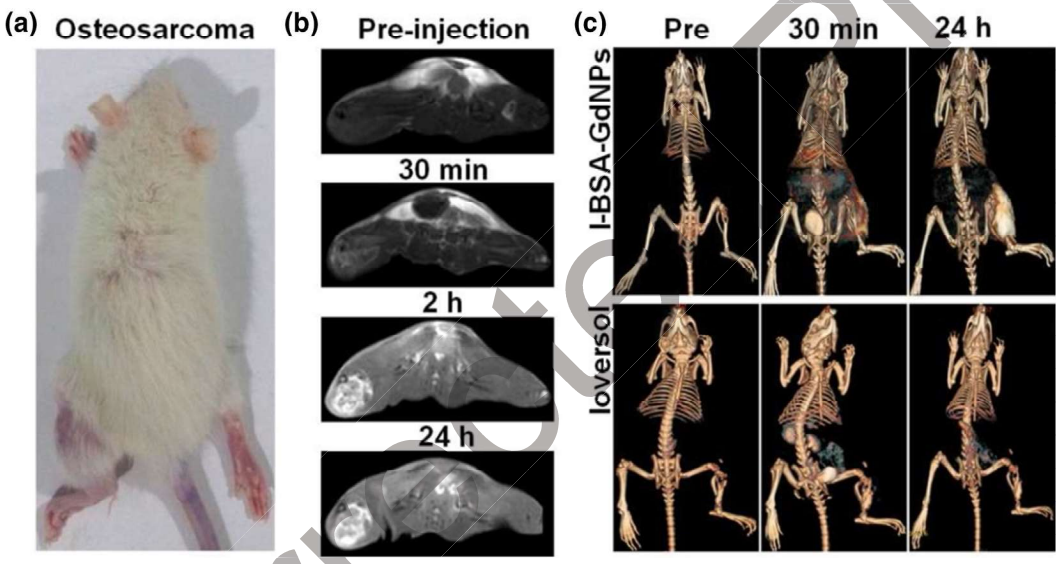

FIGURE 10

In vivo imaging of orthotopic osteosarcoma animal models using I-BSA-GdNPs. (a) Photograph of orthotopic osteosarcoma rat. (b) *In vivo* T1-weighted MRI images of orthotopic osteosarcoma rats before and at 30 min, 2 h, and 24 h after I-BSA-GdNPs injection. (c) CT 3D images of orthotopic osteosarcoma rats after Ioversol and I-BSA-GdNPs injection [273]. Reproduced with permission from Ref. [273]. Copyright 2015 American Chemical Society.

High anti-tumor activity was observed both *in vitro* and *in vivo* when treated with the DOX-loaded, FA-BSA-AuNCs, which also acted as a fluorescence imaging probe. Similarly, DOX was incorporated into BSA-AuNCs to treat HeLa cervical cancer cells (Fig. 12a) [291]. An RGD (Arg-Gly-Asp) peptide was attached to the nanomedicine to enhance cell recognition and internalization. The resulting DOX-conjugated RGD-BSA-AuNCs showed increased cell uptake and tumor penetration, and successfully inhibited cell growth both *in vitro* and *in vivo*. The long-term retention of the nanotherapeutic in the tumor after intratumoral injection was monitored by fluorescence imaging (Fig. 12b) and its efficacy was compared to tumor-bearing mice treated with PBS alone (Fig. 12c). Another strategy that has been used is conjugating both DOX and SN28 – a camptothecin derivative – through linkers that allow controlled release of both therapeutics by the change of pH and reductive state, respectively [292]. Their cytotoxicity was confirmed in 2D and 3D *in vitro* breast cancer models.

Hybrids between silica NPs and AuNCs have also been used for the delivery of combined therapeutics to combat breast cancer chemoresistance [293]. In this work, a combination of two drugs were loaded onto the nano-hybrid: (a) ZD6474, an inhibitor of tyrosine kinase activity; and (b) epigallocatechin gallate (EGCG), an Akt signaling pathway inhibitor. EGCG was first encapsulated into the silica NPs which were then functionalized with thiols to immobilize BSA-AuNCs onto the surface. ZD6474 molecules were then preferentially attached around the BSA-AuNCs through amine-gold interactions. The resulting nanoformulation only dissolved and released its cargo at acidic pH, and induced apoptosis in drug-resistant breast cancer cells.

Cationic BSA-AuNCs were cross-linked with HA and then triple-loaded with paclitaxel, indocyanine green (ICG, a U.S Food and Drug Administration (FDA)-approved contrast agent), and a nitric oxide donor [294]. The ability of the nanotherapeutic to penetrate deep within the tumor microenvironment together

Uncorrected Proof

Please cite this article in press as: I. Zare et al., Materials Today, (2020), https://doi.org/10.1016/j.mattod.2020.10.027

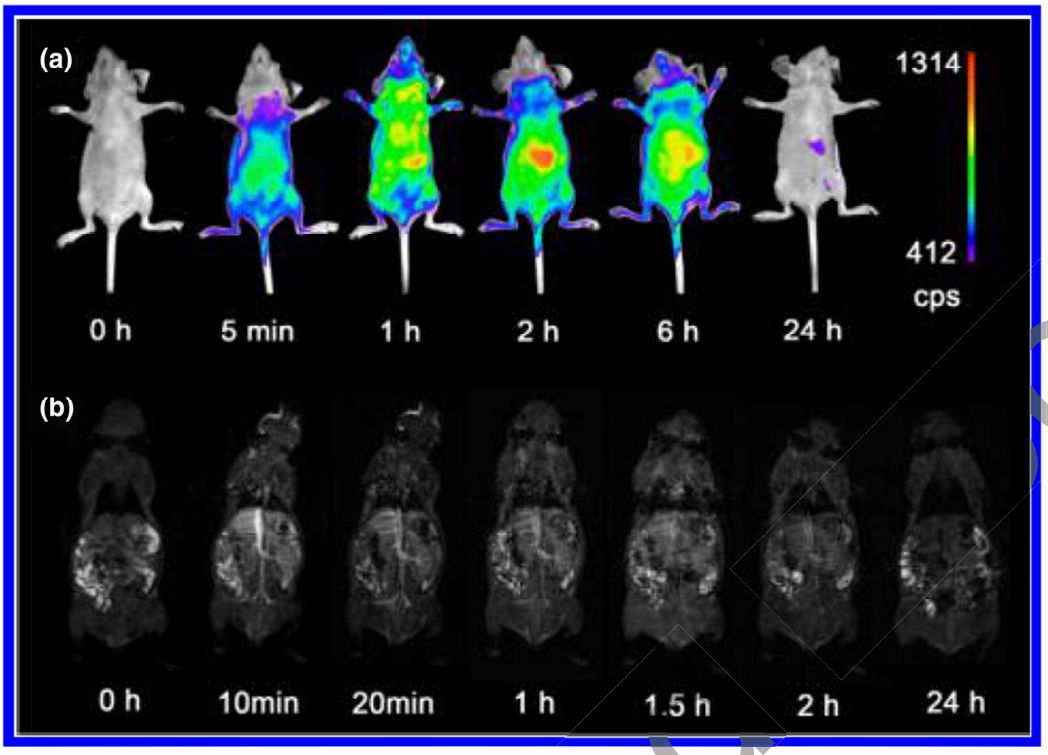

FIGURE 11

In vivo blood imaging using BSA-Gd_2O_3/Au nanoprobe. (a) NIR fluorescent imaging and (bB) magnetic resonance imaging [274]. Reproduced with permission from Ref. [274]. Copyright 2013 American Chemical Society.

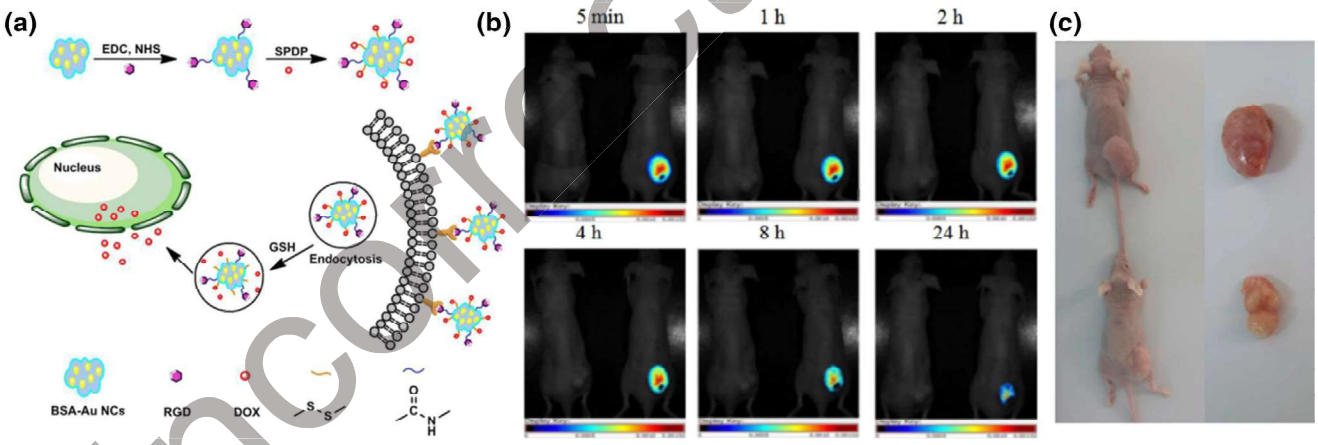

FIGURE 12

Design and performance of DOX- and RGD-conjugated AuNCs. (a) Schematic of the preparation of the BSA-templated AuNCs conjugated to DOX and RGD peptide. (b) *In vivo* fluorescence imaging of the nanoformulation after intratumoral injection to HeLa tumor-bearing mice. (c) Comparison of the mice and tumors after being treated with the nanoformulation (bottom mouse) and the control treated with PBS (upper mouse) [291]. Reproduced with permission from Ref. [291]. Copyright 2018 American Chemical Society.

Uncorrected Proof

with the combination of drugs resulted in a significant inhibition of tumor growth and reduced metastatic load in the lungs.

Croissant and his team carried out a study, describing the use of BSA-capped AuNCs as an imaging probe to track the *in vitro* and *in vivo* distribution of the nanocarrier [41]. The BSA-AuNCs acted as a cap to block the pores of MSNs that had been loaded with DOX and gemcitabine (GEM). The electrostatic interaction between the BSA-AuNCs and the MSNs allowed a high loading capacity, and pH-responsive drug release, avoiding premature leakage of the cargo by only releasing both drugs at the lysosomal pH. BSA-AuNCs have also been used as an imaging probe for a drug delivery vehicle formed from BSA [270]. The BSA-capped MSN-AuNCs loaded with DOX were able to reduce the viability of HeLa cells down to 20%, and induce apoptosis. The uptake of the nanocomposite was tracked using the intrinsic fluorescence both of the AuNCs and DOX, showing intracellular release of the drug. In another study by Pan et al., a DOX-loaded multifunctional nanocarriers (MFNCs) was designed by

Please cite this article in press as: I. Zare et al., Materials Today, (2020), https://doi.org/10.1016/j.mattod.2020.10.027

self-assembly of BSA-AuNCs, gold nanorods (AuNRs) and iron oxide (Fe_3O_4) NPs (IONPs) into a larger BSA-NP. The fluorescent, plasmonic and magnetic protein-based nanocarrier successfully carried out *in vitro* photoluminiscent imaging, plasmonic PPT, magnetic targeting and the delivery of DOX to HeLa cells.

Besides Au-based NCs, other metals have been used for the synthesis of protein MNCs for cancer therapy. For example, Trf-templated CuNCs were loaded with DOX and showed promising results as a targeted theranostic nanomedicine [295]. Tumor-bearing mice treated with this nanoformulation showed an increased life span as compared to controls due to its longer circulation time and tumor-targeted accumulation. Moreover, the results showed that healthy tissue like liver and kidneys were not affected by the treatment. In another study, bimetallic NCs formed by Au and Ag were synthesized using cationic BSA and further cross-linked to form a larger nanocomposite [27]. The resulting nanocarrier was able to deliver a suicide gene into HeLa cells reducing their viability in combination with ROS generated by the bimetallic cluster. This work proved that the intrinsic fluorescence of this type of protein-MNC could be used for simultaneous bioimaging, providing theranostic properties to the nanocarrier.

Radiotherapy

Radiotherapy is one of the most often used cancer therapies, together with chemotherapy. Typically, radiation therapy uses ionizing radiation, such as X-rays or gamma rays to treat cancer [296,297]. This ionizing irradiation damages biomolecules in tumor cells, in particular DNA, disrupting the cell division and proliferation. The DNA damage can be caused directly by the radiation absorbed by the nucleic acids, or indirectly by the creation of ROS by the radiation absorption of water. ROS play an important role in radiotherapy by triggering specific cell signaling pathways that result in apoptosis. Oxygen, in particular, can act as a radiosensitizer by producing more radicals and boosting the overall ROS effect. This is why hypoxia, a lack of oxygen inside the tumor microenvironment, is one of the main obstacles to the success of radiotherapy [298]. Nanomaterials that are able to overcome hypoxia have the potential to be efficient radiosensitizers and improve the outcomes of radiotherapy treatment [297].

In 2013, Xie and colleagues were the first to report the use of BSA-AuNCs for radiation therapy [13]. In a pilot study, they showed that intraperitoneal administration of BSA-AuNCs into tumor-bearing mice that were then irradiated with gamma rays was able to reduce tumor volume to 38% of untreated ones. Since then, most of the studies on AuNC-based radiosensitizers have utilized GSH-AuNCs, because they show better efficacy and penetration into the tumor [299–301]. However, some groups have demonstrated increased efficacy of radiotherapy using targeted and/or multifunctional protein-protected AuNCs. For example, Kefayat and colleagues, used FA [302] and aptamers [303,304] to target glioblastoma multiforme and breast cancer, respectively. In both cases, the targeting moieties were conjugated to BSA-AuNCs. After intravenous injection of FA-BSA-AuNCs and treatment with 6 Gy radiation, glioma tumor-bearing rats showed a significantly longer survival time (almost double compared to the controls) [302]. This study confirmed the ability of these AuNCs to cross the blood brain barrier – one of the most challenging biological barriers to overcome in drug discovery. The AS1411 aptamer, a RNA-like structure designed to bind to nucleolin (a protein over-expressed in cancer cells), was conjugated to the BSA-AuNCs, and their role as a radiosensitizer was first evaluated *in vitro* [303]. This preliminary study showed increased internalization of the AS1411-BSA-AuNCs in 4T1 breast cancer cells as opposed to normal cells, and exhibited enhanced cell killing when irradiated with different intensity X-rays. In a follow-up study by the same team of researchers, this system was evaluated *in vivo* [304]. AS1411-BSA-AuNCs were intraperitoneally administered to mice bearing breast cancer tumors, who were then treated with radiation. Targeted AuNCs combined with radiotherapy reduced tumor growth and enhanced survival rate in comparison to the injection of non-targeted AuNCs or radiotherapy alone.

BSA-templated nanocomposites were prepared from AuNCs plus manganese dioxide (MnO_2) as multifunctional radiosensitizers to overcome radiation resistance [305]. While the Au that accumulated in the tumor acted as an effective radiosensitizer, the MnO_2 component was able to react with endogenous H_2O_2 present within the tumor to generate additional O_2, and thus overcoming the hypoxia in the tumor microenvironment (Fig. 13). The results showed that X-ray irradiation (6 Gy) following intravenous injection of BSA-Au-MnO_2 nanocomposite, had higher efficacy at reducing tumor growth than the controls, including BSA-AuNCs (Fig. 13c). The authors hypothesized that the hypoxia-driven radiotherapy resistance is overcome with their system.

Gadolinium polytungstate NCs ($GdW_{10}O_{36}$ NCs) coated with BSA have also been synthesized and proven to be efficient radiotherapy sensitizers [306]. When these protein-MNCs were intravenously administered to tumor-bearing mice, there was high accumulation in the tumor without any toxicity. Subsequent X-ray irradiation led to significantly decreased tumor growth.

PDt

PDT is capable of destroying tumor lesions using light-sensitive photosensitizer (PS) drugs [307,308]. In PDT, light excitation of the PS produces cytotoxic ROS, such as singlet oxygen ($^1O_2$), free radicals or hydroperoxides under irradiation of the appropriate wavelength leading to the irreversible destruction of cancer cells and tissues. MNCs can have long-lived triplet excited states able to react with triplet ground state oxygen, which forms excited state $^1O_2$ [309]. Therefore protein-protected MNCs can be employed as PS in PDT by photogenerating ROS [310].

Most of the work employing AuNCs for PDT has used GSH-AuNCs [309,311,312], probably because protein-protected AuNCs have a lower $^1O_2$ generation QY. However, alkyl thiolated AuNCs co-modified with HSA and catalase (CAT) were employed as theranostic nanoagents to overcome limitations in PDT [313]. In these nanocomposites, in addition to the Au core leading to the formation of $^1O_2$ upon NIR light excitation, the CAT enzyme produces additional O_2 and relieves tumor hypoxia through decomposition of endogenous H_2O_2 inside the tumor microenvironment. Huang and colleagues designed a photo-theranostic nanomaterial for fluorescence imaging-guided PDT [314]. The material consisted of a silica construct encapsulating BSA-

Uncorrected Proof

Please cite this article in press as: I. Zare et al., Materials Today, (2020), https://doi.org/10.1016/j.mattod.2020.10.027

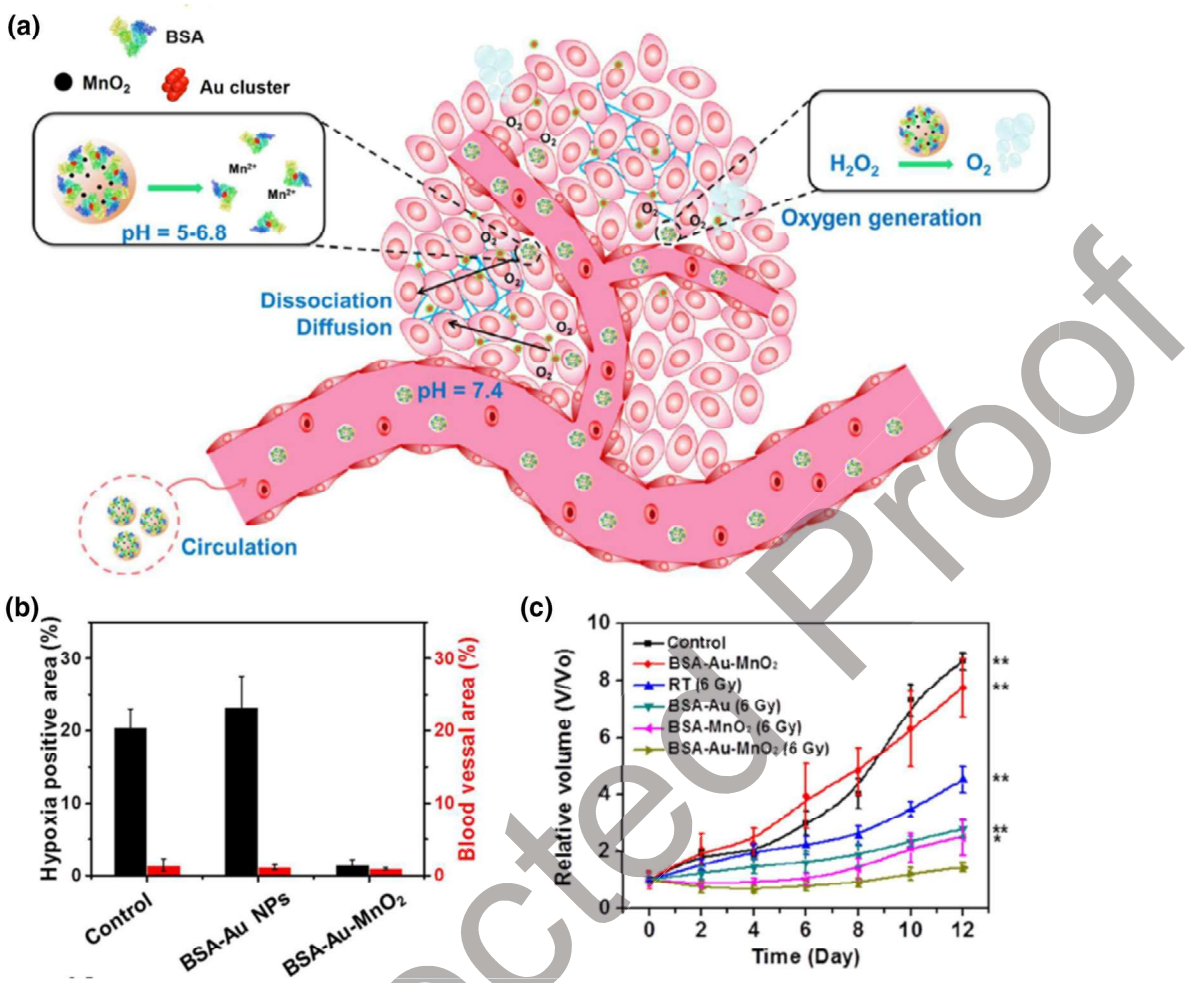

FIGURE 13

Nano-radiosensitizer formed by BSA-capped AuNCs and MnO_2 NPs. (a) Schematic of the mechanism of action of the synthesized BSA-Au-MnO_2 NPs: circulation and accumulation deep inside the tumor of the NPs until dissociation of MnO_2 in the acidic environment of the tumor generating O_2 and reducing hypoxia. (b) Quantification of the hypoxic and blood vessel areas for each treatment group measured by fluorescence intensity after staining tumors with the hypoxia-probe. (c) Tumor growth with time after radiotherapy treatment. Mice were irradiated with X-ray (6 Gy) at 6 h post intravenous injection of the nanoformulation or the controls [305]. Reproduced with permission from Ref. [305]. Copyright 2017 Royal Society of Chemistry.

AuNCs plus immobilized chlorin e6 (Ce6), a potent PS molecule. Their formulation facilitated the internalization of Ce6 into cells without non-specific release. Similarly, to enhance PS efficacy under hypoxic conditions, BSA-protected PtNCs (BSA-PtNCs) were used to coat MSNs loaded with methylene blue, a model PS agent [315]. The injected nanoformulation into HeLa xenograft models was able to inhibit tumor growth without apparent side effects when irradiated with a 635-nm laser. This study demonstrates that the BSA-PtNC biocoating onto the nanospheres generated O_2 intracellularly upon laser excitation, which led to a reduction of hypoxia and enhanced PDT efficacy. In another work, BSA-AgNCs exhibited PDT properties which could generate $^1O_2$ with high quantum efficiency comparable to commercial PS (Fig. 14) [316]. The PDT efficacy of this type of protein-MNC was shown by decreased cell viability of breast cancer cells treated with BSA-AgNC plus light irradiation (Fig. 14) [316]. Yen Nee Tan and coworkers reported protein-protected Au/Ag alloy NCs showing peculiar $^1O_2$ generation properties inversely correlated to their PL intensities [317].

PTt

PTT is defined as use of light in order to generate localized heating by specific absorption of light by specific chromophores whereby diseased cells are damaged [318]. The unique properties of protein-protected metallic nanostructures enables them to carry out photoexcited hyperthermia-induced cytotoxicity given their high conversion rate of energy to heat, resulting in the destruction of tumor cells and malignant tissue. This process therefore requires two steps: i) administering the phototherapeutic agent to the tumor; and ii) irradiating with an electromagnetic field, typically in the form of NIR light.

Plasmonic and magneto-luminescent MFNCs containing AuNRs, IONPs or BSA-AuNCs can all function as sophisticated probes for cancer theranostics, combining drug delivery, PTT

Uncorrected Proof

Please cite this article in press as: I. Zare et al., Materials Today, (2020), https://doi.org/10.1016/j.mattod.2020.10.027

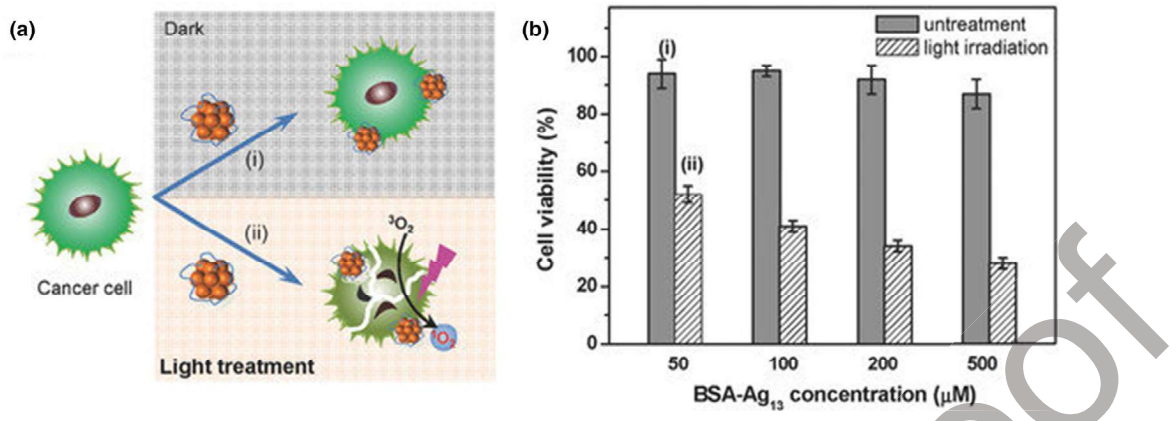

FIGURE 14

BSA-templated AgNCs as PSs for PDT. (a) Schematic diagram showing photodynamic treatment of MCF-7 cancer cells using BSA-Ag_{13} NC. (b) MTT assay histogram of MCF-7 cancer cells treated with BSA-Ag_{13} NC ranging from 50 to 500 × 10^{-6} M (Ag basis) without (i) and with light irradiation (ii) [316]. Reproduced with permission from Ref. [316]. Copyright 2016 Wiley.

and bioimaging capabilities (Fig. 15a) [277]. Irradiating MFNCs-treated HeLa cells with an 808-nm NIR laser led to a noticeable decrease in cell viability, indicating the high plasmonic PTT efficiency of the MFNCs *in vitro* (Fig. 15b) [319]. In this study, however, BSA-AuNCs were used for bioimaging purposes, without exploring their ability to induce PTT.

Gu et al. on the contrary designed polymeric nanocapsules loaded with BSA-AuNCs plus ICG, and functionalized with an RGD peptide to mediate PTT against glioblastoma [319]. The nanoformulation showed remarkable photothermal activity under 808-nm laser irradiation, killing >95% of U87-MG cells after irradiation at a power density of 2 W/cm^2. The intrinsic fluorescence of AuNCs together with the co-loaded ICG allowed for dual-modality fluorescence imaging, using either one-photon or two-photon excitation.

Using a different heat-triggered approach, Cifuentes-Rius and colleagues showed that BSA-AuNCs induced cytotoxicity to a wide range of cells when exposed to a radiofrequency (RF) field in the microwave region (1 GHz) [320]. Despite the fact that that the heating pathways of AuNCs under RF excitation are still not fully understood, the study showed that cells treated with RF without the presence of BSA-AuNCs were not killed, and likewise, BSA-AuNCs alone were non-toxic to the cells (Fig. 15c). The same group showed that the heat induced by BSA-AuNCs acted as a chemosensitizer by increasing the effectiveness of cytotoxic drugs [321], which could lead to a reduction of dosage and frequency of treatment.

Other types of protein-MNCs have been used as effective therapeutic agents for PTT. For instance, the *in vivo* hyperthermia efficiency of BSA-CuS-NCs was assessed in tumor-bearing mice [322]. Infrared thermography showed the temperature elevation at the tumor under irradiation, indicating the mild hyperthermia efficacy of BSA-CuS-NCs. Their *in vivo* PTT efficacy was evaluated after injection into tumor-bearing mice. Profound damage to tumor cells without any harm to the healthy tissue was observed indicating their potency for *in vivo* hyperthermia.

Wang et al. synthesized BSA-capped smart gadolinium oxide nanocrystals (Gd_2O_3) conjugated to Cypate, a NIR dye with potential as a clinical theranostic agent. These nanocrystals were suitable for trimodal imaging, magnetic resonance, photoacoustic and NIR fluorescence, plus mediating PTT as a therapy (Fig. 15d) [323]. These BSA-GdNCs showed good tumor ablation under NIR irradiation (Fig. 15e), as well as increased tumor accumulation and cellular internalization. The advantage of this platform was the pH-responsive photothermal effect, tailored to be more potent in the lysosomal environment after endocytosis, together with their trimodal imaging capability, enabling tracking *in vitro*, *ex vivo* and *in vivo*.

Gd-based NCs were also employed by Yang and co-workers [324]. They prepared a BSA-coated Gd:CuS hybrid nanotheranostic for PTT as well as dual imaging, magnetic resonance and photoacoustic. The protein-MNCs showed a strong NIR photothermal conversion, and potent tumor ablation capacity when irradiated with a 980-nm laser. Tumor-bearing mice treated with BSA-(Gd:CuS)NCs showed a remarkable regression in tumor growth, some of which were completely eliminated 6 days post-treatment.

Ruthenium sulfide (RuS)-based NCs have also shown enhanced photothermal activity under 808-nm laser irradiation [325]. In this work, Lu et al. used denatured BSA and polyethylene glycol (PEG) to coat RuS NCs. This nanomaterial had the ability to accumulate in the tumor to unprecedented levels, presumably due to its long circulation times. While all the control treatments showed no change in tumor growth, mice treated with BSA/PEG-(RuS)NCs had tumors that were eradicated within 4 days after treatment (Fig. 15f). This novel protein-MNC represents a potent photothermal agent for cancer PTT.

MNC-containing nanocomposites for enhanced bioimaging and controlled release

Aside from the potential of protein-protected MNCs as effective tracking probes in imaging applications, they could also be used as simultaneous delivery and therapy agents (theranostics) for human diseases in biomedical applications [45]. This capability could be attributed to good water solubility of these agents owing to the protein moiety which dissolves poorly water-soluble drugs while maintaining drug activity. More importantly, the delivery of these drugs can be tracked *via* the luminescence of the MNCs.

Uncorrected Proof

Please cite this article in press as: I. Zare et al., Materials Today, (2020), https://doi.org/10.1016/j.mattod.2020.10.027

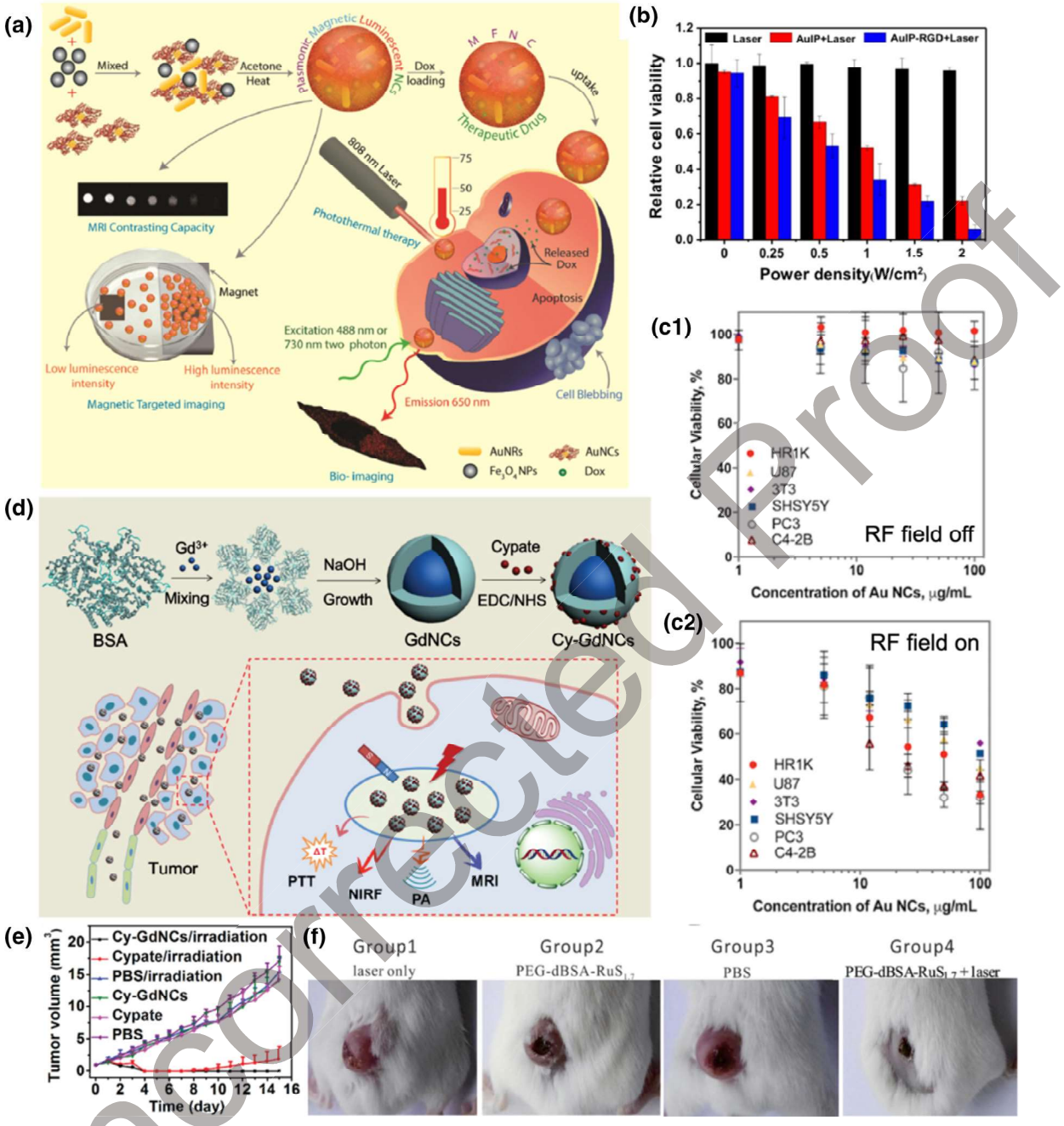

FIGURE 15

Different protein-stabilized MNCs design strategies for PTT. (a) Schematic of the synthesis and implementation of MFNCs [277] (Reproduced with permission from Ref. [277]. Copyright 2017 American Chemical Society.) and (b) their performance under NIR laser irradiation with different power densities [319]. Reproduced with permission from Ref. [319]. Copyright 2016 Royal Society of Chemistry. (c) Cytotoxicity of BSA-AuNCs to different types of cells – B-lymphocyte cells (HR1K), glioblastoma (U87), fibroblasts (3T3), neuroblastoma (SHSY5Y) and prostate cancer (PC3 and C4-2B) cells – before (1) and after (2) exposing them to a 1 GHz RF field [320]. Reproduced with permission from Ref. [320]. Copyright 2017 American Chemical Society. (d) Scheme of the strategy followed by Wang et al. in the synthesis and application of their GdNCs for dual imaging and PTT, (e) showing successful tumor eradication after 4 days of treatment [323]. Reproduced with permission from Ref. [323]. Copyright 2015 Wiley. (f) Photos of tumor-bearing mice showing tumor reduction after treatment with RuS NCs following laser irradiation (Group 4) as compared to the other controls (Group 1–3) where the tumors have kept growing [325]. Reproduced with permission from Ref. [325]. Copyright 2017 Nature Publishing Group.

In addition, MNCs allow drugs and genes to be delivered into specific target cells to inhibit their growth and kill them in a more controllable fashion [23,30,41,270,280,326–330]. This is why a lot of effort has been made to create nanocomposites composed of polymers or proteins-coating MNCs in order to provide new features for controlled release of therapeutics – triggered by external or endogenous stimuli – and simultaneous imaging.

The self-assembly of AuNCs in the presence of pH-responsive polymers was studied by Le Guevel and colleagues [331]. These nanogels were composed of GSH-AuNCs plus a cationic polymer

Uncorrected Proof

Please cite this article in press as: I. Zare et al., Materials Today, (2020), https://doi.org/10.1016/j.mattod.2020.10.027

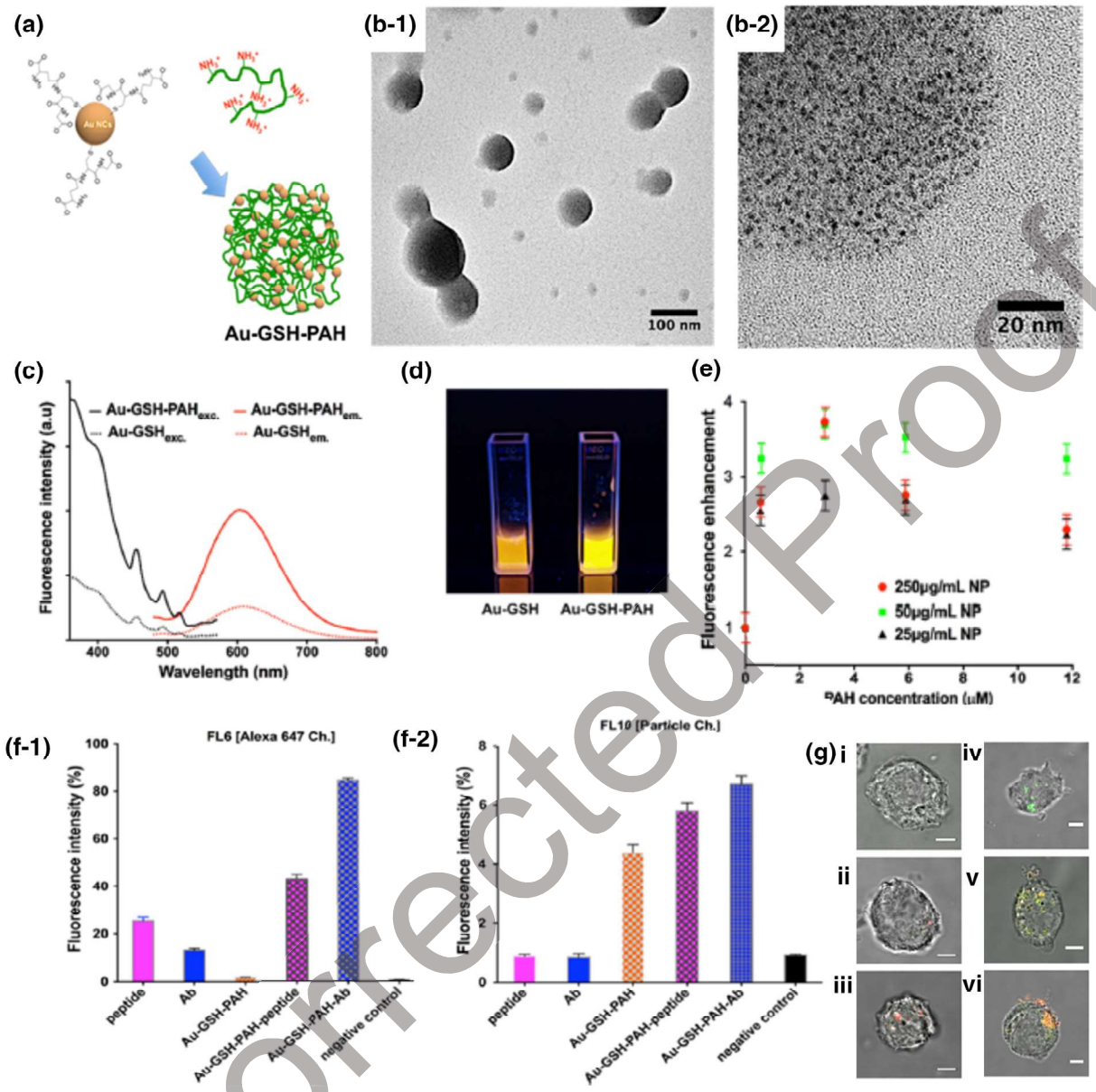

FIGURE 16

Self-assembly of AuNCs in the presence of the pH-responsive polymer (poly(allyl amine hydrochloride, PAH. (a) Scheme of the process to obtain self-assembled GSH-capped AuNCs and a cationic polymer (PAH) as cross-linking agent. (b) TEM images of the cross-linked compound at different magnifications. (c) Excitation and emission spectra of before (dashed lines) and after cross-linking with PAH (solid lines). (d) Fluorescence emission under UV illumination (λexc = 366 nm) of AuNCs before (left) and after (right) self-assembling with PAH. (e) Enhancement of the fluorescence signal (λexc/λem = 450 nm/600 nm) of the self-assembled complex with PAH concentration and NP concentration. (f) Fluorescence signal of cells incubated with fluorescently-labelled peptide or Ab-loaded complexes, unloaded complexes or free biomolecules (peptide and Ab). Detection of fluorescence by flow cytometry from (f-1) labelled biomolecules and (f-2) the self-assembled complex. (g) Confocal microscopy images of cells incubated with (1) PBS, (2) free peptide, (3) free Ab, (4) unloaded self-assembled AuNCs-PAH, (5) peptide-loaded self-assembled AuNCs-PAH and (6) Ab-loaded self-assembled AuNCs-PAH. Green: NPs; Red: free biomolecules. Scale bar: 5 μm [331]. Reproduced with permission from Ref. [331]. Copyright 2016 American Chemical Society.

Uncorrected Proof

(polyallyl amine hydrochloride (PAH)) and exhibited pH-dependent swelling ability and 4-fold enhancement of fluorescence (Fig. 16). The authors explained this increase in fluorescence by the phenomenon of AIE reported by Xie's group [332]. The reversible pH-dependent swelling capability of the nanogels, allowed the study of the cross-linking effect between AuNCs, proving that the electrostatic interaction between clusters not only enhanced the emission, but also the fluorescence lifetime. These properties were demonstrated in cell culture delivered by either Abs or peptides, and fluorescence-based imaging techniques.

Driven by the opportunities to enhance the PL efficiency of thiolated-AuNCs using the AIE phenomena, Qu's team used MOFs to achieve controlled release and fluorescence monitoring of a model compound (Fig. 17a) [333]. These 150-nm nanostructures (Fig. 17b) were able to encapsulate AuNCs, almost doubling their QY to 7.74% (Fig. 17c). Due to the pH-dependent dissociation of their MOF structure, AuNCs were able to disassemble the

Please cite this article in press as: I. Zare et al., Materials Today, (2020), https://doi.org/10.1016/j.mattod.2020.10.027

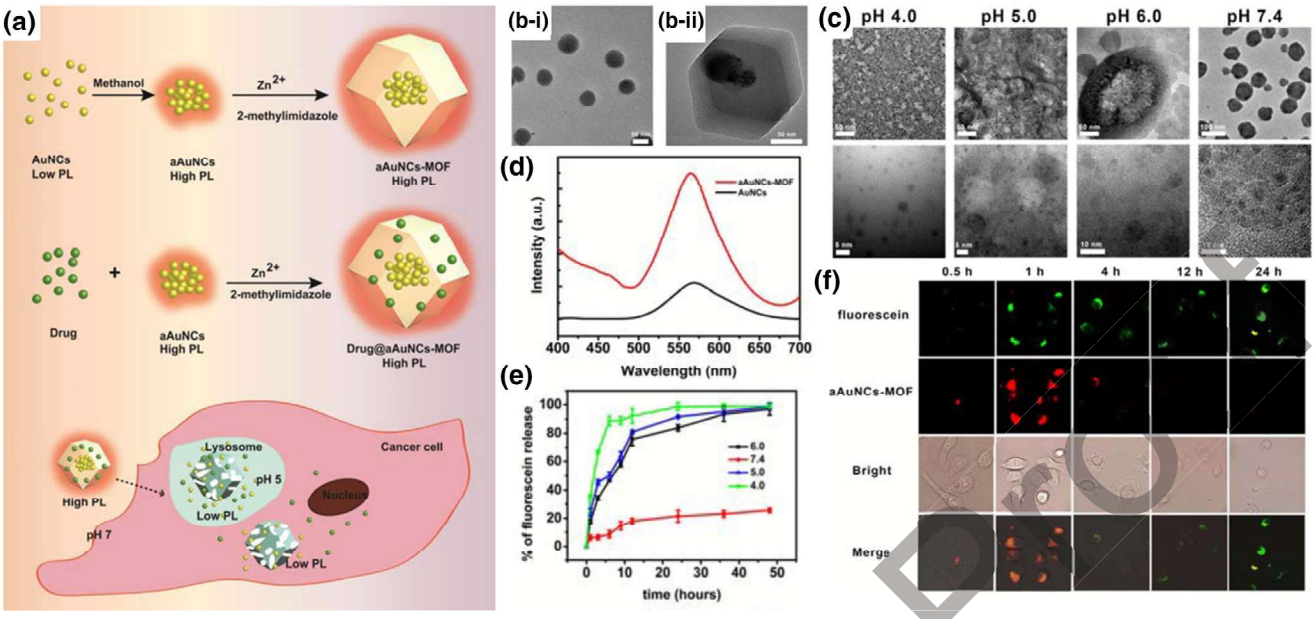

FIGURE 17

Encapsulation of AuNCs into MOFs for controlled release of therapeutics. (a) Scheme representing how aggregated AuNCs (aAuNCs) together with drugs can be encapsulated into MOFs enhancing their PL performance. This nanocomplex is a powerful tool for real-time imaging of hydrophobic drug release. (b) TEM images of (b-1) free aAuNCs and (b-2) encapsulated within the MOF. (c) TEM images of the aAuNC-MOF after 24 h in buffer at different pH values. (d) Fluorescence spectrum of well dispersed AuNCs and aAuNCs-MOFs at physiological pH. $\lambda exc = 365$ nm. (e) Release kinetics of fluorescein previously loaded into aAuNCs-MOFs at different pH for 48 h. (f) Fluorescence microscopy images of HeLa cells incubated with fluorescein-loaded aAuNCs-MOFs. Green: fluorescein; Red: aAuNCs. Magnification: 40x [333]. Reproduced with permission from Ref. [333]. Copyright 2017 Royal Society of Chemistry.

framework decreasing their luminescence providing a real-time tracking platform to monitor the release (Fig. 17c and d). Moreover, AuNCs could be co-loaded with hydrophobic drugs and dyes achieving a controlled release of both agents at pH values below 6 (Fig. 17e and f).

Serum albumin-based NPs have been shown to be non-toxic and biocompatible drug carriers [334]. Thus, the interest in encapsulating and cross-linking albumin-coated MNCs has increased. One advantage of albumin is that it possesses a variety of functionalities allowing specific conjugation and biological interactions to take place. In order to enhance pDNA loading, Dutta et al. used a cationic BSA to embed bimetallic Au-Ag MNCs into its structure [27]. Using this approach, the delivery of a therapeutic suicide gene to HeLa cancer cells accompanied with ROS generation by the clusters inducing apoptosis was possible. Moreover, they demonstrated simultaneous bioimaging to prove superior cell uptake compared to free therapeutic DNA, where the lack of positive charge caused poor cell internalization. In another work, researchers synthesized BSA-AuNCs at a high temperature (95 °C) forming BSA cross-links into a larger rod-shaped structure [335]. The binding of these nanostructures to bacterial cells could be controlled by manipulating their electrostatic charge. They used this nanostructure to not only label *E. coli* cells, but also to bind negatively charged antibiotics (ampicillin, chloramphenicol) and deliver them to bacterial cells with complete growth inhibition.

Other proteins have been used to synthesize MNCs. For example, Cyt c, a protein triggering apoptosis once it reaches the cytoplasm, was employed to produce fluorescent and cytotoxic AuNCs [336]. This work showed that once Cyt c-AuNCs were taken up by the cells, the cellular GSH replaced the capping agent, releasing free Cyt c inside the cell. Moreover, they demonstrated that the Cyt c-AuNCs accumulated into the mitochondria, showing that these NPs could be a novel mitochondria-targeted probe.

INS has also been used as a template to synthesize highly-fluorescent AuNCs [109]. In this interesting work, the functionality of INS was maintained, and therefore could be used for blood-glucose regulation as well as for cell imaging.

Protein-MNCs have also been used as a key ingredient in lipid-based nanocarriers. For example, BSA-AuNCs have been used to stabilize lipid nanocapsules loaded with curcumin. The NCs were used not only to stabilize the core–shell structure of the capsules, but also to follow their cell internalization through fluorescence microscopy [337]. Wang et al. used lipid vesicles to deliver a complex of AuNCs and Cas9 protein and single guide RNA (sgRNA) for CRISPR (clustered regularly interspaced short palindromic repeats) [338]. The positive charges of TAT (HIV-1-transactivor of transcription) peptide-protected AuNCs was bound to Cas 9 protein and sgRNA plasmid in order to facilitate the nuclear delivery of the gene editing tool. The fluorescence of the TAT-AuNCs allowed the tracking of the nanoconjugates, which accumulated near the nucleus at longer incubation times. An *in vivo* study in a subcutaneous melanoma mouse model showed effective tumor reduction (5 fold) after intratumoral injection compared to the controls.

Small interference RNA (siRNA) has recently gained a lot of attention as a potent anti-cancer modality. Taking advantage of the negative charge on the backbone structure, Jiang et al. formed a complex between nerve growth factor (NGF) siRNA

Uncorrected Proof

Please cite this article in press as: I. Zare et al., Materials Today, (2020), https://doi.org/10.1016/j.mattod.2020.10.027

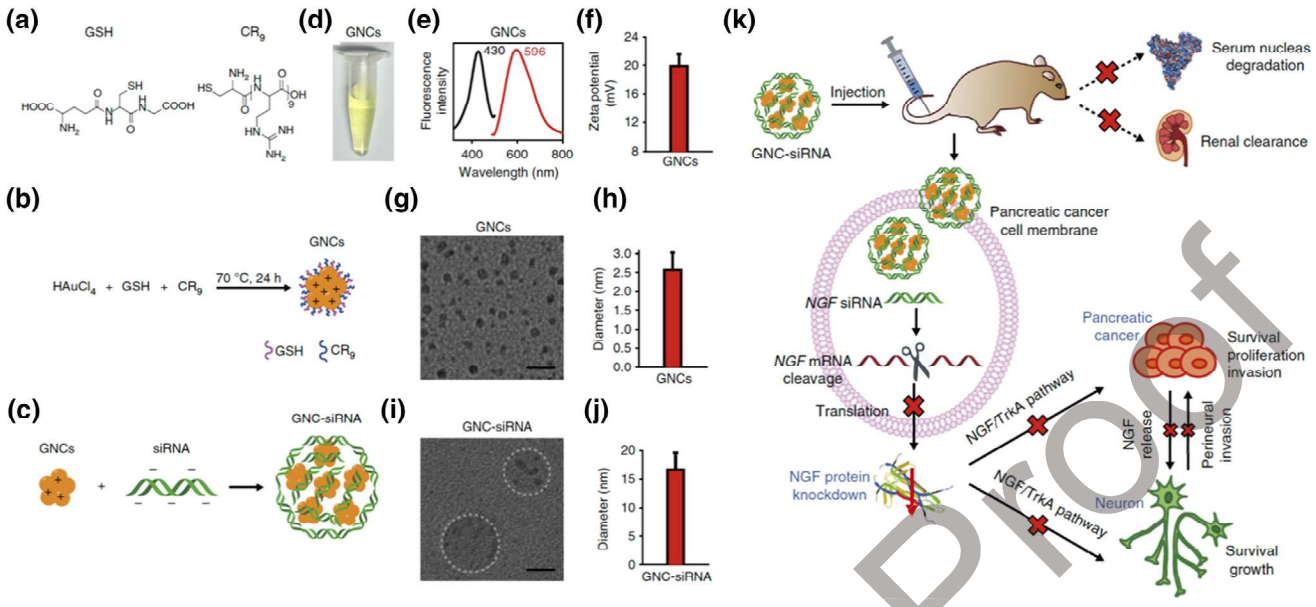

FIGURE 18

AuNC-siRNA complexes for pancreatic cancer treatment. (a) Chemical formulas of GSH and oligoarginine (CR9) and (b) the synthetic route to form AuNCs and (c) subsequent AuNCs-siRNA complexes by electrostatic interaction. (d) Visual yellow appearance and (e) excitation and emission spectra of AuNCs solution. (f) Positive surface charge of AuNCs (Mean ± SD) before forming the complex. (g, i) Cryo-TEM images and (h, j) size (Mean ± SD) of AuNCs and AuNC-siRNA, respectively. Scale bar: 20 nm. (k) Schematic of the delivery mechanism followed by the AuNC-siRNA complex NGF silencing. Importantly, the complex protects the siRNA from nuclease degradation and renal clearance, favors its accumulation to tumor cells, and allows efficient silencing in pancreatic tumors. The knockdown of NGF expression inhibits the progression of pancreatic cancer and the neurogenesis of the tumour microenvironment [339] Reproduced with permission from Ref. [339]. Copyright 2017 Nature Publishing Group.

and positively-charged AuNCs coated with GSH and oligoarginine for pancreatic cancer treatment (Fig. 18) [339]. The clusters alone had a diameter <3 nm while the siRNA-NC complex reached a size of approximately 16 nm. This size provided the nanocomplex with a prolonged blood circulation time in a subcutaneous pancreatic cancer mouse model. The intrinsic fluorescence of the AuNCs enabled tracking of the complex with enhanced permeation and retention within the tumor. In an orthotopic patient-derived xenograft model, they showed impressive results concerning anti-tumor activity and gene-knockdown using these nanocomplexes.

In addition to Au or Ag-based NCs, CdNCs have also been studied as a theranostic nanovehicle for simultaneous cancer cell imaging and drug delivery. CdNCs conjugated with HA and BSA were developed as a theranostic pH-responsive nanocarrier for MCF-7 breast cancer cells over-expressing CD44 [30].

Antibacterial activity

AuNCs (unlike AgNPs) do not show intrinsic bactericidal activity, therefore they require functionalization with proteins or other molecules to be used for antibacterial applications [340]. Some of the proteins immobilized on MNCs act either as bactericidal agents against Gram-positive and Gram-negative bacteria [341]. As an example, Chen and colleagues prepared LYZ–AuNCs via microwave assisted synthesis that could target and effectively inhibit pathogenic bacteria including, pan-drug-resistant *Acinetobacter baumannii* and vancomycin (Van)-resistant *Enterococcus faecalis* [342]. The interaction between LYZ–AuNCs and antibiotic-resistant bacteria showed enhanced antimicrobial activity compared to free LYZ. LYZ–AuNCs not only targeted bacteria as labeling agents, but also inhibited the growth of antibiotic-resistant species. In addition, Khlebtsov and coworkers synthesized BSA-AuNCs conjugated to human anti-staphylococcal immunoglobulin (antiSA–IgG) plus the photosensitizing dye Photosens™ (PS) (Au–BSA–antiSAIgG–PS) for effective photodynamic inactivation of MSSA and MRSA under 660-nm light irradiation [343]. The observed inactivation of bacteria was due to the biospecific targeting of IgG molecules to pathogenic bacteria, as well as the photodynamic activity of the PS. Yang et al. also employed papain-protected CuNCs as promising antimicrobial agents towards Gram-positive and Gram-negative bacteria and actual wound infections. The key feature of papain-CuNCs was the ability to convert added H_2O_2 to •OH to inhibit growth of the Gram-positive bacteria *S. aureus* and Gram-negative bacteria *E. coli*. Mice with infected wounds treated by papain-CuNCs plus H_2O_2 showed no erythema, edema and lesser scabs indicating the killing of bacteria in the wounds [344].

On the other hand, Nain and coworkers developed 1,3-propanedithiol/BSA–CuNCs that are able to generation of ascorbyl (Asc.) and perhydroxyl (HOO.) radicals with superior bactericidal effects against non-multidrug-resistant bacteria (*S. aureus*, *E. coli*, *Pseudomonas aeruginosa*, and *Salmonella enteritidis*) as well as multidrug-resistant bacteria such as MRSA [341]. They used the 1,3-propanedithiol, an organic compound with two thiol groups which acts as carriers for lipophilic to improve the internalization of CuNCs into bacteria [345]. They demonstrated that 1,3-propanedithiol/BSA–CuNCs was >200-fold higher bactericidal activity than 1,3-propanedithiol, which resulted in i) the destabi-

Uncorrected Proof

Please cite this article in press as: I. Zare et al., Materials Today, (2020), https://doi.org/10.1016/j.mattod.2020.10.027

lization of the bacterial membranes, ii) satisfactory biocompatibility, and iii) stronger photoluminescent intensity. Further, they revealed that 1,3-propanedithiol/BSA–CuNCs decorated carbon fiber fabrics (CFFs) possess great potential inhibitory activity against *S. aureus* and *E. coli* cells. Their results showed that 1,3-propanedithiol/BSA–CuNCs-functionalized CFFs acted as an effective antibacterial agent, where less than 5% of the bacteria remained alive, and their antifouling properties could be exploited for the fabrication of antibacterial dressings.

Conclusions and future perspectives

In this review we have summarized the burgeoning growth of interest in protein-protected MNCs for imaging and therapy in health care applications. Concerning the practical future use of MNCs in clinical applications, there is still a long way to go to provide more precise information on their performance and fate in human tissue including their circulation in blood and clearance from the body. Considering some reports on the toxicity of protein-protected MNCs, their safety over the long term should be considered a paramount issue. The accumulation of some protein-MNCs in the liver and the spleen, could cause irreparable damage, which illustrates how improved control of the size of MNCs is necessary to predict clearance and excretion from the body. Moreover, the future application in clinical practices requires considerable effort to generate reproducible highly luminescent MNCs with high photostability and longer fluorescence lifetimes. These features are prerequisites for the detection of malignant cells and infections, which may possess biomarkers at ultra-trace levels. Recent developments in optical imaging techniques, such as multi-photon excitation microscopy – which allows studies of biological interactions at a deep cellular level – has motivated intensive research in developing multi-photon absorption fluorophores. The strategies described in this review can be translated to the nonlinear optical regime (two-photon excited fluorescence for instance), that is useful for multi-photon excitation microscopy, even if this field is still in its infancy [346–350]. Despite these identified limitations, there is still scope for feasible application of protein-protected MNCs as theranostic agents.

In the last decade a wealth of information has been accumulated concerning structure–property relationships of atomically-precise MNCs, which are defined as MNCs that can be described by a precise molecular formula, including the number of metal atoms and the number of protecting ligands [1]. By the use of single crystal diffraction or through a combination of mass spectrometry, material characterization and theoretical prediction, the core and surface structure of the MNC can be elucidated or at least strongly inferred. For these systems, the optoelectronic properties of the MNCs can then be directly correlated with the structure and composition. This is not really the case for protein-MNCs. Thus far, much of MNC structural information has been deduced solely from the measured mass of metal atoms per protein molecule. More is understood regarding the combination of the protein, metal atom type and reaction conditions that can lead to particular luminescence/sensing/imaging properties (Fig. 2a). Nevertheless, there may be some commonality between thiolate-protected AgNCs and AuNCs with known structures, and those AgNCs and AuNCs stabilized by proteins which are rich in cysteine residues (*e.g.*, BSA). For example, the optical properties (absorbance, emission and photophysical properties) of BSA-AuNCs and $Au_{22}(SG)_{18}$ NCs are strikingly similar [351]. In fact, it was shown that the luminescence appeared to originate from Au_{10} catenane structures (interlocked Au-S rings) rigidified by BSA protein templates [81], because similar structural motifs (interlocking Au-S rings) had been elucidated for $Au_{22}(SG)_{18}$ NCs. Researchers should be cautioned that assuming there are structural similarities between small ligand-protected MNCs and protein-protected MNCs could be misleading, especially where there is no direct, clear structural evidence, such as is the case for $Au_{25}(SR)_{18}$ NCs and BSA-AuNCs. Due to the challenge of growing single crystals of protein-MNCs, employing modern structural characterization techniques such as single particle cryo-electron microscopy, synchrotron-based X-ray spectroscopy, or even X-ray free electron laser measurements could be necessary to understand the stabilizing interactions from the protein environment and to untangle the protein-MNC structural components within. Advances in computational chemistry and hybrid calculations of many atom systems (molecular dynamics combined with quantum mechanical treatment for systems containing 1000 s of atoms) should also make an impact on understanding the most probable binding sites for MNCs within a protein molecule and the effect of protein residues in controlling MNC size and structure. By using these advanced characterization methods, a deeper and more precise understanding of protein-MNC structure and associated properties could be achieved. Toward a better understanding of protein-MNC interactions in biological media or environments, the aforementioned electron/X-ray techniques will also be relevant for observing structural and chemical changes that occur *in situ* and in real time. With the advances in, and wider availability of, fourth-generation synchrotron light sources, *in situ* spectroscopic measurements of very dilute metals (*e.g.*, protein-MNCs inside cells) will be more achievable, leading to a better understanding of how protein-MNCs perform in biological environments and conditions and toward an improved design for their intended applications.

Instead of using protein molecules as a scaffold for synthesizing MNCs, another option is use ligand exchange or click chemistry to attach a protein molecule onto an atomically-precise MNC that has well-characterized structural and electronic properties. For example, using highly luminescent MNCs, a protecting ligand could be exchanged for a protein molecule using an extended linker to avoid adverse steric interactions. Such linkers could use a facile click-chemistry terminus that could be coupled to a reciprocal counterpart (*e.g.*, azide-alkyne cycloaddition) on the protein molecule. The MNC would then act as a luminescent marker and could be a useful approach for cellular imaging applications. Glycoprotein functionalized AuNCs could become attractive tools enabling analysis and applications of carbohydrate-protein interactions as recently demonstrated by Reichardt [153]. This specific ligand exchange reaction was studied mechanistically using a computational approach [352]. Such an approach could also preserve more of the protein bioactivity without needing amino acid residues to interact with reactive metal ion reagents. Furthermore, borrowing from progress made

Uncorrected Proof

Please cite this article in press as: I. Zare et al., Materials Today, (2020), https://doi.org/10.1016/j.mattod.2020.10.027

in the field of atomically-precise MNCs, the effect of metal atom doping or bimetallic clusters could demonstrate marked increases in QY [77,353]. Bimetallic protein-MNCs systems have been synthesized, but with a much less dramatic increase in luminescence properties. Apart from the case of atomically-precise MNCs with known crystal structures and specific metal atom locations, the arrangement and type of protein moieties that stabilize metal clusters and the structural composition are still relatively unknown. To achieve the same kind of leap forward in QY or tunable emission properties using protein-MNCs, better structural determination of the MNCs within the protein scaffold will be required.

Although several protein-templated MNCs have been designed for selective sensing of analytes, optimization of the parameters is still a challenge to meet the demands for cost effective clinical diagnostic applications involving complex biological systems. To address these issues, functionalization of the protein surface with appropriate recognition elements is very important, along with the use of lower quantities of expensive proteins for cost reduction. Nanocomposites comprised of surface-grown or deposited protein-MNCs are promising hybrid nano-bio platforms leading to synergistic energy/charge transfer properties that could enhance the emission properties or sensitivity to detect analytes [162,354,355]. In particular, a Trf-AuNCs/GO nanocomposite was fabricated as a "turn-on" NIR fluorescent probe for bioimaging cancer cells and small animals [279]. Secondly, for better quantitative evaluation of the sensing ability of the probe, single molecule techniques like fluorescence correlation spectroscopy (FCS) and single particle tracking could be employed instead of traditional fluorescence enhancement or quenching. The application of optical-based single molecule analysis in sensing studies, would never be a limitation, since the MNCs possess very good photostability and high QY.

The extraordinary properties of protein-MNCs such as tunable fluorescence, enzyme-mimicking activity, and good biocompatibility make them excellent probes for applications in the detection of neurotransmitters or pathogenic microorganisms. The signal transduction mechanisms include target-induced fluorescence quenching or enhancement, enzyme-like activity for catalysis, and fluorescent sensor arrays. Although current studies have shown great progress in this field, several issues must be addressed for their real-world application. First, most protein-MNCs are still not market-ready for *in vivo* imaging or detection due to their low QY and relatively low sensitivity. Future studies should be focused on the preparation of protein-MNCs with improved properties such as higher QY and more versatile fluorescence properties. MNCs with multiple excitation wavelengths and corresponding emission wavelengths are expected to broaden the applications for multiplex detection with enhanced accuracy. To enhance the sensitivity, dual-read-out detection methods can be employed, because some protein-MNCs can act as a "nanozyme" catalyzing reactions for signal amplification. The combination of protein-MNCs with other technologies such as enzyme-mediated signal amplification could be beneficial for *in vivo* applications with enhanced sensitivity. Secondly, as mentioned above, the precise structures of most MNCs are still under investigation. Fine control over the MNC structure is necessary to design specific nanovehicles that can be applied for detecting neurotransmitters or microorganisms. To address both applications, the structure–function relationships of protein-MNCs should be studied in more detail to understand their physicochemical properties to make further progress in biosensing applications. Protein-protected MNCs could be versatile tools for the development of ultra-sensitive immunoassays, achieving limits of detection in the range of ultra-trace amounts (ppt, nM), offering the possibility of multiplexed assays, with a wide variety of signal transduction processes either electrochemical or optical, and being able to be applied directly to a complex analytical matrix (*e.g.*, urine, serum, *etc.*). They can also act as surface modifiers, supports for the detection molecules, or even as catalysts for the detection reaction. The trend to use bimetallic MNCs and nanocomposites has opened new doors for the sensitivity of the detection step in immunoassays. Finally, miniaturization of the assay assembly are becoming a must in the development of immunoassays, due to the needs for rapid, disposable, sensitive and reliable tests for diagnostic, prognostic and follow up applications. Thus, the number of published studies using microfluidic chips, paper-based tests, *etc.* as the final platforms is increasing. Moreover, the miniaturization or simplification of the instruments – smartphones, for example - is also increasing [356,357]. These trends show the need in clinical medicine to bring this kind of device close to the patients (*i.e.*, at the bedside) and to make it user-friendly for clinicians in hospitals.

Protein-MNCs benefit from the optical features inherent in the metal core, and can be functionalized with Abs, aptamers and DNA sequences, providing tumor-recognition moieties, bio-compatibility and effective renal clearance stemming from their ultrasmall size. Nevertheless, remaining concerns are largely due to their toxicity, weak fluorescence as well as questions about biodistribution. Although the functionality of protein-MNCs suggests their superiority to other fluorescent probes, some necessary steps should be taken to adjust their functionality in order to provide precise numbers of moieties on the surface. A judicious effort should be put into gaining deeper understanding of whether adjusting the functionality affects the toxicity or not. What other variables should be controlled to address the toxicity and biodistribution? How do the functional groups control the QY of the protein-protected MNCs, which is vital in bioimaging applications? Although protein-MNCs will most likely pave a new way towards bioimaging applications, a deeper understanding of the toxicity of protein-protected MNCs, the variables determining the QY, and their biodistribution, is necessary before they are translated to clinical applications.

A large number of protein-MNCs have been developed for diagnostic purposes, relating to cancer and a wide variety of other diseases. Advances in synthetic techniques have proved to be useful for broadening their applications both *in vitro* and *in vivo*. However, only a few of these MNCs have been implemented for clinical studies, which may be partly due to the low penetration depth in living tissue of their fluorescence emission in the visible region. Although some Au-based MNCs emit fluorescence at around 800 nm, their fluorescence QY is far from satisfactory. Besides, current fluorescence probes based on MNCs need more functionality to expand their applications in bioimaging, including targeting to specific tissues or cells, and respon-

Uncorrected Proof

Please cite this article in press as: I. Zare et al., Materials Today, (2020), https://doi.org/10.1016/j.mattod.2020.10.027

siveness to stimuli either internal or external. The joint efforts of chemists, material scientists and biologists are expected to propel protein-protected MNCs to ever-greater achievements in bioimaging.

Thus far, protein-protected MNCs have shown promising performance in different therapeutic areas such as chemotherapy, radiotherapy, PTT and PDT. In general, their small diameter, good biocompatibility, intrinsic fluorescence, easy surface functionalization, and colloidal stability in biological environments make them ideal candidates as theranostic agents for cancer, due to: (i) long circulation times; (ii) accumulation deep within the tumor; and (iii) convenient tracking via fluorescence. Over recent years, there have therefore been many encouraging studies in the use of MNCs as nanomedicines in preclinical models; however, their translation into the clinical realm remains relatively unexplored. A thorough evaluation of the fate of the nanomaterials after treatment, *in vivo* biodegradability, and potential long-term side effects in both preclinical and clinical settings will be required before they are ready for translation.

Conflicts of interest

M.R.H. is on the following Scientific Advisory Boards: Transdermal Cap, Inc., Cleveland, OH; BeWell Global, Inc., Wan Chai, Hong Kong; Hologenix, Inc. Santa Monica, CA; LumiThera, Inc., Poulsbo, WA; Vielight, Toronto, Canada; Bright Photomedicine, Sao Paulo, Brazil; Quantum Dynamics LLC, Cambridge, MA; Global Photon, Inc., Bee Cave, TX; Medical Coherence, Boston MA; NeuroThera, Newark DE; JOOVV, Inc., Minneapolis-St. Paul MN; AIRx Medical, Pleasanton CA; FIR Industries, Inc. Ramsey, NJ; UVLRx Therapeutics, Oldsmar, FL; UltraluxUV, Inc., Lansing MI; Illumiheal&Petthera, Shoreline, WA; MB Lasertherapy, Houston, TX; ARRC LED, San Clemente, CA; Varuna Biomedical Corp. Incline Village, NV; Niraxx Light Therapeutics, Inc., Boston, MA; Dr Hamblin has been a consultant for Lexington Int, Boca Raton, FL; USHIO Corp, Japan; Merck KGaA, Darmstadt, Germany; Philips Electronics Nederland B.V.; Johnson & Johnson, Inc., Philadelphia, PA; Sanofi-Aventis Deutschland GmbH, Frankfurt am Main, Germany; Dr Hamblin is a stockholder in Global Photon, Inc., Bee Cave, TX; Mitonix, Newark, DE. Other authors report no conflicts of interest.

Acknowledgements

D.M.C. acknowledges research funding through a European Union Marie-Skłodowska Curie Action International Fellowship (Project: BioNanoMagnets). A.C-R. acknowledges support from the National Health and Medical Research Council (NHMRC) of Australia (Grant GNT1112432). K.L-F acknowledges support from the National Science Foundation of China (Grant Nos. 31871005, 31900981), Chinese Academy of Sciences under Grant No. YJKYYQ20180048 and Youth Innovation Promotion Association CAS (2019093). M.R.H. was funded by US NIH Grants R01AI050875 and R21AI121700. Y.X. acknowledges the "Hundred Talents Program" from Zhejiang University.

References

[1] R. Jin et al., Chem. Rev. 116 (2016) 10346–10413.
[2] Y. Tao et al., Chem. Soc. Rev. 44 (2015) 8636–8663.
[3] Y.-C. Shiang et al., J. Mater. Chem. 22 (2012) 12972–12982.
[4] M. Cui, Y. Zhao, Q. Song, TrAC, Trends Anal. Chem. 57 (2014) 73–82.
[5] J. Li, J.-J. Zhu, K. Xu, TrAC, Trends Anal. Chem. 58 (2014) 90–98.
[6] I. Chakraborty, T. Pradeep, Chem. Rev. (2017).
[7] M.G. Taylor, G. Mpourmpakis, Nat. Commun. 8 (2017) 15988.
[8] C. Deraedt et al., Nano Lett. 17 (2017) 1853–1862.
[9] R. Jin, Nanoscale 2 (2010) 343–362.
[10] B.H. Kim et al., Chem. Mater. 26 (2014) 59–71.
[11] L. Zhang, E. Wang, Nano Today 9 (2014) 132–157.
[12] X.-D. Zhang, et al., 5 (2015) 8669.
[13] X.-D. Zhang et al., Adv. Healthcare Mater. 3 (2014) 133–141.
[14] X. Yuan et al., Chemistry 8 (2013) 858–871.
[15] G. Schmid et al., Chem. Soc. Rev. 28 (1999) 179–185.
[16] M.B. Dickerson, K.H. Sandhage, R.R. Naik, Chem. Rev. 108 (2008) 4935–4978.
[17] N. Goswami, K. Zheng, J. Xie, Nanoscale 6 (2014) 13328–13347.
[18] W.J. Crookes-Goodson, J.M. Slocik, R.R. Naik, Chem. Soc. Rev. 37 (2008) 2403–2412.
[19] H. Bönnemann, Ryan M. Richards, Eur. J. Inorg. Chem. 2001 (2001) 2455–2480.
[20] H. Li et al., Sens. Actuators, B 241 (2017) 1057–1062.
[21] E. Thyrhaug et al., Nat. Commun. 8 (2017) 15577.
[22] A. Kumar, V. Kumar, Chem. Rev. 114 (2014) 7044–7078.
[23] Y. Yu et al., Chem. Commun. 50 (2014) 13805–13808.
[24] J. Zhou, Y. Yang, C.-Y. Zhang, Chem. Rev. 115 (2015) 11669–11717.
[25] J. Xie, Y. Zheng, J.Y. Ying, J. Am. Chem. Soc. 131 (2009) 888–889.
[26] H. Chen et al., ACS Nano 9 (2015) 2173–2183.
[27] D. Dutta, A. Chattopadhyay, S.S. Ghosh, ACS Biomater. Sci. Eng. 2 (2016) 2090–2098.
[28] M. Shamsipur et al., Microchim. Acta 182 (2015) 1131–1141.
[29] C. Wang et al., Nanoscale 6 (2014) 1775–1781.
[30] M. Sarparast et al., Nano Res. (2016) 1–18.
[31] J.-M. Liu, J.-T. Chen, X.-P. Yan, Anal. Chem. 85 (2013) 3238–3245.
[32] C. Shao et al., J. Mater. Chem. 21 (2011) 2863–2866.
[33] J. He et al., Colloids Surf., A 518 (2017) 80–84.
[34] G. Xavier Le, D. Nicole, S. Marc, Nanotechnology 22 (2011) 275103.
[35] A.L. West et al., ACS Appl. Mater. Interfaces 8 (2016) 21221–21227.
[36] S. Gao et al., Sci. Rep. 4 (2014) 4384.
[37] D. Chen et al., ACS Appl. Mater. Interfaces 7 (2015) 18163–18169.
[38] M.-N. Su et al., Chin. Chem. Lett. 26 (2015) 1400–1402.
[39] A.D. Kurdekar et al., Nanoscale Adv. 2 (1) (2020) 304–314.
[40] G.S. Heo et al., ACS Appl. Mater. Interfaces 11 (22) (2019) 19669–19678.
[41] J.G. Croissant et al., J. Control. Release 229 (2016) 183–191.
[42] C. Lv, S. Yin, X. Zhang, J. Hu, T. Zhang, G. Zhao, Anal. Chim. Acta (2020).
[43] C.N. Loynachan et al., Nat. Nanotechnol. 14 (9) (2019) 883–890.
[44] P.L. Xavier et al., Nano Rev. 3 (2012) 1–16.
[45] Y. Yu et al., Adv. Healthcare Mater. 5 (2016) 1844–1859.
[46] Y. Hu, W. Guo, H. Wei, Isr. J. Chem. 55 (2015) 682–697.
[47] X. Tan, R. Jin, Wiley Interdiscip. Rev. Nanomed. Nanobiotechnol. 5 (2013) 569–581.
[48] J. Liu, TrAC, Trends Anal. Chem. 58 (2014) 99–111.
[49] T. Zhao et al., J. Environ. Sci. Health, Part C 33 (2015) 168–187.
[50] A.R.D. Voet, J.R.H. Tame, Curr. Opin. Biotechnol. 46 (2017) 14–19.
[51] Y. Zhao et al., Part. Part. Syst. Char. 36 (11) (2019) 1900298.
[52] Y. Zhao et al., Method. Appl. Fluoresc. 8 (1) (2019) 012001.
[53] E. Porret, X. Le Guével, J.L. Coll, J. Mater. Chem. B 8 (11) (2020) 2216–2232.
[54] X. Meng et al., Wiley Interdiscip. Rev. Nanomed. Nanobiotechnol. 12 (3) (2020) e1602.
[55] A.S. Kumar, W.L. Tseng, Anal. Methods 12 (14) (2020) 1809–1826.
[56] L. Liu, A. Corma, Chem. Rev. 118 (2018) 4981–5079.
[57] E.A. Ivleva et al., Mater. Des. (2020) 108771.
[58] de Souza, N., 2007. All that glitters but does not blink. Nat. Methods, 4(7), 540–540.
[59] L. Shang et al., Nano Res. 5 (2012) 531–542.
[60] M.J. Meziani et al., J. Phys. Chem. B 106 (2002) 11178–11182.
[61] M. Matulionyte et al., Int. J. Mol. Sci. 18 (2017) 378.
[62] A. Dutta et al., Chem. Commun. 53 (2017) 1277–1280.
[63] L. Shang, S. Dong, G.U. Nienhaus, Nano Today 6 (2011) 401–418.
[64] Y.N. Tan, J.Y. Lee, D.I.C. Wang, J. Am. Chem. Soc. 132 (2010) 5677–5686.
[65] Y. Yue et al., Nanoscale. 4 (7) (2012) 2251–2254.
[66] D. Ghosh et al., J. Phys. Chem. C 121 (24) (2017) 13335–13344.
[67] D. Ghosh et al., J. Phys. Chem. C 123 (28) (2019) 17598–17605.
[68] D. Ghosh et al., J. Phys. Chem. C 123 (48) (2019) 29408–29417.

Uncorrected Proof

[69] J. Zheng, P.R. Nicovich, R.M. Dickson, Annu. Rev. Phys. Chem. 58 (2007) 409–431.
[70] V.W.-W. Yam, V.K.-M. Au, S.Y.-L. Leung, Chem. Rev. 115 (2015) 7589–7728.
[71] N. Xu et al., Nanotechnology 27 (2016) 425602.
[72] H. Kawasaki et al., Adv. Funct. Mater. 21 (2011) 3508–3515.
[73] Y. Chen et al., J. Colloid Interface Sci. 396 (2013) 63–68.
[74] K. Chaudhari, P.L. Xavier, T. Pradeep, ACS Nano 5 (2011) 8816–8827.
[75] J.S. Mohanty et al., Nanoscale 4 (2012) 4255–4262.
[76] J.S. Mohanty et al., J. Phys. Chem. C 123 (47) (2019) 28969–28976.
[77] S. Wang et al., Angew. Chem. Int. Ed. 53 (2014) 2376–2380.
[78] C. Guo, J. Irudayaraj, Anal. Chem. 83 (8) (2011) 2883–2889.
[79] R. Ghosh et al., ACS Appl. Mater. Interfaces 6 (6) (2014) 3822–3828.
[80] N. Goswami et al., J. Phys. Chem. Lett. 7 (2016) 962–975.
[81] D.M. Chevrier et al., Chem. Sci. 9 (2018) 2782–2790.
[82] O. Yamauchi, A. Odani, M. Takani, J. Chem. Soc., Dalton Trans. (2002) 3411–3421.
[83] J.M. Dixon, S. Egusa, J. Am. Chem. Soc. 140 (2018) 2265–2271.
[84] B. Maity, et al., 8 (2017) 14820.
[85] N. Kundu et al., J. Phys. Chem. Lett. 8 (2017) 2291–2297.
[86] X.-D. Zhang et al., Biomaterials 33 (2012) 4628–4638.
[87] L. Dong et al., Small 11 (2015) 2571–2581.
[88] A. Soleilhac, F. Bertorelle, R. Antoine, Spectrochim. Acta Part A Mol. Biomol. Spectrosc. 193 (2018) 283–288.
[89] Z. Wu, R. Jin, Nano Lett. 10 (7) (2010) 2568–2573.
[90] M. Shamsipur et al., ACS Sustainable Chem. Eng. 6 (2018) 11123–11137.
[91] D.S. Yarramala et al., ACS Sustainable Chem. Eng. 5 (2017) 6064–6069.
[92] W. Wang et al., New J. Chem. 41 (2017) 3766–3772.
[93] M.A. Habeeb Muhammed et al., Eur. J. 16 (2010) 10103–10112.
[94] G. Yang et al., Sens. Actuators, B 251 (2017) 773–780.
[95] C. Fan et al., ACS Sensors 3 (2018) 441–450.
[96] H. Liu et al., Chem. Commun. 47 (2011) 4237–4239.
[97] N. Kumar Das et al., ChemPhysChem 19 (2018) 2218–2223.
[98] M. Zhu et al., J. Am. Chem. Soc. 130 (18) (2008) 5883–5885.
[99] K.D. Weerawardene, C.M. Aikens, J. Am. Chem. Soc. 138 (35) (2016) 11202–11210.
[100] X. Wen et al., J. Phys. Chem. C 116 (35) (2012) 19032–19038.
[101] X. Wen et al., J. Phys. Chem. C 116 (21) (2012) 11830–11836.
[102] J. Zheng, C. Zhang, R.M. Dickson, Phys. Rev. Lett. 93 (2004) 077402.
[103] J. Zheng et al., *Nanoscale* 4 (2012) 4073–4083.
[104] K.G. Stamplecoskie, Y.-S. Chen, P.V. Kamat, J. Phys. Chem. C 118 (2014) 1370–1376.
[105] S. Ghosh et al., J. Phys. Chem. Lett. 6 (2015) 1293–1298.
[106] N. Goswami et al., Anal. Chem. 83 (2011) 9676–9680.
[107] C.-J. Yu et al., Nanoscale 6 (2014) 9618–9624.
[108] A. Mathew, P.R. Sajanlal, T. Pradeep, J. Mater. Chem. 21 (2011) 11205–11212.
[109] C.-L. Liu et al., Angew. Chem. Int. Ed. 50 (2011) 7056–7060.
[110] X. Le Guével et al., J. Phys. Chem. C 115 (2011) 10955–10963.
[111] H. Wei et al., Analyst 135 (2010) 1406–1410.
[112] Y.-H. Lin, W.-L. Tseng, Anal. Chem. 82 (2010) 9194–9200.
[113] Z. Lin et al., Analyst 137 (2012) 2394–2399.
[114] D. Hu et al., Analyst 135 (2010) 1411–1416.
[115] J. Xie, Y. Zheng, J.Y. Ying, Chem. Commun. 46 (2010) 961–963.
[116] N. Alkudaisi et al., J. Mater. Chem. B 7 (2019) 1167–1175.
[117] M. Zhang et al., J. Phys. Chem. C 117 (2013) 639–647.
[118] F. Wen et al., Anal. Chem. 83 (2011) 1193–1196.
[119] Y. Liu et al., Adv. Funct. Mater. 20 (2010) 951–956.
[120] K. Selvaprakash, Y.-C. Chen, Biosens. Bioelectron. 61 (2014) 88–94.
[121] G. Deng, Mater. Manuf. Processes 14 (1999) 623–625.
[122] K.E. Sapsford et al., Mater. Today 11 (2008) 38–49.
[123] M. De, P.S. Ghosh, V.M. Rotello, Adv. Mater. 20 (2008) 4225–4241.
[124] S.W. Thomas, G.D. Joly, T.M. Swager, Chem. Rev. 107 (2007) 1339–1386.
[125] J.N. Anker et al., Nat. Mater. 7 (2008) 442.
[126] Vella, F. Principles of bioinorganic chemistry: By S J Lippard and J M Berg. pp 411. University Science Books, Mill Valley, California. 1994. $30 ISBN 0-935702-73-3 (paper). Biochemical Education 1995, 23, 115-115.
[127] R.L. Brathwaite, S.D.C. Rabone, J. R. Soc. New Zealand 15 (1985) 363–370.
[128] L.-Y. Chen et al., Anal. Chem. 87 (2015) 216–229.
[129] S. Ghosh, Spectroscopic Investigations and Applications, IISER, Bhopal, 2015.
[130] F. Bray et al., CA Cancer J. Clin. 68 (2018) 394–424.
[131] O. Golubnitschaja, J. Flammer, Surv. Ophthalmol. 52 (2007) S155–S161.
[132] C.L. Sawyers, Nature 452 (2008) 548.
[133] Y. Zhou et al., Anal. Chem. 90 (2018) 10024–10030.
[134] J. Peng et al., Eur. J. 18 (2012) 5261–5268.
[135] X.-X. Wang et al., Biosens. Bioelectron. 26 (2011) 3614–3619.
[136] Y. Tao et al., Biosens. Bioelectron. 42 (2013) 41–46.
[137] Y. Tao et al., Adv. Mater. 25 (2013) 2594–2599.
[138] Y. Tao et al., Theranostics 7 (2017) 899–911.
[139] A. Retnakumari et al., Nanotechnology 21 (2009) 055103.
[140] Y. Xu et al., Microchim. Acta 185 (2018) 198.
[141] A.B. Chinen et al., Chem. Rev. 115 (2015) 10530–10574.
[142] M.F. Mousavi et al., Electroanalysis 29 (2017) 861–872.
[143] V.I. Lushchak, J. Amino Acids 2012 (2012) 26.
[144] J.R. Bhamore et al., Sens. Actuators, B 281 (2019) 812–820.
[145] T.-H. Chen, W.-L. Tseng, Small 8 (2012) 1912–1919.
[146] H. Lin et al., Biosens. Bioelectron. 41 (2013) 256–261.
[147] M.S. Mathew, K. Joseph, ACS Sustainable Chem. Eng. 5 (2017) 4837–4845.
[148] B. Alberts, A. Johnson, J. Lewis, M. Raff, K. Roberts, P. Walter, The molecular mechanisms of membrane transport and the maintenance of compartmental diversity, in: Molecular Biology of the Cell. 4th Ed. 2002. Garland Science.
[149] M. Mita et al., Anal. Chem. 91 (7) (2019) 4821–4830.
[150] E.-H. Yoo, S.-Y. Lee, Sensors 10 (2010) 4558–4576.
[151] L. Jin et al., Biosens. Bioelectron. 26 (2011) 1965–1969.
[152] C. Wang et al., RSC Adv. 5 (2015) 101599–101606.
[153] K.A. Brzezicka, S. Serna, N.C. Reichardt, Nanoscale Res. Lett. 13 (1) (2018) 360.
[154] C.E. Ahlfors, R.P. Wennberg, Semin. Perinatol. 28 (2004) 334–339.
[155] M. Jayasree et al., *Anal. Chim. Acta* 1031 (2018) 152–160.
[156] M. Santhosh et al., Biosens. Bioelectron. 59 (2014) 370–376.
[157] C. Muñoz-Bustos et al., Sens. Actuators, B 244 (2017) 922–927.
[158] X. Li et al., Talanta 195 (2019) 372–380.
[159] K. Selvaprakash, Y.-C. Chen, Biosens. Bioelectron. 92 (2017) 410–416.
[160] M. Shamsipur et al., Anal. Chem. 88 (2016) 2188–2197.
[161] S. Ghosh, U. Anand, S. Mukherjee, J. Phys. Chem. C 119 (2015) 10776–10784.
[162] M.H. Griep et al., Plasmonics 2 (2020) 1–7.
[163] Z. Chen et al., Talanta 94 (2012) 240–245.
[164] B. Aswathy, G. Sony, Microchem. J. 116 (2014) 151–156.
[165] Y. Chen et al., Anal. Chim. Acta 1026 (2018) 133–139.
[166] B. Wang et al., Talanta 178 (2018) 1006–1010.
[167] X. Cao et al., Anal. Chim. Acta 871 (2015) 43–50.
[168] L. Meng et al., Anal. Methods 9 (2017) 768–773.
[169] R. Yan et al., ACS Sustainable Chem. Eng. 6 (2018) 4504–4509.
[170] M. Jaishankar et al., Interdiscip. Toxicol. 7 (2014) 60–72.
[171] Y. Zhang et al., Sens. Actuators, B 238 (2017) 683–692.
[172] J. Zhang et al., Nano Today 11 (2016) 309–329.
[173] H. Li et al., Analyst 142 (2017) 567–581.
[174] H. Kawasaki, et al. Anal. Sci., 27 (2011), 591-591.
[175] J. Zang et al., Anal. Chem. 88 (2016) 10275–10283.
[176] S. Xu et al., Microchim. Acta 182 (2015) 2577–2584.
[177] J. Wang et al., Sens. Actuators, B 267 (2018) 342–350.
[178] S.-N. Ding, Y.-X. Guo, Anal. Methods 7 (2015) 5787–5793.
[179] T. Sanders et al., Rev. Environ. Health 24 (2009) 15–45.
[180] L.M. Gaetke, C.K. Chow, Toxicology 189 (2003) 147–163.
[181] T. Mayr et al., Anal. Chim. Acta 462 (2002) 1–10.
[182] M.E. Letelier et al., Chem. Biol. Interact. 151 (2005) 71–82.
[183] X. Yang et al., J. Mater. Chem. C 1 (2013) 6748–6751.
[184] S. Ghosh, U. Anand, S. Mukherjee, Anal. Chem. 86 (2014) 3188–3194.
[185] U.S. Akshath, P. Bhatt, S.A. Singh, J. Fluoresc. 17 (2020) 1–9.
[186] X. Liu et al., Biosens. Bioelectron. 74 (2015) 322–328.
[187] Y.-Q. Huang et al., Microchim. Acta 185 (2018) 1–10.
[188] D. Lu et al., Spectrochim. Acta Part A Mol. Biomol. Spectrosc. 121 (2014) 77–80.
[189] G. Zhang et al., Sens. Actuators, B 279 (2019) 361–368.
[190] M.-L. Cui et al., Sens. Actuators, B 188 (2013) 53–58.
[191] J. Zhang et al., Chem. Commun. 49 (2013) 2691–2693.
[192] F. Liu et al., Anal. Chem. 88 (2016) 10631–10638.
[193] A. Biswas et al., ACS Omega 2 (2017) 2499–2506.
[194] R. Shen et al., Anal. Chem. 90 (2018) 4478–4484.
[195] S. Liu et al., Anal. Chim. Acta 886 (2015) 151–156.
[196] Y.J. Ju et al., Sens. Actuators, B 275 (2018) 244–250.
[197] C.-Y. Lee et al., RSC Adv. 6 (2016) 79020–79027.
[198] K. Okabe et al., Nat. Commun. 3 (2012) 705.
[199] C. Wang et al., Nano Res. 8 (2015) 1975–1986.
[200] D. Jaque, F. Vetrone, *Nanoscale* 4 (2012) 4301–4326.
[201] X. Chen, J.B. Essner, G.A. Baker, Nanoscale 6 (2014) 9594–9598.
[202] J. Lan et al., Talanta 143 (2015) 469–473.
[203] L. Tian et al., Talanta 170 (2017) 530–539.
[204] A. Roos, W.F. Boron, Physiol. Rev. 61 (1981) 296–434.

Uncorrected Proof

[205] W. Wang et al., Analyst 139 (2014) 2990–2993.
[206] G. Zhang et al., J. Mater. Chem. C 4 (2016) 3540–3545.
[207] Y. Qiao et al., Sens. Actuators, B 220 (2015) 1064–1069.
[208] Z. Miao et al., New J. Chem. 42 (2018) 1446–1456.
[209] H. Xiong et al., Sens. Actuators, B 239 (2017) 988–992.
[210] R. Ali, S. Saleh, S. Aly, Microchim. Acta 184 (2017) 3309–3315.
[211] Y.-T. Wu et al., Nanoscale 8 (2016) 11210–11216.
[212] Y. Wei et al., Part. Part. Syst. Char. 36 (12) (2019) 1900314.
[213] S. Govindaraju, et al. Sci. Rep. 2017, 7, 40298-40298.
[214] S. Govindaraju et al., Appl. Surf. Sci. 498 (2019) 143837.
[215] H. Li et al., Analyst 139 (1) (2014) 285–289.
[216] Q. Sha et al., Sens. Actuators, B 294 (2019) 177–184.
[217] Y. He et al., Analyst 137 (17) (2012) 4005–4009.
[218] Y. Yang et al., Talanta 154 (2016) 190–196.
[219] S. Ghosh et al., Spectrochim. Acta Part A Mol. Biomol. Spectrosc. 215 (2019) 209–217.
[220] Y. Li, W. Peng, X. You, Microchim. Acta 184 (2017) 3539–3545.
[221] R.S. Aparna et al., J. Photochem. Photobiol., A 379 (2019) 63–71.
[222] D. Sharma, N. Wangoo, R.K. Sharma, Talanta 21 (2020) 121267.
[223] G. Gao et al., Biomaterials 194 (2019) 36–46.
[224] F. Tan et al., Talanta 194 (2019) 634–642.
[225] Q. Chen, R. Gao, L. Jia, Talanta 1 (2020) 121476.
[226] H. Hossein-Nejad-Ariani, T. Kim, K. Kaur, ACS Appl. Nano Mater. 1 (2018) 3389–3397.
[227] H. Ji et al., Adv. Healthc. Mater. 7 (2018) 1701370.
[228] P.-H. Chan, Y.-C. Chen, Anal. Chem. 84 (2012) 8952–8956.
[229] J. Liu et al., Talanta 134 (2015) 54–59.
[230] M. Pal et al., Anal. Chim. Acta 952 (2017) 81–87.
[231] B. Liu et al., Microchim. Acta 181 (2013) 257–262.
[232] Q. Guo et al., Microchim. Acta 182 (2015) 1483–1489.
[233] D. Tang, J. Ren, M. Lu, Analyst 142 (2017) 4794–4800.
[234] M. Lin et al., Biosens. Bioelectron. 45 (2013) 82–88.
[235] S. Lv et al., ACS Appl. Mater. Interfaces 9 (2017) 38336–38343.
[236] L.-P. Mei et al., Anal. Chem. 90 (2018) 2749–2755.
[237] X.L. Hu et al., Biosens. Bioelectron. 77 (2016) 666–672.
[238] S. Menon, K. Girish Kumar, J. Fluoresc. 27 (2017) 1541–1546.
[239] T. Peng et al., Anal. Chim. Acta 1040 (2018) 143–149.
[240] R. Li et al., Sens. Actuators, B 281 (2019) 28–33.
[241] N. Zhu et al., Talanta 199 (2019) 72–79.
[242] Q. Chen et al., Biosens. Bioelectron. 79 (2016) 364–370.
[243] L. Zhao, Z. Ma, Sens. Actuators, B 241 (2017) 849–854.
[244] T. Peng et al., Microchim. Acta 185 (2018) 1–8.
[245] Z. Zhang et al., Anal. Chim. Acta 1035 (2018) 168–174.
[246] N. Kaur et al., Nanoscale Res. Lett. 13 (2018) 302.
[247] Lei YuLei Yu, Qiao Zhang, Qi Kang, Bin Zhang, Dazhong Shen, and Guizheng Zou. Anal. Chem. 92 (2020) 7581-7587.
[248] Quan-Quan Zhuang et al., ACS Appl. Mater. Interfaces 11 (2019) 31729–31734.
[249] Bioimaging: principles and techniques. In Introduction to Biophotonics; pp. 203–254.
[250] D.L. Farkas et al., Comput. Med. Imaging Graph. 22 (1998) 89–102.
[251] P. Zhang et al., Nanoscale 6 (2014) 2261–2269.
[252] C.-Y. Tsai et al., J. Fluoresc. 26 (2016) 1239–1248.
[253] H. Chen et al., Nanoscale 4 (2012) 6050–6064.
[254] D. Hu et al., Theranostics 4 (2014) 142–153.
[255] Z. Teng et al., J. Agric. Food. Chem. 61 (2013) 2556–2564.
[256] H. Li et al., Talanta 158 (2016) 118–124.
[257] Y. Wang, J. Chen, J. Irudayaraj, ACS Nano 5 (2011) 9718–9725.
[258] T. Zhao et al., J. Mater. Chem. B 3 (2015) 2388–2394.
[259] N. Hashemi et al., Microchim. Acta 185 (2017) 60.
[260] L. Shang, G.U. Nienhaus, APL Mater. 5 (2017) 053101.
[261] C. Zhou et al., Angew. Chem. 123 (2011) 3226–3230.
[262] U. Prabhakar et al., Cancer Res. 73 (2013) 2412–2417.
[263] D. Rosenblum et al., Nat. Commun. 9 (2018) 1410.
[264] P. Reineck, B.C. Gibson, Opt. Mater. 5 (2017) n/a-n/a.
[265] S.L. Raut et al., Nanoscale 6 (2014) 2594–2597.
[266] P. Zhao et al., Anal. Chem. 87 (2015) 9998–10005.
[267] X. Wu et al., Nanoscale 2 (2010) 2244–2249.
[268] Z. Li et al., ACS Appl. Mater. Interfaces 10 (2018) 83–90.
[269] S.L. Raut et al., Chem. Phys. Lett. 561–562 (2013) 74–76.
[270] R. Khandelia et al., Small 11 (2015) 4075–4081.
[271] H. Al Kindi et al., J. Photochem. Photobiol., A 357 (2018) 168–174.
[272] Y. Liu et al., J. Mater. Chem. B 4 (2016) 1276–1283.
[273] Q. Wang et al., Anal. Chem. 87 (2015) 4299–4304.
[274] S.-K. Sun et al., Anal. Chem. 85 (2013) 8436–8441.
[275] H. Cui et al., ACS Appl. Mater. Interfaces (2017).
[276] L. Han et al., ACS Appl. Mater. Interfaces 9 (2017) 6941–6949.
[277] U.N. Pan et al., ACS Appl. Mater. Interfaces 9 (2017) 19495–19501.
[278] F. Gao et al., ACS Nano 9 (2015) 4976–4986.
[279] Y. Wang, J.-T. Chen, X.-P. Yan, Anal. Chem. 85 (2013) 2529–2535.
[280] H. Chen, B. Li, X. Ren, S. Li, Y. Ma, S. Cui, Y. Gu, Biomaterials 33 (2012) 8461–8476.
[281] H. Hu et al., Biomaterials 35 (2014) 9868–9876.
[282] C. Ding, Y. Tian, Biosens. Bioelectron. 65 (2015) 183–190.
[283] J. Qiao et al., Chem. Commun. 49 (2013) 8030–8032.
[284] L. Kong et al., ChemistrySelect 1 (2016) 1096–1103.
[285] H.-D. Cui et al., Chin. Chem. Lett. 28 (2017) 1391–1398.
[286] D.-H. Hu et al., Nanoscale 5 (2013) 1624–1628.
[287] Y. Kong et al., Nanoscale 5 (2013) 1009–1017.
[288] J. Lin et al., Nanoscale Res. Lett. 8 (2013) 170.
[289] J. Wang et al., Sci. Rep. 3 (2013) 1157.
[290] F. Zhou et al., Theranostics 6 (2016) 679–687.
[291] C. Ding et al., ACS Appl. Mater. Interfaces 10 (2018) 8947–8954.
[292] A. Latorre et al., Cancers 11 (7) (2019) 969.
[293] B.N.P. Kumar et al., Mol. Pharm. 15 (2018) 2698–2713.
[294] R. Liu et al., J. Control. Release 278 (2018) 127–139.
[295] U. Goswami et al., ACS Appl. Mater. Interfaces 10 (2018) 3282–3294.
[296] H. Wang et al., Trends Pharmacol. Sci. 39 (2018) 24–48.
[297] J. Xie et al., Adv. Mater. 31 (2019) 1802244.
[298] S. Zhu, Z. Gu, Y. Zhao, Adv. Ther. 1 (2018) 1800050.
[299] X.-D. Zhang et al., J. Mater. Chem. B 3 (2015) 4735–4741.
[300] D. Huo et al., ACS Nano 11 (2017) 10159–10174.
[301] X.-D. Zhang et al., Adv. Mater. 26 (2014) 4565–4568.
[302] A. Kefayat et al., Nanomed. Nanotechnol. Biol. Med. 16 (2019) 173–184.
[303] F. Ghahremani et al., RSC Adv. 8 (2018) 4249–4258.
[304] F. Ghahremani et al., Nanomedicine 13 (2018) 2563–2578.
[305] J. Chen et al., Nanoscale 9 (2017) 14826–14835.
[306] Y. Yong et al., NPG Asia Mater. 8 (2016) e273.
[307] P. Agostinis et al., CA Cancer J. Clin. 61 (4) (2011) 250–281.
[308] A.P. Castano, P. Mroz, M.R. Hamblin, Nat. Rev. Cancer 6 (7) (2006) 535–545.
[309] R. Ho-Wu, S.H. Yau, T. Goodson, J. Phys. Chem. B 121 (2017) 10073–10080.
[310] V. Poderys et al., J. Photochem. Photobiol., B 204 (2020) 111802.
[311] C. Zhang et al., Adv. Funct. Mater. 25 (2015) 1314–1325.
[312] F. Xia et al., Biomaterials 170 (2018) 1–11.
[313] Q. Chen et al., Nano Res. 11 (2018) 5657–5669.
[314] P. Huang et al., Biomaterials 34 (2013) 4643–4654.
[315] Y. Li et al., ACS Appl. Mater. Interfaces (2019) 17215–17225.
[316] Y. Yu et al., Adv. Healthcare Mater. 5 (2016) 2528–2535.
[317] Y. Yu, W. Di Lee, Y.N. Tan, Mater. Sci. Eng., C 109 (2020) 110525.
[318] M. Abbas et al., Adv. Mater. 29 (2017) 1605021.
[319] W. Gu et al., J. Mater. Chem. B 4 (2016) 910–919.
[320] A. Cifuentes-Rius et al., ACS Appl. Mater. Interfaces 9 (2017) 41159–41167.
[321] A. Cifuentes-Rius, et al. Small 13 (2017) 1701201-n/a.
[322] T. Yang et al., Adv. Mater. 28 (2016) 5923–5930.
[323] Y. Wang et al., Adv. Mater. 27 (2015) 3874–3882.
[324] W. Yang et al., ACS Nano 10 (2016) 10245–10257.
[325] Z. Lu, et al., Sci. Rep. 7 (2017), 41571-41571.
[326] T. Chen et al., ACS Appl. Mater. Interfaces 4 (2012) 5766–5774.
[327] H. Ding et al., ACS Appl. Mater. Interfaces 7 (2015) 4713–4719.
[328] C. Wang et al., Angew. Chem. Int. Ed. 50 (2011) 11644–11648.
[329] B. Khlebtsov et al., J. Innov. Opt. Health Sci. 09 (2016) 1650004.
[330] X. Bai et al., TrAC, Trends Anal. Chem. 73 (2015) 54–63.
[331] A. Yahia-Ammar et al., ACS Nano 10 (2016) 2591–2599.
[332] Z. Luo, e, et al., J. Am. Chem. Soc. 134 (2012) 16662–16670.
[333] F. Cao et al., Nanoscale 9 (2017) 4128–4134.
[334] R.R. Kudarha, K.K. Sawant, Mater. Sci. Eng., C 81 (2017) 607–626.
[335] P. Liu et al., Part. Part. Syst. Char. 32 (2015) 749–755.
[336] S. Chattoraj, M.A. Amin, K. Bhattacharyya, ChemPhysChem 17 (2016) 2088–2095.
[337] C. Fu et al., Mater. Sci. Eng., C 87 (2018) 149–154.
[338] P. Wang et al., Adv. Sci. 4 (2017) 1700175.
[339] Y. Lei et al., Nat. Commun. 8 (1) (2017) 1–5.
[340] Y. Zhao, X. Jiang, Nanoscale 5 (2013) 8340–8350.
[341] A. Nain et al., J. Hazard. Mater. 389 (2020) 121821.
[342] W.-Y. Chen et al., Nanomedicine 5 (2010) 755–764.
[343] B. Khlebtsov et al., RSC Adv. 5 (2015) 61639–61649.

Uncorrected Proof

Please cite this article in press as: I. Zare et al., Materials Today, (2020), https://doi.org/10.1016/j.mattod.2020.10.027

[344] H. Miao et al., Nanoscale 7 (2015) 19066–19072.
[345] P. Domenico et al., Antimicrob. Agents Chemother. 41 (8) (1997) 1697–1703.
[346] K. Brach et al., Langmuir 33 (36) (2017) 8993–8999.
[347] F. Bertorelle et al., ACS Omega 3 (11) (2018) 15635–15642.
[348] F. Bertorelle et al., ChemPhysChem 19 (2) (2018) 165–168.
[349] J. Olesiak-Banska et al., Chem. Soc. Rev. 48 (15) (2019) 4087–4117.
[350] V. Bonačić-Koutecký, R. Antoine, Nanoscale. 11 (26) (2019) 12436–12448.
[351] Y. Yu et al., J. Am. Chem. Soc. 136 (2014) 1246–1249.
[352] V. Rojas-Cervellera et al., Nanoscale 9 (2017) 3121–3127.
[353] G. Soldan et al., Angew. Chem. Int. Ed. 55 (2016) 5749–5753.
[354] H. Bagheri et al., Biosens. Bioelectron. 89 (2017) 829–836.
[355] C. Guo et al., ACS Appl. Mater. Interfaces 47 (2017) 41188–41199.
[356] J.M. Campbell et al., Int. J. Mol. Sci. 19 (2018) 2731.
[357] S.K. Vashist, J.H.T. Luong, Smartphone-based immunoassays. Handbook of Immunoassay Technology 2018, chapter 16.

Uncorrected Proof

Please cite this article in press as: I. Zare et al., Materials Today, (2020), https://doi.org/10.1016/j.mattod.2020.10.027